Mathematical Modeling and Simulation for Microbial Enhanced Oil Recovery Optimization

Master's Thesis in Applied and Computational Mathematics

Abay Molla Kassa

Department of Mathematics

University of Bergen

May, 2016

Acknowledgement

During my study, I was fortunate to interact with a number of people from whom I have benefited greatly. I am grateful to those who have offered their advice, assistance, encouragement and friendship. Most of all, my thanks goes to my supervisors; Kundan Kumar (PhD, Assoc. Prof.) and Florin A. Radu (PhD, Prof.). I appreciate their invaluable unreserved material and moral support to start my study earlier and to complete it on time. Their encouragement, active interest in my work, discussion on the topic and appreciation during the entire year have been very indispensable. I consider myself very fortunate to have been under their direction. Our interaction has for me been an invaluable learning experience.

I would like to thank the Mathematics department of University of Bergen(UoB) and Lanekassen for giving me the opportunity to do my graduate work and teaching me far more about life than Mathematics. I also grateful to Quality Renhold A/S who gave me a part time work which greatly support my living expense.

I am thankful to all my Ethiopian community friends in Bergen and fellow of UoB who helped me going through it. I thank Vincent Teyekpiti and Mahlet Berhanu for their valuable comments and suggestions to improve the earlier version of this thesis.

Finally, I would like to forward my grateful thanks to Kassa's family. Specially, special thanks goto my elder sisters Eneye Molla and Asres Molla. They encourage, help and advise me from the beginning of my life. Without them none of this would have mattered.

Abay Molla Kassa,
May, 2016.

Dedication

This thesis is dedicated to Semu Mitiku Kassa (PhD, Assoc. Prof.)

Abstract

In this study, we developed a mathematical model for 2D microbial EOR technology. It consists of an average pressure formulation of two-phase flow and component advection-diffusion reactive transport models. An IFT reduction mechanism has been used to couple porous media flow and transport phenomenon. A cell centered control volume and backward Euler methods were applied to discretize the flow and transport equations. An iterative linearization technique is implemented in Matlab to solve the resulting system of non-linear algebraic equations. Numerical experiments were conducted on two-phase flow, advection-diffusion transport and the coupled microbial EOR models for different mobility and capillary pressure parameterizations. Moreover, we have proposed a new microbial EOR optimization model to maximize the sweep efficiency by controlling the slug size injection strategy. In this thesis, we have also proposed a new optimization algorithm based on gradient accent and iterative linearization methods to handle the microbial EOR optimization model numerically. A number of illustrative numerical experiments have been done to analyse the effect of slug size and cost of microbial concentration.

Keywords: two-phase flow, advection-diffusion transport, microbial EOR, slug size injection strategy and microbial EOR optimization.

Contents

Acknowledgement ii

Abstract v

1 General Introduction 6

2 Background and Literature Review 10

2.1 Flow in Porous Media . . . 10

2.1.1 Basic Definitions . . . 11

2.1.2 Saturation and Relative Permeability . . . 12

2.1.3 Capillary Force and Inter-facial Tension . . . 12

2.2 EOR: Enhanced Oil Recovery . . . 13

2.2.1 Physicochemical Methods . . . 14

2.2.2 Biological Methods . . . 15

2.2.2.1 Physical and Chemical Challenge of Microbial EOR Processes . . . 16

2.3 Literature Review on Multi-phase Flow and Transport Models . . . 17

3 Flow and Transport Models 20

3.1 Two-phase Flow Reservoir Modeling . . . 20

3.1.1 Mean-value Formulation . . . 22

3.1.1.1 Boundary and Initial Conditions . . . 22

3.2 Reactive Transport Models . . . 23

3.2.1 Relation Between Growth, Consumption and Production . . . 25

4 Numerical Modeling 27

4.1 Midpoint Rule and Temporal Discretization . . . 27

4.2 Multi-point Flux Approximation (MPFA) . . . 29

4.2.1 Discretization of Boundary Conditions . . . 31

4.2.1.1 Dirichlet Boundary Condition . . . 31

4.2.1.2 Neumann Boundary Condition . . . 33

4.2.2 Finite volume Discretization of Flow Problem . . . 33

4.2.2.1 Pressure Equation . . . 34

4.2.2.2 The Saturation Equation . . . 35
4.2.3 Finite Volume Discretization for Transport Equation . . . 36

5 Numerical Results and Convergence Analysis 40
5.1 Discrete L_2 Error Estimation . . . 40
5.2 Matlab Code Implementation Validation for Different Fluid Parameterizations . . . 41
5.2.1 Linear Relative Permeabilities and Quadratic Capillary Pressure . . . 42
5.2.2 Van Genuchten Parameterizations . . . 42
5.2.3 Matlab Code Implementation Validation Test for two-phase Flow with Constant Mobilities and Quadratic Capillary Force . . . 43
5.2.4 Matlab Code Implementation Validation Test for Two-phase Flow Problem with Linear Relative Permeabilities and Quadratic Capillary Pressure . . . 45
5.2.5 Code Validation Test for Two-phase Flow Problem with van Genuchten Parametrization 48
5.2.6 Analytic Solution validation Test Case for Transport Model . . . 51

6 Mathematical Models for Microbial EOR Processes 55
6.1 Capillary Pressure, Residual Oil and Relative Permeabilities . . . 55
6.1.1 Effect of Microbial Concentration on Capillary Pressure and Relative Permeabilities . 57
6.1.2 Effect of Microbial activity on Residual Oil . . . 57
6.2 Coupling Flow and Transport Equations . . . 58
6.2.1 The Coupled Model Validation Test Case with an Analytical Solutions . . . 59

7 Optimal Control Theory 64
7.1 Extremal of Functionals and The Fundamental Theorem of Variational Calculus . . . 64
7.2 Optimal Control Problem Formulation . . . 65
7.3 Discrete Maximum Principle . . . 67
7.3.1 Necessary Conditions for Explicit Discretization . . . 67
7.3.2 Necessary Conditions for Implicit Discretization . . . 69

8 Economic Mathematical Modeling for 2D Microbial EOR 73
8.1 Mathematical Model for Production-Injection Wells . . . 73
8.1.1 Performance of Production Wells . . . 74
8.2 Introducing Wells to the Coupled Microbial EOR Model . . . 75
8.2.1 Numerical Simulation for the Integrated Models of Wells and Microbial EOR . . . 76
8.2.1.1 The Effect of Pure Water Injection . . . 76
8.2.1.2 The Effect of Water and Microbes Injection . . . 77
8.3 Slug Size Injection Strategy . . . 79
8.4 Numerical Optimization Methods and Results . . . 80
8.4.1 Maximum Principle and Solution Algorithm . . . 80
8.4.1.1 Description of Solution Algorithm . . . 82
8.4.2 Optimization Results and Sensitivity Analysis . . . 83

9 Conclusion and Future Work **90**

Appendices **92**

Bibliography 95

List of Tables

2.1 Bio-products of microbes and their effects 16

5.1 Error analysis for two-phase flow problem with constant mobilities and quadratic capillarity force. 45
5.2 Error analysis for two-phase flow problem with linear mobilities and quadratic capillarity force. 48
5.3 Error analysis for two-phase flow with van Genuchten parametrization. 51
5.4 Error analysis for transport model. 52

6.1 Iterative linearization algorithm. 59
6.2 Parameters used to validate the coupled model. 60
6.3 Error analysis the coupled reservoir system of pressure and saturation. 62
6.4 Error analysis the coupled reservoir system of Microbial concentration. 62

8.1 Parameters used to simulate the coupled model reservoir. 77

List of Figures

2.1.1 Contact angle From [7] . . . 13

4.0.1 Cell-centered finite volume regular mesh . . . 28
4.2.1 Cell-center finite volume discretization. . . . 29
4.2.2 1D cell-centered finite volume Discretization for boundary conditions. . . . 32

5.2.1 Concave Capillary Pressure (left) and phase relative permeabilities (right). . . . 42
5.2.2 Capillary Pressure (left) and Relative permeabilities (right) of van Genuchten parametrization. 43
5.2.3 Approximate (left) and exact (right) average pressure solutions for constant mobilities and quadratic capillary pressure. . . . 45
5.2.4 Approximate (left) and exact (right) water phase saturation solutions for constant mobilities and quadratic capillary pressure. . . . 46
5.2.5 Error plot for constant mobilities and quadratic capillary pressure. . . . 46
5.2.6 Approximate average pressure solution (left) and exact average pressure solution (right) for linear relative permeabilities and quadratic capillary pressure. . . . 47
5.2.7 Approximate (left) and exact (right) saturation profile for linear relative permeabilities and quadratic capillary pressure. . . . 47
5.2.8 Error Plot of average pressure and water phase saturation for two phase flow problem with linear relative permeabilities and quadratic capillary pressure parameterizations. . . . 48
5.2.9 Approximate average pressure (left) and exact pressure (right) solutions for van Genuchten parametrization. . . . 50
5.2.10 Approximate wetting saturation (left) and exact wetting saturation (right) solutions for van Genuchten parametrization. . . . 50
5.2.11 Error plot for two-phase flow problem with van Genuchten parameterizations. . . . 51
5.2.12 Comparative plot of approximate (left) and exact (right) solutions for transport model . . . 52
5.2.13 Error plot for component transport models. . . . 52

6.1.1 IFT vs microbial concentration. . . . 56
6.1.2 Residual oil vs oil-water IFT (left) and Residual oil vs microbial concentration (left). . . . 58
6.2.1 Approximate (left) and exact (right) average pressure solutions for the coupled system. . . . 61
6.2.2 Approximate (left) and exact (right) water phase saturation profiles for the coupled system. . 61
6.2.3 Approximate (left) and exact (right) microbial concentration solutions for the coupled system. 61

6.2.4 Error plot for the coupled system of the oil reservoir. 62

8.2.1 Initial Water injection strategy. 77
8.2.2 Final Reservoir Profile for water injection. 78
8.2.3 Injection policy for water (left) and microbial concentration (right). 78
8.2.4 Final time reservoir condition for water and microbial concentration injection. 79
8.4.1 Optimal Injection Policy. 84
8.4.2 Final Reservoir Condition with injection strategy of Figure 8.4.1. 84
8.4.3 Performance functional. 85
8.4.4 Optimal injection policy with zero cost of microbes 86
8.4.5 Final time fluids distribution for Injection 8.4.4 86
8.4.6 Optimal water (left) and microbial concentration (right) injection profiles corresponding to the highest cost of microbes 87
8.4.7 Performance functional for high cost of microbes 87
8.4.8 Effect of microbial concentration cost on performance functional. 88

Chapter 1

General Introduction

Since 1856, researchers from science and engineering disciplines started exploring and investigating fluid flow and transport in subsurface reservoirs and to use the information acquired to forecast, manage and control the process as it takes place in a system ([1–15] to list a few). This kind of study often involves building simulation models that can mimic actual fluid flow behaviours within reservoirs. The models should represent porous medium (the reservoir), with all appropriate physics, reservoir properties and geology as closely as possible. In reservoir mathematics, multi-phase flow models embrace the properties of the reservoir domain and motion of multiple fluids (ranging from immiscible/incompressible to miscible/compressible fluids) through the voids of a porous media [1]. In this sort of fluid transport, fluids flow together, allowing distinct interface between phases due to phase pressure differences.

Multi-phase flow in porous media are widely applicable in real life phenomenon, such as ground water contamination, CO2 sequestration, nuclear waste management and enhanced oil recovery (EOR) [1, 2, 4–6, 9, 11, 16–25]. Since the world's energy consumption has risen tremendously, crude fuels remain in the market as a key supply of energy source. Thus, simulation of fluid dynamics in subsurface reservoir has been received an increasing interest in industries as well as academia ([4–6, 11, 15, 17, 23–25] to name a few) and it is also the interest of this thesis, particularly microbial EOR.

Fluid dynamics in oil petroleum reservoir is governed by non-linear and complex systems of partial differential equations (PDEs). As a consequence, it is difficult and quite challenging to give a qualitative solution analysis unless one can make strong assumptions, which indeed cannot describe the physical phenomena and lead to invalid forecast for fluid flow problems. This enforces to weaken the assumptions in order to have a comparable realistic mathematical flow models. Moreover, the need to explore the effect of adding microbes to an oil reservoir for enhancing the recovery has a significant additional complexity on the governing mathematical model. Thus, numerical methods should be employed to understand, analyse and forecast multi-phase flow and mass transport in porous media.

This thesis aims to investigate the effect of microbial activities on residual oil by reduction of interfacial tension (IFT) mechanism. This is often done by setting a mathematical reservoir model consisting of two-phase flow (the oil phase and water phase, for which the flow is governed by the Darcy's law and mass conservation for each phase) and the transport mechanism of microbes (it has been modelled by the advection–diffusion equations). The flow and transport equations are coupled by introducing microbes effect on the capillary pressure and relative permeabilities (see the developments in Chapter 6) which would give a complete and coupled mathematical model (we call it microbial EOR model) to govern fluid flow and transport of microbes in porous media. This mathematical model is used to simulate the contribution of microbes on recovery of oil by capillary pressure reduction mechanism.

In addition to microbial EOR simulation, this thesis has shown the interaction between slug size injection, microbial EOR model and well production performance by proposing a new mathematical model that controls the injection size of water and microbial concentration. This part aims to investigate the effect of slug size injection over the residual oil. The resulting model is an optimization model that controls the injection volumetric rate and searches a way to maximize the profit from the oil recovery processes.

In general, the resulting mathematical models are non-linear and fully coupled systems which lead to the use of numerical methods and simulation mechanism providing better correlation between the physical model, the mathematical model and the numerical model. As a result, we have employed a cell center finite volume and backward Euler discretization in space and time respectively followed by iterative linearization to simulate two-phase flow, microbial transport and microbial EOR models. Furthermore, we adopt this iterative linearization solver and gradient accent optimization method in order to solve and analyse the effect of injection slug size on the performance of oil production.

This thesis is organised as follows;

† Chapter 2 introduces basic notions and concepts of multi-phase flow in porous media. Moreover, it discusses existing EOR methods, particularly it gives a detail discussion on microbial EOR method. Literature review on mathematical models that govern two-phase flow and transport phenomena with the corresponding numerical methods have been introduced in this chapter.

† A Darcy–type mathematical model is given in Chapter 3 that presents a two dimensional average pressure formulation of incompressible two-phase flow. An advection-diffusion reactive component transport models are also discussed in this chapter. The growth, deposition and reaction terms of microbial concentration are also introduced.

† The mathematical models discussed in Chapter 3 are discretized in Chapter 4 by the help of cell centered finite volume method. Moreover, a two point flux approximation is used to obtain harmonic average approximate value of boundary rock permeability at each control volume. Furthermore, an average and upwind streaming methods are formulated to obtain an approximate value of boundary relative permeabilities at each control volume.

† In Chapter 5, numerical modeling and implementation validation test are discussed and analysed for two-phase flow models with different fluid parameterizations and a simple transport model through comparing the numerical solutions with the manufactured analytical solutions.

† In Chapter 6, an IFT mathematical model is developed and used to couple the two-phase flow and microbial transport models. An iterative linearization method is adapted to solve the resulting microbial EOR model. Furthermore, a numerical convergence and Matlab code implementation validation test of a method is discussed along with an analytical solution.

† Chapter 7 introduces a preliminary introduction for maximum principles of variational calculus and discrete optimal control problems. The developments of implicit and explicit necessary conditions for discrete optimal control problems are also discussed briefly.

† In Chapter 8, we have integrated an injection/production wells with a microbial EOR model. An optimization model is also proposed to determine the slug injection policy in order to maximize the production of oil. Furthermore, a benefit based comparison study between traditional injection processes and the predicted optimal injection processes has been discussed.

† The thesis culminates with conclusion in Chapter 9. It also suggests future works.

Chapter 2

Background and Literature Review

This chapter begins with basic concepts, definitions, terminologies and properties of multiple fluids flow in porous media. Then a comparison type study on well known enhanced oil recovery methods is discussed. Moreover, literatures on mathematical models of two-phase flow and convective-dispersive transport with corresponding numerical methods are reviewed.

2.1 Flow in Porous Media

Most of subsurface formation comprises of a solid matrix with an interconnected void space for which fluids are allowed to flow through it. Subsurface void spaces might be filled with multiple fluids that are either able to flow or are trapped within rock skeletons, and commonly referred to as multi-phase flow in porous media, represent fluid dynamics of great complexity involving a wide range of physical phenomena. A subsurface formation is mainly characterized by its porosity which is a ratio of the void space to the *Representative Elementary Volume*, (REV). Other properties of the medium (e.g., permeability, tensile strength, electrical conductivity) can sometimes be derived from the respective properties of its constituents (solid matrix and fluid), the medium porosity and pores structure [26], but such a derivation is usually complex. In general, the rock formations are typically heterogeneous at all length scales in between and phenomena at all length scales can have a profound impact on flow, making flow in subsurface reservoirs a true multi-scale problem. In any phenomenon that involves a porous material, one must deal with the complex pore structure of the medium and how it affects the distribution, flow, displacement of one or more fluids, or dispersion (i.e., mixing) of one fluid in another.

Fluids with different properties are found within sedimentary rocks that have sufficient interconnected void space to store and transmit these fluids. The hydrocarbons typically carried in rock zones that are a few tens of meters thick but extend several kilometres in the lateral directions [1]. In this case, the use of REV is employed in mathematical modeling processes instead of concerned with how fluid moves around and in

the pore network. Based on macroscopic scale or REV, fluid flow and microbial transport in representative porous domain (volume, V) are governed by mass conservation principle and given as

$$\left\{\begin{array}{c}\text{Change}\\ \text{of mass}\\ \text{in V}\end{array}\right\} = \left\{\begin{array}{c}\text{Mass}\\ \text{entered}\\ \text{into V}\end{array}\right\} - \left\{\begin{array}{c}\text{Mass}\\ \text{leave}\\ \text{from V}\end{array}\right\} + \left\{\begin{array}{c}\text{Source}\\ \text{or Sink}\\ \text{iside V}\end{array}\right\}$$

where the source/sink term will account for production/consumption of mass within the volume.

In general, flow and transport phenomena in porous media, fractured rock as well as industrial synthetic porous materials arise in many diverse fields of science and technology, ranging from agricultural, biomedical, construction, ceramic, chemical, and petroleum engineering, to food and soil sciences, and powder technology.

2.1.1 Basic Definitions

In the processes of developing a flow model in subsurface systems, it is important to realize that fluid flows are governed in large part by (absolute) permeability, K, of the medium which is a measure of a single fluid flow conductivity in the porous medium and the porosity of a reservoir ϕ, which is a measure of its void space given as a dimensionless ratio

$$\phi = \frac{\text{volume of void}}{\text{REV}}.$$

Rock permeability and porosity have a complicated connection, but Kozeny-Carman equation is used to interpret their relationship [26] as follows

$$K = \frac{1}{8\tau\tilde{S}^2}\frac{\phi^3}{(1-\phi)^2},$$

where $\tilde{S}$ is a ratio of the internal rock surface area to the volume of the rock, whereas τ is the tortuosity which is a ratio of the length of a pore to the distance between its endpoints.

The Kozeny-Carman equation does serve to acquire estimates of scalar permeability, or porosity, which might be suitable for homogeneous medium. However, most fluids can flows easily through sandstone in each direction, due to this K is usually designed as a tensor. If a rock formation like sandstone transmit fluids readily, then they are called *permeable*. Moreover, the medium is called an *isotropic*, if K is independent of direction. Conversely, when K changes value depending on the direction being considered, then the medium is referred to as *anisotropic*. Furthermore, if K depends on special location then the system is called *heterogeneous* whereas it is known to be homogeneous medium. On the other side, a subsurface region might be completely occupied by the solid matrix which refuses fluid flow in the region is referred to as impermeable.

2.1.2 Saturation and Relative Permeability

In literature, ([5, 27, 28] to list few) effective saturation has been used for parametrization purpose. The effective saturation can be defined mathematically as

$$\Theta = \frac{w_c - w_c^{\text{res}}}{w_c^{\max} - w_c^{\text{res}}},$$

where $w_c = \phi S_w$ is water content and S_w is water saturation which is the ratio of water volume to void volume.

In multi-phase flow, the pore space is filled with more than one fluid; in this case there is a blocking of path ways and space of one by another. This property of fluid leads to relative permeabilities which is taken to be an empirical function of the wetting phase saturation (water saturation in our case) and assumed to be direction independent. Decrease in saturation of one phase results in a decreased permeability of the phase. This decreased permeability is called effective permeability of the phase and is expressed as the ability of the reservoir rock to transmit a fluid as related to its ability to transmit another fluid in the same circumstance [27, 28]. Mathematically:

$$K_{\text{eff}} = KK_{r\alpha}.$$

In the system of multi-phase flow, the sum of relative permeabilities is always less than or equal to 1. That is,

$$\sum_{\alpha} K_{r\alpha} \leq 1.$$

2.1.3 Capillary Force and Inter-facial Tension

On molecular level adhesive forces attract fluid molecules to the solid surface and cohesive force attracts molecules of a fluid to another fluid. At the fluid-fluid interface these forces are not at equilibrium leading to a kind of curved interface and this interface is well defined if the fluids in the reservoir are immiscible [19]. Since the cohesion between fluid molecules at one side of the interface is different from that of the other side, the interface is characterized by some surface energy (*surface tension* for liquid-gas fluids and *interfacial tension* for liquid-liquid fluids), which is a measure of the forces that must be overcome to change its shape. One consequence of the existence of the surface/interfacial tension is the difference in the equilibrium fluids pressures separated by a curved interface, due to unbalanced tangential forces at the dividing surface. The pressure drop across the interface is denoted in this context as the capillary pressure which is connected with interfacial tension and the mean curvature radius r_c by Laplace equation:

$$P_c = \frac{2\sigma_{ow}}{r_c}$$

where σ_{ow} is oil-water IFT force. From Laplace equation, we can observe that the capillary force is higher in magnitude for smaller void space. In other words, the wetting phase will retreat to smaller pores during drainage process of saturated medium. Based on this, macroscopic capillary force increases while the wetting

phase saturation decrease in REV. This capillary force usually parameterized as an algebraic function of water saturation [1, 28] which relates the pressure difference of the two fluids, thus,

$$P_c(S_w) = P_o - P_w,$$

where $P_c \geq 0$ around the interface. The interaction with the cohesive/adhesive forces leads to a specific

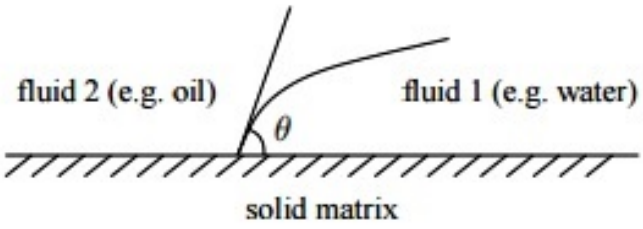

Figure 2.1.1: Contact angle From [7]

contact angle θ, between the solid surface and fluid-fluid interface which depends on the properties of fluids. Most of the time, a fluid has been classified as a wetting phase fluid when the contact angle $\theta \leq 90^o$ and the other treated as non-wetting fluid [1, 19]. In Figure 2.1.1, one can consider the water as a wetting fluid and oil as non-wetting fluid.

2.2 EOR: Enhanced Oil Recovery

The world's energy consumption has risen tremendously since 1930's for which fossil fuel such as oil has been used as a primary source of energy to meet the rising demand. As a result, Enhanced Oil Recovery (EOR) methods are used in the oil industry to increase the ultimate recovery of crude oil after primary and secondary productions. The residual oil is retained in the pore space due to viscous and capillary forces commonly influenced by interfacial tension, wettability and permeability. EOR is aimed to alter these parameters in beneficial ways [29–31, 63].

Mobility ratio and capillary number have been used in analysis of the expected oil production from the application of different EOR mechanisms. In [33] the mobility ratio is given by,

$$M = \frac{\lambda_D}{\lambda_d},$$

where λ_D and λ_d are mobilities of the displacing and displaced fluids respectively. The case $M < 1$ tells us the mobility of the displacing fluid is smaller than that of the displaced fluid which implies that the displaced fluid can be mobilized. On the other hand, the Capillary number N_c, is defined as (see [34])

$$N_c = \frac{\mu q}{\sigma},$$

where q is Darcy velocity, μ is the viscosity of displacing fluid and σ is fluid-fluid interfacial tension. A low interfacial tension σ, results in weak capillary forces which is of great importance for displacement and gives high N_c. In other word, high N_c lowers the residual oil saturation.

In the following subsequent Sections, we will review well known EOR techniques being used to recover the residual oil from subsurface and can be categorized as physicochemical and biological approaches.

2.2.1 Physicochemical Methods

In this subsection most commonly used physical and chemical EOR are discussed. Though there are several EOR technologies which have been known to recover the residual oil, we have mentioned few of them in this study. The type of EOR method that used for a specific reservoir mainly depends on the properties of the reservoir and fluid.

For instance, thermal EOR methods are generally applicable to heavy, viscous crude reservoirs [29]. The method introduces heat energy to the reservoir through steam flooding, steam stimulation, and in-situ combustion. The increase in heat reduces the surface tension, increases the permeability of the oil and improves the reservoir seepage conditions [35]. The heated oil may also vaporise and then condense, forming improved oil. This approach however, requires substantial investment in special equipment. Due to the heat effect on the reservoir, this method may cause severe damage to the underground well structure as well as it may pose safety risks in the larger production process and as a consequence, the method is not widely used, though it contributes approximately 2 million oil barrels per day [29].

Chemical EOR methods lived their best times in 1980s and most of them are applicable in sandstone reservoirs [30]. This method is still applied in China these days as a main EOR technique. Injection of various chemicals, usually as dilute solutions, have been used to aid mobility and the reduction of surface/interfacial tension. Chemical processes includes surfactant-polymer injection, and caustic flooding. Polymer flooding improves the vertical and real sweep efficiency as a consequence of improving the water/oil mobility ratio [36]. On the other hand, caustic flooding will result in the production of soap that may lower the IFT enough to increase production if the oil reservoir has naturally occurring organic acids [36]. However, this type of chemical reaction would take place in a poor reservoir so it will also produce oil pollution and the capacity for water absorption would be damaged. Most wells cannot achieve a satisfactory result using this method, making it counterproductive, with the negative effects outweighing the benefits. For instance, this method faces significant challenges in light oil reservoirs. One of the reasons is the availability, or lack of, compatible chemicals in high temperature and high salinity environments [29].

Gas flooding such as miscible hydrocarbon displacement, carbon dioxide injection, and inert gas injection have been the most widely used recovery methods of light, condensate and volatile oil reservoirs [30]. The main idea is to use a miscible gas that reduces the IFT between water and oil, hence improving the displacement of oil in deep, high-pressure. It is believed that in light oil reservoirs, N_2 flooding can reach miscible conditions. However, immiscible N_2 injection has also been used for pressure maintenance, cycling of condensate reservoirs, and as a drive gas for miscible slugs [31]. In general, gas injection is an EOR method most frequently applied in carbonate formations when compared to chemical and thermal EOR methods.

All methods discussed above involve the injection of large amounts of rather expensive fluids into oil bearing

reservoir formations. Moreover, the methods are task challenging since most of them involves a significant change in the reservoir condition and others even cause a permanent damage to the reservoir.

2.2.2 Biological Methods

The challenge to increase oil recovery from reservoirs is a driving force behind the efforts to come up with alternative recovery processes like microbial EOR which is the interest of this study. Microbial EOR was fist proposed by Beckman in 1926 [37], and it has done a little work up to 1940s. Afterwards, ZoBell in 1947 described and patented processes by which bacterial products such as gases, acids, solvents, surface-active agents, and cell biomass, release oil from sandpack columns in laboratory tests [37]. Since, 1950s works came out with great advances of looking at how microbes can benefit the recovery of oil from petroleum reservoir and many of the laboratory studies have been promising. However, the occurrence of biological, chemical, and physical processes in the reservoir are not fully understood. As consequence, results from field applications are oscillating between success and failure [8, 38].

In most cases, microbial EOR methods have been applied in either *in situ/tradational* or *ex situ* processes. The *in situ* is done based on the production of bio-products by either injection of specially selected microbes (i.e., microbes that are capable of living and breading in harsh reservoir environment) with appropriate nutrients into the reservoir or stimulating indigenous microbes through nutrient injection. If the reservoir environment is favorable for exogenous microbes, then it is of great importance in which the concerned body might be free to choose the right microbe to hit his/her own interest in the processes, but microbe transportation is not an easy task in addition to computation of nutrition with indigenous microbes. Lazare *et al* [37], reported the basic nature and existence of indigenous microbes in oil reservoir. This motivates injection of nutrients to the reservoir in order to stimulate the indigenous microbes. But, the existing indigenous microbes may not give the desired outcome. Moreover, the sulphate reducing bacteria may overgrow due to the injection of nutrients, which are a source of hydrogen sulfide, H_2S [8]. The alternative approach is introduction of *ex situ* produced bio-products [39, 40] into the reservoir. This is done where the reservoir environment is not suitable for exogenous microbes and the existence as well as functionality of bio-products from indigenous microbes are in question. Though it is the simplest and well accepted in field scale operations [8, 41], cost of bio-reactor operations and purification push it to the bottom corner [8, 38].

In general, microbial EOR process aims to get bio-products (like, surfactant and polymers to name few) which have an important role in altering the properties of the reservoir and leads to a significant improvement in oil recovery in several ways such as reduction of IFT and viscosity of oil-water phases to list few (See Table 2.1, to get a summarized products of microbes and their effects on the system [8, 37–41]). One of the crucial activity of microbes in oil reservoir is their ability of stickiness to all surfaces leads to clogging/plugging for which the flow divert to another direction, helps to displace immobilized oils [8, 37, 38, 41].

Both an indigenous and exogenous micro-organisms are subject to physical (i.e., temperature, pressure, pore size), chemical (like acidity, salinity and oxidation potential) and biological (i.e., growth, decay, and

Bio-products	Surfactant	polymers	Gases	Biomass	Solvents	Acid
Effects	Interfacial tension reduction and Emulsification	Mobility Control and plugging	Reservoir pressurization and Viscosity Reduction	Altering wettability and reduction of oil viscosity	Oil dissolving	degradation of rock and reduction of oil viscosity

Table 2.1: Bio-products of microbes and their effects

attachement/detachement) factors. Besides these factors the survival of microbes originates from their ability to form spore which can resist high temperature and acidity. Moreover, micro-organisms are complex in their way of responding to the surrounding environment. The cells change physiological state to have maximum chances of survival which may lead to the change in substrate consumption, growth, and metabolite production significantly.

2.2.2.1 Physical and Chemical Challenge of Microbial EOR Processes

Microbes may be able to grow and function well up to 100°C [42]. However, oil reservoir temperature may rise up to 150°C, which can disrupt the microbe's enzyme function due to denaturation around the catalyzing sites. In addition to temperature, reservoir pressure also has its own effect on growth and activities of microbes [15, 42]. Though, we use the general term microbe in previous Sections, bacterium are mainly applied when we come to microbial oil recovery due to their small size. However, Bacillus strain rod measures 6 μm which might be in the same order of magnitude as pore size. In 2008 Marshal [42] reported that bacteria penetration through the reservoir is guaranteed for pore diameter of 6-10 μm, but it must be above 2 μm. If this is not the case, microbes may not be transported to the target zone. Even if we assume that the pore spaces are relatively large, losses of injectivity may occur due to well-bore plugging. According to Magot *et al.,* [15], a reservoir with high pressure allows gases to mix with fluids for which the reservoir may have strong acidic components. In [15], it is reported that the acidity determines microbial surface charge which affects the transport of microbes as well. Moreover, transport of bacteria influenced by its physiology. For instance, a bacteria with hydrophobic surface tends to stick together and transported in flocs, whereas the hydrophilic bacteria often get suspended and transported alone along with the fluid [11].

Though the fundamental mechanisms of controlling microbial transport, growth and deposition are well understood in laboratory experiments, the results are often not directly relevant to processes occurring in subsurface and engineered systems [16]. The inherent physical, chemical and biological heterogeneity of these systems presents a highly complex environment to mimic [16].

2.3 Literature Review on Multi-phase Flow and Transport Models

The study of fluid dynamics in porous media dates back to 1850s. Multiple fluids flow in geological reservoir encounter many fluid and rock properties that could influence the motion of fluids. Due to the absence of uniformity in factors that determine the flow, the corresponding mathematical models that govern the flow always results in non-linear and possibly discontinuous form of partial differential equations. People have been using conservation laws and Darcy's law to model multi-phase flow in porous media followed by manipulation and combination of those balance equations into modified forms, with concomitant introduction of ancillary functions that we will refer to as the fractional flow such as, global pressure [1, 7, 9, 14, 19, 20, 43–46], and average pressure formulation [1, 5, 25, 47]. The global pressure or total velocity approach treats the multi-phase flow problem as a total fluid flow of a single mixed fluid, and then describes the individual phases as fractions of the total flow whereas the average pressure formulation considers the average of the two pressures and the wetting phase saturation as primary variables, but it introduces the capillary pressure as a function of wetting saturation in pressure as well as saturation equation. These mathematical models have been used to forecast fluid distributions in porous reservoir. Moreover, there might be components that could be transported along with fluids which are not considered in the above mathematical settings. These components (if any) might potentially affect the flow behaviour significantly.

According to [16, 17], there have been considerable ongoing efforts aimed at understanding the transport, deposition behavior, growth of microbes in porous media and their effect on oil recovery since 1920s. Since then, mathematical models have been developed and used to simulate the activities and propagations of microbes in porous reservoir, for example [17, 21, 23, 24, 48]. Reactive convective-dispersive transport equations usually coupled with microbial aspects such as net growth, nutrient consumption and metabolite production processes, see Section 3.2. To the best of author's knowledge, previous studies didn't address all of the consequences of microbial growth. For instance, clogging, wettability alteration, nutrient and metabolite adsorption and salinity effect on mobility of phase are not properly investigated.

Multi-phase fluids flow models should be coupled with component transport models to simulate the effect of microbes on the distribution of fluids and reservoir. For instance, reduction of IFT and viscosity reduction mechanisms are reported in [4, 5, 11, 17, 25] to investigate the effect of microbial activities on residual oil. The resulting coupled equations (flow equations and transport equations) have been used to simulate microbial EOR processes.

Since the governing equations for microbial EOR processes are highly nonlinear and complex, efficient numerical and stable schemes have to be employed to forecast an approximate information about the physical phenomenon within the reservoir. In 1962, Peaceman *et al.,* [10] presented a finite-difference method for predicting oil displacement and they noticed that the proposed method suffers instability when applied to immiscible, multi-phase flow in porous media. According to Kukreti *et al.,*, [18] finite element method was introduced by Lewis and his co-authors in 1974 to treat two-phase immiscible flow in porous medium. On-

wards, considerable developments have been established on finite element methods for multi-phase flow in porous media (for example, see [18, 49]) but, each approach has its own limitation when we come to stability. Kumar *et al.,* [50] in 2013 have reported a convergence result on a mixed finite element discretization for up-scaled reactive flows in porous medium. The convergence results are discussed by considering a semi-discrete form (discrete in time and continuous weak variational form in space) and fully discrete form in separate sheet. Moreover, they have presented an illustrative example of a numerical convergence result of the method as well. In [51] a theoretical convergence analysis and error estimation for finite element discretization of precipitation-dissolution transport equations in porous medium has been discussed in the same fashion as [50]. In general, a unifying and concrete documentation of finite element methods for general elliptic as well as transient problems can be found in [1, 52–54].

Both the finite difference and finite element methods are unable to meet the local conservative property. For this reason finite volume methods have got an attention for numerical simulation of various types of conservation laws for which the flux is of importance [12, 19, 55–57]. Apart from finite difference, both finite element and finite volume methods are suited for heterogeneous media [56]. Besides, we refer to see [14] for a conservative mixed finite element discretization for two-phase flow in porous medium.

On the other hand, temporal discretization has become a topic of great interest in academia and industry. In hydrology applications, researches (for instance, [19, 20]) have been using fully implicit schemes predominantly. However, it doesn't mean that fully implicit scheme is designed only for hydrology applications. For instance, [4] have applied implicit scheme to simulate microbial transport in oil reservoir.

The petroleum engineering literature contrasts with the hydrology literature with the predominant approach being explicit or semi-implicit and IMPES (implicit pressure, explicit saturation) scheme has been frequently used in most applications [1, 43, 57]. This scheme has been favored because it decouples the pressure and saturation equations, thus reducing the computational effort required for their solution. However, it exhibits unacceptable oscillatory solutions unless one can control the time step appropriately and there is no convergence theory on the title. On the other hand, the fully implicit method is unconditionally stable but it converges locally and is computationally expensive. We recommend to see [58] for a comparison study between implicit and IMPES methods.

Development of a robust iterative methods for two phase flow in porous media got attention in recent years. For example, Radu *et al.,* [12] have proposed an iterative linearization method for a finite volume based discretization of two-phase flow models. Moreover, they have shown that the proposed method converges at leat linearly. A survey of iterative methods (Newton, Picard, and L–method) for Rechards' equation has been done in [13]. In the paper it is shown that the mixed methods (i.e., Newton/Picard, L/Newton) are robust but first order. On the other side, the Newton method is quadratic convergent. But, locally convergent and even failure of Newton's method can occur (See the example in [13]). A convergent analysis for three of the methods is also discussed and convergence of L–method is verified.

Chapter 3

Flow and Transport Models

This chapter discusses about the development of mathematical models that govern multiple fluids flow and component concentrations transport in subsurface porous media. The combination of these dynamic models have been used to simulate microbial EOR mechanisms. In this thesis, we have adopted an average/mean-value pressure formulation and thus, average pressure, wetting phase saturation and component concentrations are dependent variables of interest in microbial EOR simulation.

3.1 Two-phase Flow Reservoir Modeling

The continuum approach has been assumed to be a valid approximation for physical processes in subsurface, when the mean free path length of fluid molecules is much smaller than the physical domain of interest, i.e., the length of the void space [19]. However, this study considers a macroscopic level model, where each point in the continuum is assigned average values over elementary volumes of quantities on the microscopic level. This approach does not need exact description of the microscopic configuration (like a mathematical modeling approach at microscopic level) [7], rather only measurable statistical properties of the porous medium and fluids are required. Further we assume that the diameter of the void space must be small enough, so that the fluid flow is controlled by adhesive forces at fluid solid interface and cohesive forces at fluid-fluid interface which separates cases like a network of pipes from the definitions of a porous medium [3, 19].

Since a French Engineer Henry Darcy developed a relationship between the fluid velocity relative to the solid and the pressure head gradient, flow in porous media has been extensively studied [1, 5, 9, 12, 13, 18–20, 43, 45, 46, 50, 51]. In this Section we try to come up with a mathematical model which describes the flow of multiple fluids in porous reservoir. To save time and space, we do not attempt to derive Darcy's differential equation and transport of fluids in porous media starting from ground level, rather, we reviewed these equations and get used of them for the required purpose. Moreover, we consider a two-phase flow in which the effect of gravity is negligible. Considering the above assumptions, multi-phase flow in porous

medium could be described in deferential form as an extension of Darcy's law for single phase flow which could be read as follows

$$q_\alpha = -\frac{K_{r\alpha}K}{\mu_\alpha}\nabla P_\alpha \qquad \text{in } \Omega, \tag{3.1.1}$$

where Ω is a porous domain, $\alpha = \{o, w\}$, K [m^2] is absolute permeability, $K_{r\alpha}$ [-] is relative permeability of phase α, P_α [Pa] is pressure of phase α and q_α [$m.s^{-1}$] stands for Darcy's velocity of fluid α and μ_α [Pa.s] is viscosity of phase α.

The Darcy's equation (3.1.1) must be supplemented with phase mass balance equation,

$$\phi\rho_\alpha\frac{\partial S_\alpha}{\partial t} + \nabla\cdot(\rho_\alpha q_\alpha) = F_\alpha \qquad \text{in } \Omega \tag{3.1.2}$$

where ϕ [-] is porosity, S_α [-] is saturation of phase α, ρ_α [Kg/m^3] is density of fluid α and F_α stands for source or sink term. To simplify things in equation (3.1.2), we assume incompressible flow and the pore volume is filled with only two fluids, thus,

$$\sum_\alpha S_\alpha = 1. \tag{3.1.3}$$

The pressure difference at the interface of phases commonly related with the static capillary pressure as in equation (3.1.4)

$$P_o - P_w = P_c(S_w), \tag{3.1.4}$$

where, the indices o and w stands for oil and water phases respectively. However, there are assumptions in which the two fluids may not reach equilibrium [45, 59, 61] and interested reader can see the references there in. Nevertheless, combining the above four equations (3.1.1)–(3.1.4) with appropriate boundary and initial conditions describe multi-phase flow in porous media and read as

$$\begin{cases} \phi\frac{\partial(\rho_\alpha S_\alpha)}{\partial t} + \nabla\cdot(\rho_\alpha u_\alpha) = F_\alpha & \text{in } \Omega, \\ q_\alpha = -\frac{K_{r\alpha}K}{\mu_\alpha}\nabla P_\alpha & \text{in } \Omega, \\ \sum_\alpha S_\alpha = 1, & \\ P_o - P_w = P_c(S_w), & \\ \text{Boundar Conditions} & \text{on } \partial\Omega, \\ \text{Initial Conditions} & \text{in } \Omega, \end{cases} \tag{3.1.5}$$

where $\partial\Omega$ is the boundary of a porous domain, Ω. The system of equations in (3.1.5) can be rewritten as phase flow equations in the following way

$$\begin{cases} \phi\frac{\partial S_o}{\partial t} + \nabla\cdot(-\frac{K_{ro}K}{\mu_o}\nabla P_o) = \frac{F_o}{\rho_o} & \text{in } \Omega, \\ \phi\frac{\partial S_w}{\partial t} + \nabla\cdot(-\frac{K_{rw}K}{\mu_w}\nabla P_w) = \frac{F_w}{\rho_w} & \text{in } \Omega, \\ S_w = 1 - S_o, & \\ P_o - P_w = P_c(S_w), & \\ \text{Boundar Conditions} & \text{on } \partial\Omega, \\ \text{Initial Conditions} & \text{in } \Omega. \end{cases} \tag{3.1.6}$$

We add the phase equations in (3.1.6) to eliminate the nonwetting/oil saturation term to yield,

$$\begin{cases} -\nabla \cdot K(\frac{K_{ro}}{\mu_o}\nabla P_o + \frac{K_{rw}}{\mu_w}\nabla P_w) = \frac{F_o}{\rho_o} + \frac{F_w}{\rho} & \text{in } \Omega \\ \phi\frac{\partial S_w}{\partial t} + \nabla \cdot (-\frac{K_{rw}K}{\mu_w}\nabla P_w) = \frac{F_w}{\rho_w} & \text{in } \Omega, \\ P_o - P_w = P_c(S_w), & \\ \text{Boundary Conditions} & \text{on } \partial\Omega, \\ \text{Initial Conditions} & \text{in } \Omega. \end{cases} \tag{3.1.7}$$

To know how the pressure and saturation behaves, we can couple or decouple the first two equations in the system above (3.1.7) as alternative formulation. In order to couple the system, researchers have been using different pressure formulations, among these global pressure and mean-value formulations are commonly used as reviewed in section 2.3. In this investigation, we will use mean-value pressure formulation.

3.1.1 Mean-value Formulation

The mean-value formulation considers the average of the two fluid pressures and is written as

$$P_{\text{av}} = \frac{1}{2}(P_o + P_w). \tag{3.1.8}$$

Combining equation (3.1.4) and (3.1.8) gives the following relations

$$\begin{cases} P_o = P_{\text{av}} + \frac{1}{2}P_c(S_w), \\ P_w = P_{\text{av}} - \frac{1}{2}P_c(S_w). \end{cases} \tag{3.1.9}$$

Now we can substitute (3.1.9) into (3.1.7) to obtain the following fully coupled pressure-saturation equation, which describes the flow of two fluids

$$\begin{cases} -\nabla \cdot K(\lambda_t \nabla P_{\text{av}} + \frac{1}{2}\lambda_d \nabla P_c(S_w)) = F_t & \text{in } \Omega, \\ \phi\frac{\partial S_w}{\partial t} - \nabla \cdot (\lambda_w \nabla(P_{\text{av}} - \frac{1}{2}P_c(S_w))) = \frac{F_w}{\rho_w} & \text{in } \Omega, \\ \text{Boundary Conditions} & \text{on } \partial\Omega, \\ \text{Initial Conditions} & \text{in } \Omega. \end{cases} \tag{3.1.10}$$

where F_t stands for total source/sink term, $\lambda_t = \frac{K_{ro}}{\mu_o} + \frac{K_{rw}}{\mu_w}$ is commonly named as total mobility, whereas $\lambda_d = \frac{K_{ro}}{\mu_o} - \frac{K_{rw}}{\mu_w}$ and $\lambda_w = \frac{K_{rw}}{\mu_w}$. In the case of microbial EOR simulation by bio-clogging mechanism, the change in porosity and absolute permeability should be taken into account in the flow equation (3.1.10).

Dirichlet and Neuman type boundary conditions are the two commonly arising boundary conditions of flow and transport in porous media, which are described in the following subsections.

3.1.1.1 Boundary and Initial Conditions

A two phase flow mathematical model developed so far is not complete unless necessary boundary and initial conditions are specified. The two commonly used boundary condition are the Dirichlet and Neumann

boundary conditions. In this case, the first type will give unique solution whereas the later type will give us a unique solution upto constant unless it is supported by initial conditions. To impose the boundary conditions in the system (3.1.10), we denote $\partial\Omega$ for the external boundary of the porous medium domain, Ω, under consideration. When the average pressure and water phase saturation are specified as a known function of position, the boundary condition reads,

$$\begin{cases} P_{\text{av}} = g_1(x,y) \text{ on } \partial\Omega, & \frac{\partial P_{\text{av}}}{\partial \vec{\text{n}}} = h_1(x,y) \text{ on } \partial\Omega, \\ S_w = g_2(x,y) \text{ on } \partial\Omega, & \frac{\partial S_w}{\partial \vec{\text{n}}} = h_2(x,y) \text{ on } \partial\Omega, \end{cases} \tag{3.1.11}$$

where $\vec{\text{n}}$ stands for a unit normal vector pointing outward to the boundary.

Incorporating the boundary conditions (3.1.11) and appropriate initial reservoir information into system (3.1.10) would give complete multi-phase flow problem. The resulting two-phase flow problem is non-linear and very difficult to give qualitative profile. However, one can solve them using non-linear solvers/iterative linearization schemes once discretization in space and temporal variables are done, see chapter 4.

3.2 Reactive Transport Models

Transport of micro-organisms, nutrients and metabolites/bio-surfactant through porous media governs many phenomena in subsurface system. In porous medium, microorganisms may be found suspended in water phase or attached to the porous skeleton. In this thesis, we assume the density of the microorganism is less than that of water and hence sedimentation of micro-organisms is negligible. In EOR, the term microorganisms are used frequently, however, we only consider one family of bacteria for this particular study. Moreover, we assume the nutrients and metabolites are not adsorbed by the solid body. The three components in water and/or oil phase (if any) are subjected to convective-dispersive transport due to fluids motion [17, 21, 22, 48, 60] and generally described as follows,

$$\sum_j \frac{\partial \phi S_j C_{ij}}{\partial t} + \sum_j \nabla \cdot (q_j C_{ij} - \phi \nabla (D_i S_j C_{ij})) = Q_i + R_i, \quad \text{in } \Omega \tag{3.2.1}$$

where S_j is saturation of phase j, C_{ij} is concentration of component i in phase j, D_i dispersion coefficient for component i, q_j is velocity of phase j, Q_i and R_i stand for source/sink and reaction term for component i respectively.

The reservoir comprises the pore volume, ϕ and the porous matrix $(1-\phi)$. We assume the pore volume consists of three phases, namely, water, oil and biofilm. In most papers, the bio-film saturation is denoted by σ, but we replace it by ψ to ignore the confusion with IFT. In [24] the concentration of bacteria in biofilm was modelled as conservation of mass in separate equation. On the other hand, [22, 23] have applied one of an empirical approach, Langmuir isotherm partitioning expression [62] which introduces the maximum adsorption capacity of the surface in homogeneous aquifer. To simplify things, we assume the biofilm consists of only the attached bacteria and the bacteria can only be adsorbed from the water phase to enter the biofilm. Thus, we assume that the water phase concentration of bacteria determines the amount of bacteria attached

to the pore walls and can be stated as follows,

$$a_b = \frac{L_1 C_{\max} C_{bw}}{1 + L_2 C_{bw}}, \tag{3.2.2}$$

where a_b [Kg/m^2] is the mass of bacteria adsorbed per unit area, L_1 and L_2 are Langmuir constants related to the bonding energy, $C_{\max}$ is the maximum adsorbed concentration when all active surface sites are occupied.

It is clear that the amount of bacteria that adsorbed depends on the pore wall area available. The contact area between pore walls and the water phase is assumed to reflect the area available for adsorption and thus the efficient surface area S_{area} is the specific surface area scaled with the water phase saturation, which can be described mathematically as,

$$S_{\text{area}} = \frac{\tilde{S}}{\phi} \frac{S_w}{S_W^{max}}, \tag{3.2.3}$$

where $\tilde{S}$ is the ratio of surface area to volume of porous rock which ranges between $10^5 - 10^6$ m^2/m^3 [15].

Combining (3.2.2) and (3.2.3) gives the amount of bacteria adsorbing to the pore walls as a function of water phase concentration of bacteria,

$$\psi \rho_b = S_{\text{area}} \cdot a_b, \tag{3.2.4}$$

where $\psi \rho_b$ is the concentration of adsorbed bacteria and C_{bw} is the concentration of suspended bacteria after apparent equilibrium has been reached. It shows that the slope of the increasing part of the curve equals $S_{\max} L_1$ and that the curve finally reaches $S_{\max}$. When $L_2 C_{bw} < 1$, the Langmuir equation may be linearized to obtain a linear relationship:

$$\psi \rho_b = S_{\text{area}} L_1 C_{bw}. \tag{3.2.5}$$

The bio-film formation behavior of microbes leads to a porosity change, which is usually measured as

$$\phi = \phi_0 - \psi,$$

where ϕ_0 describes an initial porosity distribution of a reservoir. This porosity change usually results in a reduction of absolute permeability, and related as follows

$$K = K_0 \left(\frac{\phi}{\phi_0} \right)^c$$

where c is a real scalar constant and K_0 is initial rock permeability.

One can insert the developments above into the flow as well as transport equations in appropriate way to consider a bio-clogging mechanism for microbial EOR processes.

3.2.1 Relation Between Growth, Consumption and Production

Though the Monod expression is empirical regarding with microbial growth, it has been used widely to describe the relation between the bacterial growth rate and substrate [4, 16, 17, 21–23, 48]. And thus, the Monod type growth rate for one limiting substrate is given as

$$G_b = G_{\max} \frac{C_s}{K_s + C_s}, \tag{3.2.6}$$

where K_s is half-saturation constant, $G_{\max}$ maximum growth rate, and C_s is the limiting substrate concentration in the water phase. In practice, bacterial decay occurs, but we assume, that the growth rate covers the net growth rate.

If we further assume the growth inhibition does not occur, the corresponding reaction/source term R_b is expressed as

$$R_b = Y_{sb} G_b C_b, \tag{3.2.7}$$

where Y_{sb} is the yield of bacteria on substrate.

It is convenient to assume that metabolite/bio-surfactant production occurs in both the planktonic (unattached) and sessile (attached) phases of bacteria. An empirical equation is used to calculate metabolite production rate as growth rate of bacteria. The source term for metabolite equation can be stated as

$$R_m = Y_{sm} C_b G_b. \tag{3.2.8}$$

As can be seen above microbial growth and metabolite production are granted by substrates consumption which is given by

$$R_s = -R_b - R_m. \tag{3.2.9}$$

In other words, equation (3.2.9) describes the reaction term after the injected substrate contributed to the growth of bacteria and production of bio-surfactant.

We recommend to see [21, 22, 48] in order to have more insight into the empirical relations discussed above. These relations could be incorporated into the convective-dispersive transport equation (3.2.1) to describe the microbial EOR processes, at least partly.

Chapter 4

Numerical Modeling

Dynamical system of equations like the governing equations developed for multi-phase flow and transport models so far are challenging to address by qualitative approaches. As a consequence, numerical techniques have been used frequently to obtain approximate information, though most of these equations have their solutions in the infinite dimensional horizon. For instance, people from applied mathematics, control science and engineering basically have been using the three numerical methods namely, finite difference (for example, [4, 6, 10, 11, 55]), finite/control volume (see, [5, 6, 12, 25, 55]) and finite element (see, [1, 13, 18, 47, 49–54]) to obtain approximate solution for partial differential equations (PDEs) arising from practical problems. Among these we adapt the finite volume method to have an approximate information for two-phase flow and component transport equations in this particular study. The method of finite volume subdivides the spatial domain into small pieces but finite control volumes. For 2D two-phase flow problems, the control volumes can be figured out by setting finite points in the domain followed by connecting them through non-intersecting strait lines. Then one can possibly choose the center of the control volume as grid/node points and the approach is called cell-centred finite volume. As can be seen in Figure 4.0.1, the discretization in this thesis is established on structured rectangular mesh in space as well as time. Basically, the cell-centered finite volume associates the unknowns with the center of the control volume. For non-complex geometrise, structured grids are computationally efficient and accurate than unstructured grids. Moreover, for the same number of grid points, structured meshes require less memory to store than unstructured meshes, because of the simpler connectivity.

4.1 Midpoint Rule and Temporal Discretization

If we use the end points of the sub-intervals in either x or y direction to approximate the integral, we run the risk that the values at the end points do not accurately represent the average value of the function on the control volume. A point which is more likely to be close to the average would be the midpoint of each control volume. Consider a function f defined on a 2D domain. The 2D midpoint rule begins by dividing the

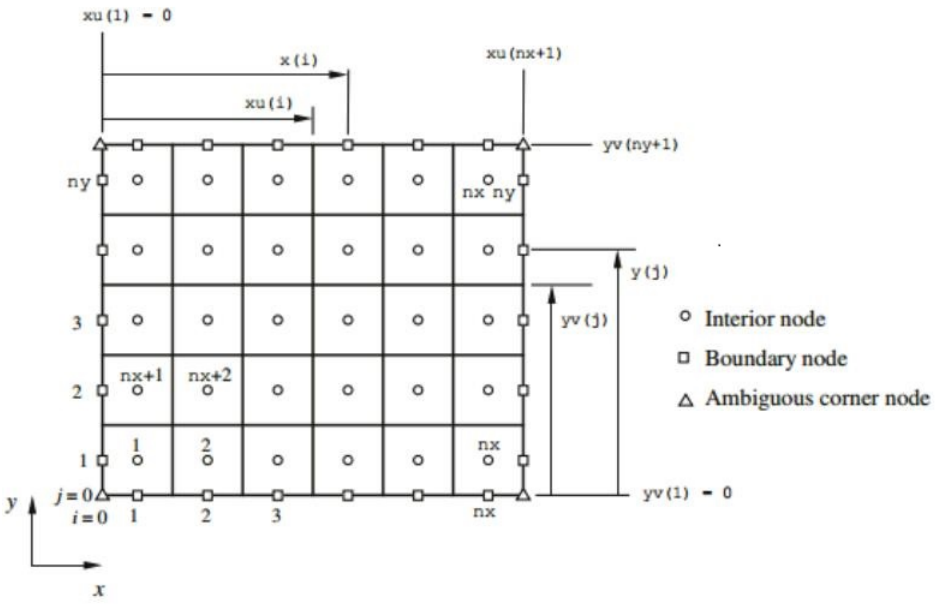

Figure 4.0.1: Cell-centered finite volume regular mesh

given region into a set of little rectangular sub-domains (control volume), each with length x and width y as in Figure 4.0.1. The approximate integral of f over each control volume $\Omega_i = [x_{i-\frac{1}{2}}, x_{i+\frac{1}{2}}] \times [y_{i-\frac{1}{2}}, y_{i+\frac{1}{2}}]$, using the help of midpoint rule is given by;

$$\int_{\Omega_i} f dA = f(\circ) \triangle x \triangle y$$

In this thesis, we use *forward* and *backward* Euler method for temporal discretization of saturation and concentration equations respectively. The forward Euler method approximates the given system of ODE explicitly at the current time step $n+1$ as follows

$$y^{n+1} = y^n + tf(t_n, y^n),$$

where t is the step length. On the other hand, the backward Euler method reads as,

$$y^{n+1} = y^n + tf(t_{n+1}, y^{n+1}),$$

where t is the step size for time discretization. Both backward as well as forward Euler methods converge linearly.

The explicit approach controls the time step to ensure convergence of the method. This is not the case for fully implicit methods, but the accuracy of the solution is of course depending on the magnitude of the time step.

4.2 Multi-point Flux Approximation (MPFA)

Since we are using a cell-center finite volume method with quadrilateral grids, it can be seen that there are four fluxes entering/leaving the approximate equation over each control volume, see Figure 4.2.1. The method constructs an expression for the pressure gradient using linear approximations inside the control volume and also uses two entities, the control volume and an interaction region for calculating the fluxes.

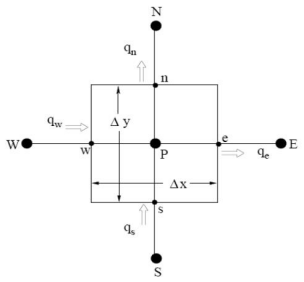

Figure 4.2.1: Cell-center finite volume discretization.

Consider the following Poison equation:

$$-\nabla \cdot (K(x,y)\nabla P) = f(x,y), \tag{4.2.1}$$

where $K(x,y)$ and $f(x,y)$ are absolute permeability and source term respectively.

Let $q = -K\nabla P$, then equation (4.2.1) can be rewritten as,

$$\nabla \cdot q = f(x,y). \tag{4.2.2}$$

Since we are dealing with two dimensional domain of interest, equation(4.2.2) can be restated as;

$$\frac{\partial q_x}{\partial x} + \frac{\partial q_y}{\partial y} = f(x,y), \tag{4.2.3}$$

where q_x and q_y stand for Darcy's velocities along the x and y directions respectively.

Now let us define the control volume $\Omega_k = [x_{i-\frac{1}{2}}, x_{i+\frac{1}{2}}] \times [y_{j-\frac{1}{2}}, y_{j+\frac{1}{2}}]$ $k = 1, 2, \cdots, \mathrm{nx}^2$, and the points (x_i, y_j) for $i, j = 1, 2, \ldots, \mathrm{nx}$ being node points which are the center points of the control volumes. Further, the walls/boundaries of a control volume on the east and the west are given by $\mathrm{E} = x_{i-\frac{1}{2}} \times [y_{j-\frac{1}{2}}, y_{j+\frac{1}{2}}]$ and $\mathrm{W} = x_{i+\frac{1}{2}} \times [y_{j-\frac{1}{2}}, y_{j-\frac{1}{2}}]$ respectively and similarly on the south and the north we have the walls $\mathrm{S} = [x_{i-\frac{1}{2}}, x_{i+\frac{1}{2}}] \times y_{j-\frac{1}{2}}$ and $\mathrm{N} = [x_{i-\frac{1}{2}}, x_{i+\frac{1}{2}}] \times y_{j+\frac{1}{2}}$ respectively. We can integrate equation (4.2.2) over each control volume as;

$$\int_{\Omega_k} \bigtriangledown \cdot q dA = \int_{\Omega_k} f(x,y) dA. \tag{4.2.4}$$

By using Gauss divergence theorem, the above volume integral equation (4.2.4) can be reformulated as follows,

$$\int_{\partial\Omega_k} q \cdot \vec{\mathrm{n}} dS = \int_{\Omega_k} f(x,y) dA, \tag{4.2.5}$$

where $\vec{\mathrm{n}}$ is a unit normal vector pointing outward to the boundary $\partial\Omega_k = \mathrm{E} \cup \mathrm{W} \cup \mathrm{S} \cup \mathrm{N}$. Thus, equation (4.2.5) can be rewritten as linear combination of surface integrals as follows;

$$\int_{\mathrm{E}} q \cdot [-1,0] dS + \int_{\mathrm{W}} q \cdot [1,0] dS + \int_{\mathrm{S}} q \cdot [0,-1] dS + \int_{\mathrm{N}} q \cdot [0,1] dS = \int_{\Omega_k} f(x,y) dA \tag{4.2.6}$$

Now equation (4.2.6) can be approximated by midpoint rule to give

$$[q_x(x_{i+\frac{1}{2}}, y_j) - q_x(x_{i-\frac{1}{2}}, y_j)] \triangle y + [q_y(x_i, y_{j+\frac{1}{2}}) - q_y(x_i, y_{j-\frac{1}{2}})] \triangle x = f(x_i, y_j) \triangle y \triangle x. \tag{4.2.7}$$

But, we know that $q = -K\nabla P$, which implies $q_x = -K\frac{\partial P}{\partial x}$ and $q_y = -K\frac{\partial P}{\partial y}$. We used these relations to approximate the fluxes at the boundary of the control volume provided that the fluxes are continuous across the volume. Thus, we have

$$\frac{q_x}{K} = -\frac{\partial P}{\partial x} \quad \text{and} \quad \frac{q_y}{K} = -\frac{\partial P}{\partial y}. \tag{4.2.8}$$

Now let us integrate equation (4.2.8) from x_i to x_{i+1} and y_j to y_{j+1} respectively to approximate $q_x(x_{i+\frac{1}{2}}, y_j)$ and $q_y(x_i, y_{j+\frac{1}{2}})$;

$$\int_{x_i}^{x_{i+1}} \frac{q_x}{K} dx = \int_{x_i}^{x_{i+1}} -\frac{\partial P}{\partial x} dx \quad \text{and} \quad , \int_{y_i}^{y_{i+1}} \frac{q_y}{K} = \int_{y_i}^{y_{i+1}} -\frac{\partial P}{\partial y}. \tag{4.2.9}$$

Since the fluxes q_x and q_y are constants with respect to x and y respectively inside control volumes, integration of equation (4.2.9) can give the following expression

$$\begin{aligned} q_x(x_{i+\frac{1}{2}}, y) \int_{x_i}^{x_{i+1}} \frac{1}{K(x,y)} dx &= -[P(x_{i+1}, y) - P(x_i, y)], \\ q_y(x, y_{j+\frac{1}{2}}) \int_{y_j}^{y_{j+1}} \frac{1}{K(x,y)} dy &= -[P(x, y_{j+1} - P(x, y_j)]. \end{aligned} \tag{4.2.10}$$

To have the fluxes as a pressure difference, we need to approximate $\int_{x_i}^{x_{i+1}} \frac{1}{K(x,y)} dx$. Since, we are integrating over two neighbouring cells/control volumes, it can be rewritten as follows;

$$\int_{x_i}^{x_{i+1}} \frac{1}{K(x,y)} dx = \int_{x_i}^{x_{i+\frac{1}{2}}} \frac{1}{K(x,y)} dx + \int_{x_{i+\frac{1}{2}}}^{x_{i+1}} \frac{1}{K(x,y)} dx. \tag{4.2.11}$$

Now let us assume that the absolute permeability is constant in a specific control volume. Then, we can introduce the following notion;

$$\begin{cases} \frac{1}{K(x_i, y_j)} = 2\frac{\int_{x_i}^{x_{i+\frac{1}{2}}} \frac{1}{K(x,y)} dx}{\triangle x}, \\ \frac{1}{K(x_{i+1}, y_j)} = 2\frac{\int_{x_{i+\frac{1}{2}}}^{x_{i+1}} \frac{1}{K(x,y)} dx}{\triangle x}. \end{cases} \tag{4.2.12}$$

Substitute the results in (4.2.12) into equation (4.2.11) to approximate the integral as;

$$\int_{x_i}^{x_{i+1}} \frac{1}{K(x,y)} dx = \frac{\triangle x}{2K(x_i, y_j)} + \frac{\triangle x}{2K(x_{i+1}, y_j)}. \tag{4.2.13}$$

Similarly, we have,

$$\int_{y_j}^{y_{j+1}} \frac{1}{K(x,y)} dy = \frac{\triangle y}{2K(x_i, y_j)} + \frac{\triangle y}{2K(x_i, y_{j+1})}. \tag{4.2.14}$$

The approximate values (4.2.13) and (4.2.14) can be substituted into equation (4.2.10) to approximate the flux at boundaries of the control volume as follows

$$\begin{cases} q_x(x_{i+\frac{1}{2}}, y_j) = -\frac{[P(x_{i+1},y_j)-P(x_i,y_j)]}{\frac{\triangle x}{2K(x_i,y_j)}+\frac{\triangle x}{2K(x_{i+1},y_j)}} \\ q_y(x_i, y_{j+\frac{1}{2}}) = -\frac{[P(x_i,y_{j+1})-P(x_i,y_j)]}{\frac{\triangle y}{2K(x_i,y_j)}+\frac{\triangle y}{2K(x_i,y_{j+1})}} \end{cases} \tag{4.2.15}$$

Which then can be substituted into equation (4.2.7) to obtain:

$$\begin{aligned} &[-\frac{[P(x_{i+1}, y_j) - P(x_i, y_j)]}{\frac{\triangle x}{2K(x_i,y_j)} + \frac{\triangle x}{2K(x_{i+1},y_j)}} - (-\frac{[P(x_i, y_j) - P(x_{i-1}, y_j)]}{\frac{\triangle x}{2K(x_i,y_j)} + \frac{\triangle x}{2K(x_{i-1},y_j)}}] \triangle y), \\ &+[-\frac{[P(x_i, y_{j+1}) - P(x_i, y_j)]}{\frac{\triangle y}{2K(x_i,y_j)} + \frac{\triangle y}{2K(x_i,y_{j+1})}} - (-\frac{[P(x_i, y_j) - P(x_i, y_{j-1})]}{\frac{\triangle y}{2K(x_i,y_j)} + \frac{\triangle y}{2K(x_i,y_{j-1})}}] \triangle x = f(x_i, y_j) \triangle y \triangle x. \end{aligned} \tag{4.2.16}$$

In this thesis, we consider a uniform mesh (equidistant grid; $\triangle x_i = \triangle y_j$). Now let us set

$$a_{i,j} = \frac{1}{(\frac{1}{2K(x_i,y_j)} + \frac{1}{2K(x_{i-1},y_j)})} \text{ and } \alpha_{i,j} = \frac{1}{\frac{1}{2K(x_i,y_j)} + \frac{1}{2K(x_i,y_{j-1})}}, \tag{4.2.17}$$

in equation (4.2.16) to get:

$$\begin{aligned} &-a_{i+1,j}[P(x_{i+1}, y_j) - P(x_i, y_j)] + a_{i,j}[P(x_i, y_j) - P(x_{i-1}, y_j)], \\ &-\alpha_{i,j+1}[P(x_i, y_{j+1}) - P(x_i, y_j)] + \alpha_{i,j}[P(x_i, y_j) - P(x_i, y_{j-1})] = f(x_i, y_j)\triangle x^2. \end{aligned} \tag{4.2.18}$$

Thus, we have a system of nx^2 linear equations with $(\mathrm{nx}+2)^2 - 4$ unknown. In order to obtain a unique solution, we need to impose boundary conditions in the discrete system. Since this study considers only the two commonly used boundary conditions, we will discretize these boundary conditions in the following Subsection.

4.2.1 Discretization of Boundary Conditions

Though it is known that finite volume methods are promising and simple to implement, imposing boundary conditions into the discrete system (4.2.18) is not an easy task. In particular, the Dirichlet boundary condition is difficult for cell-centered finite volume method, whereas the Neumann boundary condition is also challenging for vertex centered finite volume approach. In following subsequent sections, we will see the treatment of discrete boundary unknowns with the boundary values such as: Dirichlet and Neumann boundary values.

4.2.1.1 Dirichlet Boundary Condition

The Dirichlet boundary condition has been imposed on the discrete system by adding ghost cells at the most exterior boundaries of the domain. Let us do this for 1D and it is straightforward for 2D problem.

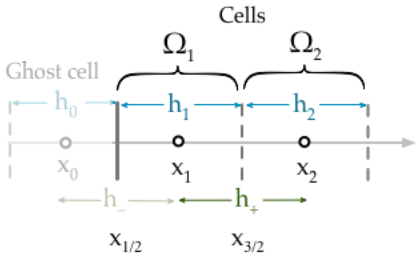

Figure 4.2.2: 1D cell-centered finite volume Discretization for boundary conditions.

Consider the following 1D mesh, Figure 4.2.2. Now let us see how to impose the Dirichlet boundary condition $P|_{x_{\frac{1}{2}}} = g$ on the discrete equation;

$$-\frac{P(x_2) - P(x_1)}{\triangle x} + \frac{P(x_1) - P(x_0)}{\triangle x} = f(x_1)\triangle x. \tag{4.2.19}$$

Note that equation (4.2.19) is a finite volume approximation of $\frac{\partial^2 P}{\partial x^2} = f(x)$ in Ω_1 and $P(x_0)$ is indeed out of the domain and ultimately we need to discard this term from the equation. Let us define the linear interpolation from the centre of cell Ω_0 to the centre of cell Ω_1. Conveniently this line passes through $x_{\frac{1}{2}}$, so this is how the Dirichlet conditions enter into the system of discrete equations, and since we are using a uniform mesh discretization approach, the interpolation could be given by,

$$g(x_{\frac{1}{2}}) = \frac{P(x_0) + P(x_1)}{2}. \tag{4.2.20}$$

Rearranging equation (4.2.20) will give us $P(x_0) = 2g(x_{\frac{1}{2}}) - P(x_1)$ and one can substitute this relation into equation (4.2.19) to obtain

$$-\frac{P(x_2) - P(x_1)}{\triangle} + \frac{P(x_1) - (2g(x_{\frac{1}{2}}) - P(x_1))}{\triangle} = \triangle x f(x_1). \tag{4.2.21}$$

The above discretized equation (4.2.21) can be further simplified to give

$$-\frac{P(x_2)}{\triangle x} + \frac{3P(x_1)}{\triangle x} = f(x_1)\triangle x + \frac{2g(x_{\frac{1}{2}})}{\triangle x}. \tag{4.2.22}$$

The above discussion incorporates the left Dirichlet boundary condition into the system. The right hand side Dirichlet boundary condition can also be imposed in similar fashion as discussed above and will yield

$$-\frac{P(x_{n-1})}{\triangle x} + \frac{3P(x_n)}{\triangle x} = f(x_n)\triangle x + \frac{2g(x_{n+\frac{1}{2}})}{\triangle x}. \tag{4.2.23}$$

Equations (4.2.22) and (4.2.23) can work fine for any fixed value y_j which helps to impose the left and right Dirichelet boundary condition into the discrete system for 2D problem and can be stated as follows

$$\begin{cases} -\frac{P(x_2,y_j)}{\triangle x} + \frac{3P(x_1,y_j)}{\triangle x} = hf(x_1,y_j) + \frac{2g(x_{\frac{1}{2}},y_j)}{\triangle x}, \\ -\frac{P(x_{n-1},y_j)}{\triangle x} + \frac{3P(x_n,y_j)}{\triangle x} = f(x_n,y_j)\triangle x + \frac{2g(x_{n+\frac{1}{2}},y_j)}{\triangle x} \end{cases} \tag{4.2.24}$$

Similarly, the south and north boundary conditions can be incorporated into the system as above without additional effort and can be given as

$$\begin{cases} -\frac{P(x_i,y_2)}{\triangle x} + \frac{3P(x_i,y_1)}{\triangle x} = f(x_i,y_1)\triangle x + \frac{2g(x_i,y_{\frac{1}{2}})}{\triangle x}, \\ -\frac{P(x_i,y_{n-1})}{\triangle x} + \frac{3P(x_i,y_n)}{\triangle x} = f(x_i,y_n)\triangle x + \frac{2g(x_i,y_{n+\frac{1}{2}})}{\triangle x}. \end{cases} \tag{4.2.25}$$

Equation (4.2.24) and (4.2.25) can be possibly incorporated into the discrete system (4.2.18) to give the complete system of equations. A technique discussed above is a higher order boundary condition discretization. Besides, Thomas [55] suggested first order simple approach to handle Dirichlet boundary condition which simply assigns the Dirichlet boundary values to the most exterior boundary unknowns as follows

$$\begin{cases} P(x_0, y_j) = P(x_{\frac{1}{1}}, y_j), \ P(x_{n+1}, y_j) = P(x_{n+\frac{1}{2}}, y_j) \\ P(x_i, y_0) = P(x_i, y_{\frac{1}{2}}), \ P(x_i, y_{n+1}) = P(x_i, y_{n+\frac{1}{2}}) \end{cases},$$

and this study employs this technique, to simplify the computational complexity.

4.2.1.2 Neumann Boundary Condition

Without loss of generality let us consider homogeneous Neumann boundary condition, i.e., no flux boundary condition, which can be described mathematically as follows

$$q \cdot \vec{\mathrm{n}} \quad = \quad 0. \tag{4.2.26}$$

In rectangular 2D domain, equation (4.2.26) can be rewritten as

$$\begin{cases} \frac{\partial K(x_{\frac{1}{2}}, y) P_{\mathrm{av}}(x_{\frac{1}{2}}, y)}{\partial y} = 0, & \frac{\partial K(x_{n+\frac{1}{2}}, y) P_{\mathrm{av}}(x_{n+\frac{1}{2}}, y)}{\partial y} = 0, \\ \frac{\partial K(x, y_{\frac{1}{2}}) P_{\mathrm{av}}(x, y_{\frac{1}{2}})}{\partial x} = 0, & \frac{\partial K(x, y_{n+\frac{1}{2}}) P_{\mathrm{av}}(x, y_{n+\frac{1}{2}})}{\partial y} = 0. \end{cases} \tag{4.2.27}$$

Setting the permeabilities at the ghost cells as

$$\begin{cases} K(x_0, y) = K(x_1, y), \ K(x_n, y) = K(x_{n+1}, y) \\ K(x, y_0) = K(x, y_1), \ K(x, y_n) = K(x, y_{n+1}) \end{cases},$$

which can be discarded from equation (4.2.27), and discretizing each of equations in (4.2.27) using central finite difference yields,

$$\begin{cases} P_{\mathrm{av}}(x_1, y) = P_{\mathrm{av}}(x_0, y) \text{ and } P_{\mathrm{av}}(x_{n+1}, y) = P_{\mathrm{av}}(x_n, y), \\ P_{\mathrm{av}}(x, y_1) = P_{\mathrm{av}}(x, y_0) \text{ and } P_{\mathrm{av}}(x, y_n) = P_{\mathrm{av}}(x, y_{n+1}). \end{cases} \tag{4.2.28}$$

Substituting the above expression (4.2.28) into the system of linear equations (4.2.18) to give a complete discretization of conservation equation with Neumann boundary conditions.

4.2.2 Finite volume Discretization of Flow Problem

In Chapter 3, a mathematical model for two phase flow with average pressure formulation is discussed. In this Section we will discretize the pressure and saturation equations one by one in separate sheet using previously discussed cell-centered finite volume method as a tool. For instance, one can discretize the pressure gradients in the same way as discussed in Section 4.2 and the saturation equation is discretized in the same way in space and applying Euler forward method for temporal discretization.

4.2.2.1 Pressure Equation

The pressure equation can be recalled from equation (3.1.10) as

$$-\nabla \cdot K(\lambda_t \nabla P_{\text{av}} + \frac{1}{2}\lambda_d \nabla P_c(S_w) = F_t. \tag{4.2.29}$$

The cell-centered flux approximation could be used to discretize equation (4.2.29) as discussed in Section 4.2 over the control volume Ω_k as follows

$$-\int_{\Omega_k} \nabla \cdot (K\lambda_t \nabla P_{\text{av}})dA - \frac{1}{2}\int_{\Omega_k} \nabla \cdot (K\lambda_d \nabla P_c(S_w))dA = \int_{\Omega_k} F_t dA. \tag{4.2.30}$$

Here again the Gauss-divergence theorem can be applied to equation (4.2.30) to obtain

$$-\int_{\partial\Omega_k} (K\lambda_t \nabla P_{\text{av}}) \cdot \vec{\text{n}}dA - \frac{1}{2}\int_{\partial\Omega_k} (K\lambda_d \nabla P_c(S_w)) \cdot \vec{\text{n}}dA = \int_{\Omega_k} F_t dA. \tag{4.2.31}$$

Let us make a notations on differences to have a readable presentation as follows

$$\begin{cases} \Delta_x^+ \chi = \chi(i+1,j) - \chi(i,j) \\ \Delta_x^- \chi = \chi(i,j) - \chi(i-1,j) \end{cases}$$

and similarly we can have the differences in y direction as follows

$$\begin{cases} \Delta_y^+ \chi = \chi(i,j+1) - \chi(i,j) \\ \Delta_x^- \chi = \chi(i,j) - \chi(i,j-1) \end{cases}$$

where χ can be the average pressure, saturation or capillary pressure. As we have discussed above, the mid-point rule and a kind of central difference approach is employed in equation (4.2.31) to obtain the following discrete approximation

$$\begin{aligned} &-(K_{i+\frac{1}{2},j}\lambda_t(S^{n+1}_{i+\frac{1}{2},j})\Delta_x^+ P^{n+1}_{\text{av}} - K_{i-\frac{1}{2},j}\lambda_t(S^{n+1}_{i-\frac{1}{2},j})\Delta_x^- P^{n+1}_{\text{av}}) \\ &-(K_{i,j+\frac{1}{2}}\lambda_t(S^{n+1}_{i,j+\frac{1}{2}})\Delta_y^+ P^{n+1}_{\text{av}} - K_{i,j-\frac{1}{2}}\lambda_t(S^{n+1}_{i,j-\frac{1}{2}})\Delta_y^- P^{n+1}_{\text{av}}) \\ &= \frac{1}{2}(K_{i+\frac{1}{2},j}\lambda_d(S^{n+1}_{i+\frac{1}{2},j})\Delta_x^+ P_c^{n+1} - K_{i-\frac{1}{2},j}\lambda_d(S^{n+1}_{i-\frac{1}{2},j})\Delta_x^- P_c^{n+1}) \\ &\quad +\frac{1}{2}(K_{i,j+\frac{1}{2}}\lambda_d(S^{n+1}_{i,j+\frac{1}{2}})\Delta_y^+ P_c^{n+1} - K_{i,j-\frac{1}{2}}\lambda_d(S^{n+1}_{i,j-\frac{1}{2}})\Delta_y^- P_c^{n+1}) + F_t(i,j)\Delta x^2, \end{aligned} \tag{4.2.32}$$

where $S = S_w$ is used throughout this chapter to make the presentation clear and readable.

Here again the number of unknowns are greater than that of the number of equations. To have a unique solution for the above system of algebraic equation (4.2.32), one can impose boundary conditions and move them to the right hand side of the equation. Moreover, the permeability of the medium, K, at the boundaries $(i+\frac{1}{2},j)$ and $(i,j+\frac{1}{2})$ is approximated by harmonically averaging over two adjacent control volumes as discussed in Section 4.2 which can be recalled as

$$K(i+\frac{1}{2},j) = \frac{1}{\frac{1}{2}(\frac{\Delta x_i}{K(i,j)} + \frac{\Delta x_{i+1}}{K(i+1,j)})} \text{ and } K(i,j+\frac{1}{2}) = \frac{1}{\frac{1}{2}(\frac{\Delta y_i}{K(i,j)} + \frac{\Delta y_{i+1}}{K(i,j+1)})} \text{ respectively.}$$

However, since this thesis is restricted to uniform grid, the above relations can be simplified to give

$$K(i+\frac{1}{2},j) = \frac{1}{\frac{\triangle x}{2}(\frac{1}{K(i,j)} + \frac{1}{K(i+1,j)})} \text{ and } K(i,j+\frac{1}{2}) = \frac{1}{\frac{\triangle y}{2}(\frac{1}{K(i,j)} + \frac{1}{K(i,j+1)})}.$$

The relative permeabilities at the boundaries of a control volume have been approximated by taking an arithmetic average over the two adjacent control volumes which can be stated mathematically as follows

$$\begin{cases} \lambda_t(S_{i+\frac{1}{2},j}) = \frac{\lambda_t(S_{i+1,j})+\lambda_t(S_{i,j})}{2} \\ \lambda_t(S_{i,j+\frac{1}{2}}) = \frac{\lambda_t(S_{i,j+1})+\lambda_t(S_{i,j})}{2}. \end{cases} \tag{4.2.33}$$

However, arithmetic averaging has not been applied in most cases because of its instability condition. As a result, it is much popular to employ an upstream approximation which could be stated as,

$$\lambda_t(S_{i+\frac{1}{2},j}) = \begin{cases} \lambda_t(S_{i+1,j}) & \text{if } P_{\text{av}}(i,j) < P_{\text{av}}(i+1,j) \\ \lambda_t(S_{i,j}) & \text{if } P_{\text{av}}(i,j) \geq P_{\text{av}}(i+1,j) \end{cases} \tag{4.2.34}$$

and

$$\lambda_t(S_{i,j+\frac{1}{2}}) = \begin{cases} \lambda_t(S_{i,j+1}) & \text{if } P_{\text{av}}(i,j) < P_{\text{av}}(i,j+1) \\ \lambda_t(S_{i,j}) & \text{if } P_{\text{av}}(i,j) \geq P_{\text{av}}(i,j+1) \end{cases} \tag{4.2.35}$$

The arithmetic averaging approach is quite simple to implement and employed into the flux equations. On the other hand, the upstreaming approach can be implemented by determining the direction of flow by choosing the upstream cell for the calculations of relative permeabilities, which is a physical property that moves with the flow [55, 57]. Pressure based upstream weighting scheme is easy to implement as well. However, it violates the important flux continuity property across the interfaces between control volumes [57].

Since we are applying an iterative semi-implicit scheme, the mobilities and capillary pressure in equation (4.2.32) are calculated from the previous time step saturation, whereas the average pressure is calculated at the current time step. Thus, equation (4.2.32) can be rewritten as follows

$$\begin{aligned} &-(K_{i+\frac{1}{2},j}\lambda_t(S^{n+1,k}_{i+\frac{1}{2},j})\Delta_x^+ P^{n+1,k+1}_{\text{av}} - K_{i-\frac{1}{2},j}\lambda_t(S^{n+1,k}_{i-\frac{1}{2},j})\Delta_x^- P^{n+1,k+1}_{\text{av}}) \\ &-(K_{i,j+\frac{1}{2}}\lambda_t(S^{n+1,k}_{i,j+\frac{1}{2}})\Delta_y^+ P^{n+1,k+1}_{\text{av}} - K_{i,j-\frac{1}{2}}\lambda_t(S^{n+1}_{i,j-\frac{1}{2}})\Delta_y^- P^{n+1,k+1}_{\text{av}}) \\ &= \frac{1}{2}(K_{i+\frac{1}{2},j}\lambda_d(S^{n+1,k}_{i+\frac{1}{2},j})\Delta_x^+ P_c^{n+1,k} - K_{i-\frac{1}{2},j}\lambda_d(S^{n+1,k}_{i-\frac{1}{2},j})\Delta_x^- P_c^{n+1,k}) \\ &\quad +\frac{1}{2}(K_{i,j+\frac{1}{2}}\lambda_d(S^{n+1,k}_{i,j+\frac{1}{2}})\Delta_y^+ P_c^{n+1,k} - K_{i,j-\frac{1}{2}}\lambda_d(S^{n+1,k}_{i,j-\frac{1}{2}})\Delta_y^- P_c^{n+1,k}) + F_t(i,j)\Delta x^2, \end{aligned} \tag{4.2.36}$$

where k is the inner loop index. Equation (4.2.36) can be linearized and solved for the average pressure by assuming the value of $S^{n+1,k}$ is known.

4.2.2.2 The Saturation Equation

The approach used to discretize the average pressure equation in subsubsection 4.2.2.1 can be used directly to discretize the saturation equation in space for which it can be reduced to an ODE,

$$\phi\frac{\partial S}{\partial t} = \nabla\cdot(\lambda_w\nabla(P_{\text{av}} - \frac{1}{2}P_c)) + \frac{f_w}{\rho_w}. \tag{4.2.37}$$

Now we can discretize equation (4.2.37) in time using explicit/forward-Euler method to have;

$$\phi\frac{S^{n+1}-S^n}{\triangle t} - \nabla\cdot(\lambda_w^{n+1}\nabla(P^{n+1}_{\text{av}} - \frac{1}{2}P_c^{n+1})) = \frac{f_w^n}{\rho_w}, \tag{4.2.38}$$

where S^n, is previous time step saturation of water, λ_w^n, and P_c^n are water relative permeability and the capillary pressure at current time step respectively whereas S^{n+1} and P_{av}^{n+1} stand for current saturation and average pressure values respectively.

A cell-centered finite volume approach can be applied once more to discretize equation (4.2.38) in spatial variables which then can be given as

$$\begin{aligned}
\frac{\phi S^{n+1}-S^n}{\triangle t}\Delta x^2 &= K_{i+\frac{1}{2},j}\lambda_t(S^{n+1}_{i+\frac{1}{2},j})\Delta_x^+ P_{\text{av}}^{n+1} \\
-K_{i-\frac{1}{2},j}\lambda_t(S^{n+1}_{i-\frac{1}{2},j})\Delta_x^- P_{\text{av}}^{n+1} &+ K_{i,j+\frac{1}{2}}\lambda_t(S^{n+1}_{i,j+\frac{1}{2}})\Delta_y^+ P_{\text{av}}^{n+1} \\
-K_{i,j-\frac{1}{2}}\lambda_t(S^{n+1}_{i,j-\frac{1}{2}})\Delta_y^- P_{\text{av}}^{n+1} &- \frac{1}{2}K_{i+\frac{1}{2},j}\lambda_d(S^{n+1}_{i+\frac{1}{2},j})\Delta_x^+ P_c^n \\
+K_{i-\frac{1}{2},j}\lambda_d(S^{n+1}_{i,j-\frac{1}{2}})\Delta_x^+ P_c^{n+1} &- \frac{1}{2}K_{i,j+\frac{1}{2}}\lambda_d(S^{n+1}_{i,j+\frac{1}{2}})\Delta_y^+ P_c^{n+1} \\
&+K_{i,j-\frac{1}{2}}\lambda_d(S^{n+1}_{i,j-\frac{1}{2}})\Delta_y^- P_c^{n+1}) + F_t(i,j)\Delta x^2.
\end{aligned} \tag{4.2.39}$$

The discretized version of the water phase saturation equation (4.2.39) can be modeled in semi-implicit way by introducing an inner loop index k as we did for an average pressure equation,

$$\begin{aligned}
\phi\frac{S^{n+1,k+1}-S^{n+1,k}}{\triangle t}\Delta x^2 &= K_{i+\frac{1}{2},j}\lambda_t(S^{n+1,k}_{i+\frac{1}{2},j})\Delta_x^+ P_{\text{av}}^{n+1,k+1} \\
-K_{i-\frac{1}{2},j}\lambda_t(S^{n+1,k}_{i-\frac{1}{2},j})\Delta_x^- P_{\text{av}}^{n+1,k+1} &+ K_{i,j+\frac{1}{2}}\lambda_t(S^{n+1,k}_{i,j+\frac{1}{2}})\Delta_y^+ P_{\text{av}}^{n+1,k+1} \\
-K_{i,j-\frac{1}{2}}\lambda_t(S^{n+1,k}_{i,j-\frac{1}{2}})\Delta_y^- P_{\text{av}}^{n+1,k+1} &- \frac{1}{2}K_{i+\frac{1}{2},j}\lambda_d(S^{n+1,k}_{i+\frac{1}{2},j})\Delta_x^+ P_c^{n+1,k} \\
+K_{i-\frac{1}{2},j}\lambda_d(S^{n+1,k}_{i,j-\frac{1}{2}})\Delta_x^- P_c^{n+1,k} &- \frac{1}{2}K_{i,j+\frac{1}{2}}\lambda_d(S^{n+1,k}_{i,j+\frac{1}{2}})\Delta_y^- P_c^{n+1,k} \\
&+K_{i,j-\frac{1}{2}}\lambda_d(S^{n+1,k}_{i,j-\frac{1}{2}})\Delta_y^- P_c^{n+1,k}) + F_t(i,j)\Delta x^2.
\end{aligned} \tag{4.2.40}$$

The combination of the above discretized equations (4.2.36) and (4.2.40) with appropriate boundary and initial conditions are enough to have an approximate solution for two-phase incompressible and immiscible flow models. However, since the part of this thesis is aimed to have a simulation for microbial EOR process, we need to have a numerical model for component transport equations and the following discussion is devoted to this subject.

4.2.3 Finite Volume Discretization for Transport Equation

Once we obtained the solutions for average pressure and water phase saturation at the new time step, we can proceed to compute the microbial concentration C, using backward Euler method for temporal variables followed by control volume discretization in spatial variables. Though we have developed a general multi-component transport model in section 3.2, it is convenient to deal with single component transport equation for discretization purpose and the same procedure can be employed to other components. Let us consider only the microbial component which can have an expression of the form,

$$\phi\frac{\partial(SC)}{\partial t} + \nabla\cdot(q_w C - D\nabla(\phi SC)) = Q, \tag{4.2.41}$$

where S is water saturation, ϕ is porosity D is dispersion coefficient and Q stands for reaction/source or sink term.

An implicit Euler method is used to approximate the temporal derivative in equation (4.2.41) to give

$$\phi\frac{S^{n+1}C^{n+1}-S^nC^n}{\Delta t}+\nabla\cdot(q_wC^{n+1}-D\nabla(\phi S^{n+1}C^{n+1}))=Q^n. \tag{4.2.42}$$

Similarly, we can apply a control volume method to discretize equation (4.2.42) in space which could be started with integrating it over a control volume Ω_k as

$$\int_{\Omega_k}\phi\frac{S^{n+1}C^{n+1}-S^nC^n}{\Delta t}dA+\int_{\Omega_k}\nabla\cdot(q_wC^{n+1}-D\nabla(\phi S^{n+1}C^{n+1}))dA+\int_{\Omega_k}Q^ndA=0. \tag{4.2.43}$$

Applying the Gauss-divergence theorem will give us,

$$\int_{\Omega_k}\phi\frac{S^{n+1}C^{n+1}-S^nC^n}{\Delta t}dA+\int_{\partial\Omega_k}(q_wC^{n+1}-D\nabla(\phi S^{n+1}C^{n+1}))\cdot\overrightarrow{n}dS=\int_{\Omega_k}Q^ndA. \tag{4.2.44}$$

The integral equation (4.2.44), can be approximated by employing the midpoint rule (see section 4.2) to obtain

$$\begin{aligned}&\phi\frac{S^{n+1}_{i,j}C^{n+1}_{i,j}-S^n_{i,j}C^n_{i,j}}{\Delta t}\Delta x^2+\\&(-D\frac{\partial(\phi S^{n+1}C^{n+1})}{\partial x}+q_wC^{n+1})_{i+\frac{1}{2},j}\Delta y-(q_wC^{n+1}-D\frac{\partial(\phi S^{n+1}C^{n+1})}{\partial x})_{i-\frac{1}{2},j}\Delta y+\\&(u_wC^{n+1}-D\frac{\partial(\phi S^{n+1}C^{n+1})}{\partial y})_{i,j+\frac{1}{2}}\Delta x-(q_wC^{n+1}-D\frac{\partial(\phi S^{n+1}C^{n+1})}{\partial y})_{i,j-\frac{1}{2}}\Delta x=Q_{ij}\Delta x^2.\end{aligned} \tag{4.2.45}$$

Approximating the space derivatives in equation (4.2.45) by a central finite difference approach and averaging of bacteria concentration over the nodes of the adjacent control volumes for the convective term gives the following discrete system

$$\begin{aligned}\phi\frac{S^{n+1}_{ij}C^{n+1}_{ij}-S^n_{ij}C^n}{\Delta t}\Delta x^2+(q_{w,i+\frac{1}{2},j}&\frac{C^{n+1}_{i+1,j}+C^{n+1}_{i,j}}{2}-D\phi\frac{S^{n+1}_{i+1,j}C^{n+1}_{i+1,j}-S^{n+1}_{i,j}C^{n+1}_{i,j}}{\Delta x})\Delta y-\\(q_{w,i-\frac{1}{2},j}&\frac{C^{n+1}_{i,j}+C^{n+1}_{i-1,j}}{2}-D\phi\frac{S^{n+1}_{i,j}C^{n+1}_{i,j}-S^{n+1}_{i-1,j}C^{n+1}_{i-1,j}}{\Delta x})\Delta y+\\(q_{w,i,j+\frac{1}{2}}&\frac{C^{n+1}_{i,j+1}+C^{n+1}_{i,j}}{2}-D\phi\frac{S^{n+1}_{i,j+1}C^{n+1}_{i,j+1}-S^{n+1}_{i,j}C^{n+1}_{i,j}}{\Delta y})\Delta x-\\(u_{w,i,j-\frac{1}{2}}&\frac{C^{n+1}_{i,j}+C^{n+1}_{i,j-1}}{2}-D\phi\frac{S^{n+1}_{i,j}C^{n+1}_{i,j}-S^{n+1}_{i,j-1}C^{n+1}_{i,j-1}}{\partial y})\Delta x=Q_{ij}\Delta x^2.\end{aligned} \tag{4.2.46}$$

After some mathematical rearrangement, equation (4.2.46) can be rewritten as

$$\beta_{i-1,j}C^{n+1}_{i-1,j}+a_{i,j}C^{n+1}_{i,j}+\alpha_{i+1,j}C^{n+1}_{i+1,j}+\alpha_{i,j+1}C^{n+1}_{i,j+1}+\beta_{i,j-1}=f_{i,j}, \tag{4.2.47}$$

where $a_{i,j}=\phi S^{n+1}_{i,j}(\frac{\Delta x^2}{\Delta t}+4D)+\frac{\Delta y}{2}(q_w(S^{n+1}_{i+\frac{1}{2},j},C^n_{i-\frac{1}{2},j})-q_w(S^{n+1}_{i-\frac{1}{2},j},C^n_{i-\frac{1}{2},j}))+\frac{\Delta x}{2}(q_w(S^{n+1}_{i,j+\frac{1}{2}},C^n_{i-\frac{1}{2},j})-q_w(S^{n+1}_{i,j-\frac{1}{2}},C^n_{i-\frac{1}{2},j}))$, $\beta_{i-1,j}=-D\phi S^{n+1}_{i-1,j}-q_w(S^{n+1}_{i-\frac{1}{2},j},C^n_{i-\frac{1}{2},j})\frac{\Delta y}{2}$, $\alpha_{i+1,j}=q_w(S^{n+1}_{i+\frac{1}{2},j},C^n_{i+\frac{1}{2},j})\frac{\Delta y}{2}-D\phi S^{n+1}_{i+1,j}$, $\alpha_{i,j+1}=q_w(S^{n+1}_{i,j+\frac{1}{2}}C^n_{i,j+\frac{1}{2}})\frac{\Delta x}{2}-D\phi S^{n+1}_{i,j+1}$, and $\beta_{i,j-1}=-D\phi S^{n+1}_{i,j-1}-q_w(S^{n+1}_{i,j-\frac{1}{2}},C^n_{i,j-\frac{1}{2}})\frac{\Delta x}{2}$

One can introduce the inner loop index k, in equation (4.2.47) to linearize the flux at $C^{n+1,k}$ as we did for pressure and saturation equations. Moreover, we can impose given boundary conditions appropriately as

we did in Section 4.2.1. The resulting system of equations could be coupled with pressure and saturation equations (see chapter 6 for coupling processes of the flow and transport equation) and solved for the microbial concentration C^{n+1} at the new time step and can be ready to be used in the flow equation for the next time step.

Chapter 5

Numerical Results and Convergence Analysis

In Chapter 4, we have developed 2D cell-centered finite volume models from continuous two-phase flow and convictive-dispersive reactive transport models. This chapter aims to investigate the accuracy and convergence of the discretized flow and transport models to the corresponding continuous models. We have manufactured twice continuously differentiable analytical solutions to perform a validation test for our discretization scheme and Matlab code implementation of two-phase flow and advection-diffusion reactive transport equations.

5.1 Discrete L_2 Error Estimation

In order to validate our numerical model, as well as analyzing the numerical convergence of the method used to solve the model, we should compare the computed numerical solution with the analytical solution for different fluid parametrization and grid resolution of space and time. To compare the numerical solution with the analytical one, we require some form of measure for the difference between them, in the form of a norm. The simplest measure can be with respect to Euclidean norms, either $L_2(\Omega)$ or infinity norm, L_∞. For any square integrable function f, these norms are defined as

$$\|f\|_{L_2} = \left(\int_\Omega f^2\right)^{\frac{1}{2}} \tag{5.1.1}$$

and,

$$\|f\|_\infty = \max_\Omega |f|. \tag{5.1.2}$$

In our specific case f can be an average pressure P_{av}, water saturation, S_w or microbial concentration C. Thus, the distance between the numerical solution to the constructed analytical solution can be measured

in the same way as defined above and given by

$$E = \|f_{\text{an,j}} - f_{\text{nu,j}}\| = \left(\int_{\Omega} (f_{\text{an,j}} - f_{\text{nu,j}})^2 dA \right)^{\frac{1}{2}}, \tag{5.1.3}$$

where $f_{\text{an,j}}$ and $f_{\text{nu,j}}$ stand respectively for analytical and numerical solutions for $j = P_{\text{av}}, S_w, C$.

In the course of discretization of two phase flow and transport equations, we have divided the domain of interest Ω, (in this particular chapter we considered $\Omega = [0,1] \times [0,1]$ into sub-domains which we call cells/control volumes, and made an integration over each cell as seen in chapter 4. A similar thing has been done here, for which we arrive at

$$E^2 = \|f_{\text{an,j}} - f_{\text{nu,j}}\| = \left(\sum_i \int_{\Omega_i} (f_{\text{an,j}} - f_{\text{nu,j}})^2 dA \right)^{\frac{1}{2}}. \tag{5.1.4}$$

To determine the convergence order of numerical methods, the above square L_2 error E^2 can be related to the temporal step size as follows,

$$E^2 = k^2 (\triangle t)^{2p}, \tag{5.1.5}$$

where p is the convergence rate and k a real constant. Thus, the i-th and $(i+1)$-th error can be related to the rate of convergence as follows:

$$E_i^2 = k^2 (\triangle t)^{2p} \text{ and } E_{i+1}^2 = k^2 (\frac{\triangle t}{2})^{2p}. \tag{5.1.6}$$

Taking the quotient will give us the reduction of the error

$$\frac{E_i}{E_{i+1}} = \frac{k^2 (\triangle t)^{2P}}{k^2 (\frac{\triangle t}{2})^{2p}}. \tag{5.1.7}$$

Taking $\log_2$ both sides will give the rate of convergence p as follows,

$$p = \log_2 (\frac{E_i}{E_{i+1}}).$$

This relation is used to obtain rate of convergence in numerical methods. For example, we use it in the following subsequent test cases to validate our Matlab code implementation and to determine the convergence of numerical solutions to the exact solutions.

5.2 Matlab Code Implementation Validation for Different Fluid Parameterizations

In this section, we will see three different test case models defined on a rectangular domain, $\Omega = [0,1] \times [0,1]$ to validate and analyse the convergence of numerical solutions to exact solutions of two-phase flow problem. Moreover, we have discussed a validation test case for transport model. We have employed an iterative linearization method [12] on the discretized models of these test cases to conclude and analyse the convergence of the numerical models to the continuous models of flow equations. The flow as well as transport test case

models are designed by choosing possible solutions followed by constructing source terms and boundary conditions. To ease the construction of the source terms, we consider unit magnitude for rock as well as fluid parameters, (i.e., $\rho_w = \rho_o = \mu_w = \mu_o = \phi = K = 1$) throughout this chapter.

5.2.1 Linear Relative Permeabilities and Quadratic Capillary Pressure

It seems natural to consider a linear relative permeabilities and concave quadratic capillary pressure parameterizations as a constitutive relation for two-phase flow in porous media. If the water saturation is high, these parameterizations might give us high relative permeabilities and capillary force as compared to the well known parameterizations like van Genuchten parametrization. Nevertheless, these parameterizations are modeled as a function of the wetting phase saturation as follows,

$$\begin{cases} P_c(S_w) = 1 - S_w^2, \\ K_{ro}(S_w) = 1 - S_w, \\ K_{rw}(S_w) = S_w. \end{cases}$$

See Figure 5.2.1 for the curves of these parameterizations. One can easily observe that the capillary pressure

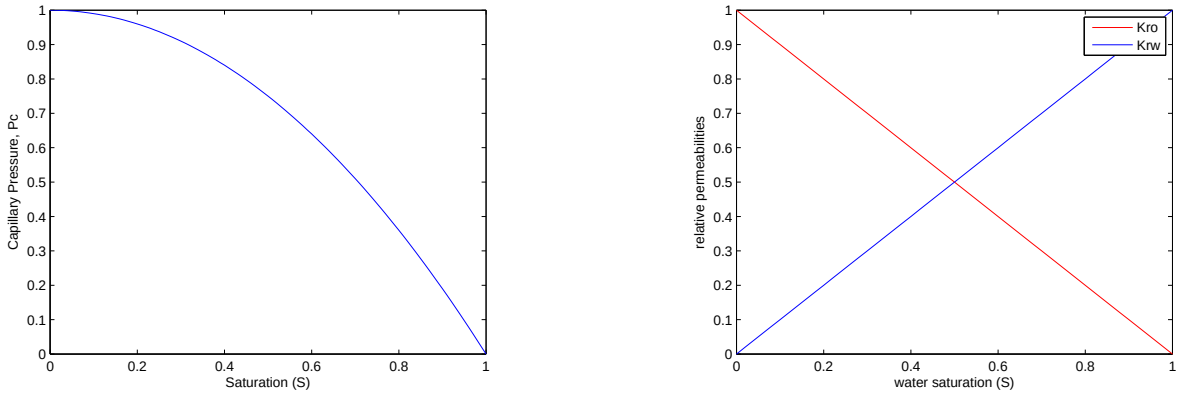

Figure 5.2.1: Concave Capillary Pressure (left) and phase relative permeabilities (right).

is monotonically decreasing as the water phase saturation increases. On the other hand, the relative permeability of water is directly proportional to the water phase saturation whereas the non-wetting phase relative permeability is inversely related with water phase saturation. Furthermore, $P_c(0) = K_{ro}(0) = K_{rw}(1) = 1$, and $P_c(1) = K_{ro}(1) = K_{rw}(0) = 0$. All of these properties make the above parametrization physically acceptable.

5.2.2 Van Genuchten Parameterizations

In the study of two phase flow in porous medium, the van Genuchten parametrization has been widely used to relate static capillary pressure and relative permeabilities to the wetting fluid saturation, see [1, 19, 28]. Since this study considers the water saturation as a wetting phase, relative permeabilities and capillary

pressure of the system are related with water phase saturation, and can be given as:

$$\begin{aligned} P_c(S_w) &= \left(S_w^{-\frac{1}{\mathrm{M}}} - 1\right)^{\frac{1}{\mathrm{N}}}, \\ K_{ro}(S_w) &= \sqrt{1-S_w}\left(1 - S_w^{\frac{1}{\mathrm{M}}}\right)^{2\mathrm{M}}, \\ K_{rw}(S_w) &= \sqrt{S_w}\left(1 - \left(1 - S_w^{\frac{1}{\mathrm{M}}}\right)^{\mathrm{M}}\right)^2, \end{aligned} \tag{5.2.1}$$

where M is pore volume distributions of the porous domain and can be related to N as $\mathrm{M} = \frac{1}{\mathrm{N}}$. Curves for the van Genuchten parameterizations are depicted in Figure 5.2.2. The capillary pressure and the non-wetting

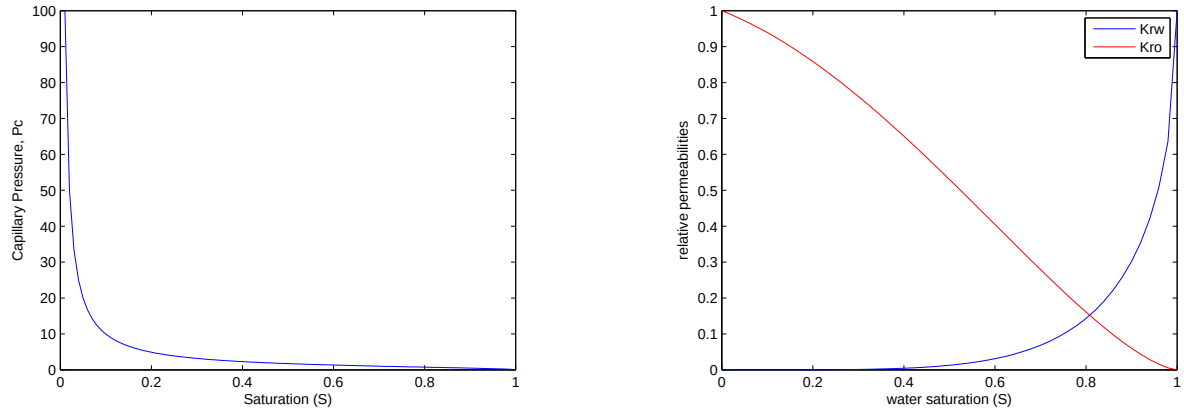

Figure 5.2.2: Capillary Pressure (left) and Relative permeabilities (right) of van Genuchten parametrization.

relative permeability are decreasing functions, while the wetting phase relative permeability increases as the wetting saturation increases.

5.2.3 Matlab Code Implementation Validation Test for two-phase Flow with Constant Mobilities and Quadratic Capillary Force

This test case is relatively simple and may not represent a realistic physical problem. It considers a concave capillary pressure and constant relative permeabilities for two-phase flow problem (3.1.10) with Dirichlet boundary condition. Now we recall equation (3.1.10) as follows

$$\begin{cases} -\nabla \cdot K(\lambda_t \nabla P_{\mathrm{av}} + \frac{1}{2}\lambda_d \nabla P_c(S_w)) = F_t \quad \text{in} \quad \Omega \\ \phi \frac{\partial(S_w)}{\partial t} - \nabla \cdot (\lambda_w \nabla P_{\mathrm{av}} - \frac{1}{2} P_c(S_w)) = \frac{F_w}{\rho_w} \quad \text{in} \quad \Omega \\ P_{\mathrm{av}} = P_0 \quad \text{on} \quad \partial\Omega \\ S_w = S_w^0 \quad \text{on} \quad \partial\Omega \end{cases} \tag{5.2.2}$$

where the right hand sides of the first two equations, F_t and F_w, can be constructed from the chosen analytical solutions for average pressure and saturation of water

$$\begin{cases} P_{\mathrm{av}} = x(1-x)y(1-y) \\ S_w = x(1-x)y(1-y) + 0.5 \end{cases} \tag{5.2.3}$$

In this test example, we consider $\lambda_t = 1$ and $\lambda_d = -\frac{1}{2}$ provided that $\lambda_n = \frac{1}{4}$ and $\lambda_w = \frac{3}{4}$. Thus, the flow equation can be reduced to

$$\begin{aligned} -\nabla \cdot K(\nabla P_{\text{av}} - \frac{1}{4}\nabla P_c(S_w)) &= F_t \quad \text{in} \quad \Omega \\ \frac{\partial S_w}{\partial t} - \nabla \cdot \frac{3}{4}(\nabla P_{\text{av}} - \frac{1}{2}\nabla P_c(S_w)) &= F_w \quad \text{in} \quad \Omega \\ P_{\text{av}} &= 0 \quad \text{on} \quad \partial\Omega \\ S &= 0.5 \quad \text{on} \quad \partial\Omega. \end{aligned} \tag{5.2.4}$$

To construct the source terms from the chosen exact solutions (5.2.3), one can differentiate the given solutions and capillary pressure with respect to x and y to obtain

$$\nabla P_{\text{av}} = \begin{bmatrix} t(1-2x)y(1-y) \\ t(1-2y)x(1-x) \end{bmatrix} \text{ and } \begin{bmatrix} \frac{\partial^2 P_{\text{av}}}{\partial x^2} \\ \frac{\partial^2 P_{\text{av}}}{\partial y^2} \end{bmatrix} = \begin{bmatrix} -2ty(1-y) \\ -2tx(1-x) \end{bmatrix} \tag{5.2.5}$$

$$\nabla P_c = -2\begin{bmatrix} t(1-2x)y(1-y)S \\ t(1-2y)x(1-x)S \end{bmatrix} \text{ and } \begin{bmatrix} \frac{\partial^2 P_c}{\partial x^2} \\ \frac{\partial^2 P_c}{\partial y^2} \end{bmatrix} = \begin{bmatrix} (4ty(1-y)S - 2(t(1-2x)y(1-y)))^2 \\ 4tx(1-x)S - 2(t(1-2y)x(1-x)))^2 \end{bmatrix},$$

and substituting these derivatives (5.2.5) into the flow equation (5.2.2) will give us the following source terms for average pressure and wetting phase saturation

$$\begin{aligned} F_t &= -\triangle P_{\text{av}} + \frac{1}{4}\triangle P_c, \\ F_w &= \frac{\partial S_w}{\partial t} - \frac{3}{4}\triangle P_{\text{av}} + \frac{3}{8}\triangle P_c(S_w), \end{aligned}$$

where $\triangle P_{\text{av}} = \frac{\partial^2 P_{\text{av}}}{\partial x^2} + \frac{\partial^2 P_{\text{av}}}{\partial y^2}$ and $\triangle P_c = \frac{\partial^2 P_c}{\partial x^2} + \frac{\partial^2 P_c}{\partial y^2}$. Thus, we have a continuous two-phase flow model defined over a rectangular reservoir domain Ω.

The discretization scheme discussed in subsection 4.2.2 and iterative linearization solver are applied to obtain average pressure and wetting phase saturation profiles as depicted in Figure 5.2.3 and Figure 5.2.4, with an L_2 norm errors of pressure and saturation as, eP = 3.5263e-05 and eS = 2.1266e-05, respectively. These errors are found for (1.6e+03)-number of elements/control volumes and (1.6e+03)-number of time steps. However, the results obtained above doesn't tell us about the convergence of the numerical model, which is the objective of this particular chapter. To see the convergence of the numerical solution to the chosen exact solution, we have refined the number of cells and time step by a factor of 2 starting from small number of cells and step size.

For instance, we have started with 25-number of cells and 300-number of time step. The data in Table 5.1 are obtained by resolution of the starting number of cells and step size. As can be seen in Table 5.1, the numerical model converges quadratically to the constructed continuous model. Figure 5.2.5 is an error plot against number of elements/control volumes, which indeed verifies the quadratic convergence of the method and the corresponding Matlab code implementation.

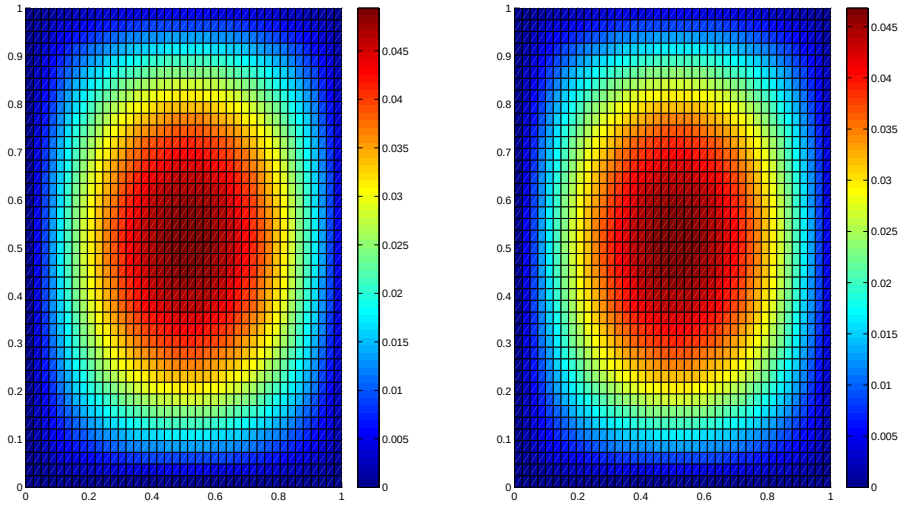

Figure 5.2.3: Approximate (left) and exact (right) average pressure solutions for constant mobilities and quadratic capillary pressure.

No. step	No. cells	App. Error for P_{av}	App. Error for S_w	$\frac{E_i^{P_{\text{av}}}}{E_{i+1}^{P_{\text{av}}}}$	$\frac{E_i^{S_w}}{E_{i+1}^{S_w}}$	rate for P_{av}	rate for S_w
250	25	0.0029	0.0015	-	-	-	-
500	100	6.3439e-04	3.5543e-04	4.5713	4.2202	2.1926	2.0773
1e+03	400	1.4675e-04	8.6279e-05	4.3229	4.1195	2.1120	2.0425
2e+03	1.6e+04	3.5255e-05	2.1210e-05	4.1625	4.0678	2.0575	2.0242
4e+03	6.4e+03	8.6377e-06	5.2553e-06	4.0815	4.0359	2.0291	2.0129

Table 5.1: Error analysis for two-phase flow problem with constant mobilities and quadratic capillarity force.

5.2.4 Matlab Code Implementation Validation Test for Two-phase Flow Problem with Linear Relative Permeabilities and Quadratic Capillary Pressure

This test case advances the discussed test case above in subsection 5.2.3 by considering a linear relative permeabilities (i.e., $K_{rw} = S_w$, and $K_{ro} = 1 - S_w$). Here again we consider the flow equation with Dirichlet boundary conditions. Using these relative permeabilities and capillary pressure, we will construct the source terms for average pressure and water phase saturation equations. In order to construct the source terms, one need to find first and second order derivatives of the exact pressure, mobilities and capillary pressure

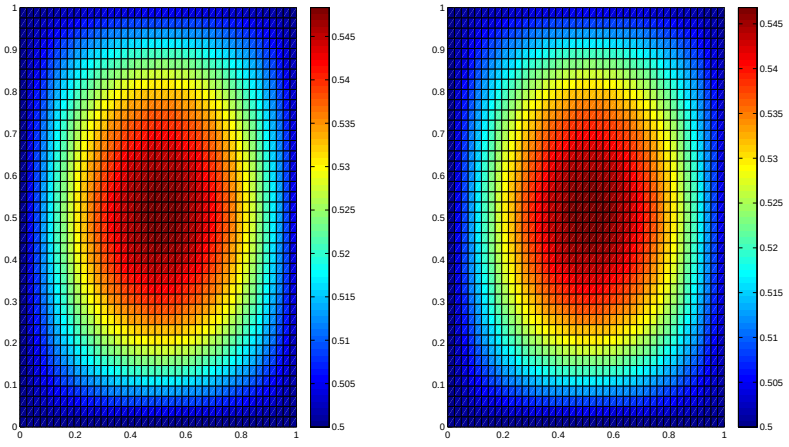

Figure 5.2.4: Approximate (left) and exact (right) water phase saturation solutions for constant mobilities and quadratic capillary pressure.

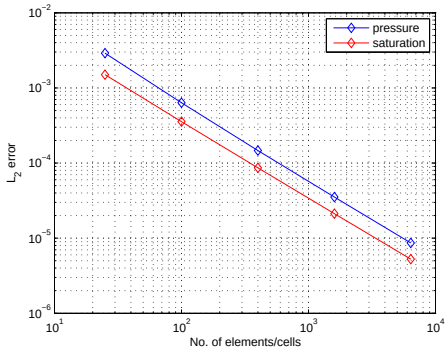

Figure 5.2.5: Error plot for constant mobilities and quadratic capillary pressure.

with respect to x and y as follows

$$\begin{aligned}
\nabla P_{\text{av}} &= \begin{pmatrix} t(1-2x)y(1-y) \\ t(1-2y)x(1-x) \end{pmatrix} \text{ and } \nabla K_{rw} = \begin{pmatrix} t(1-2x)y(1-y) \\ t(1-2y)x(1-x) \end{pmatrix} \\
\nabla K_{ro} &= -\begin{pmatrix} t(1-2x)y(1-y) \\ t(1-2y)x(1-x) \end{pmatrix} \text{ and } \nabla P_c = -2\begin{pmatrix} t(1-2x)y(1-y)S \\ t(1-2y)x(1-x)S \end{pmatrix} \qquad (5.2.6) \\
\begin{pmatrix} \frac{\partial^2 P_{\text{av}}}{\partial x^2} \\ \frac{\partial^2 P_{\text{av}}}{\partial y^2} \end{pmatrix} &= \begin{pmatrix} -2ty(1-y) \\ -2tx(1-x) \end{pmatrix} \text{ and } \begin{pmatrix} \frac{\partial^2 P_c}{\partial x^2} \\ \frac{\partial^2 P_c}{\partial y^2} \end{pmatrix} = \begin{pmatrix} (4ty(1-y)S - 2(t(1-2x)y(1-y)))^2 \\ 4tx(1-x)S - 2(t(1-2y)x(1-x)))^2 \end{pmatrix},
\end{aligned}$$

where the derivatives above are obtained from properly manufactured exact solutions of the average pressure and wetting phase saturation, which are given as

$$\begin{aligned}
P_{\text{av}} &= tx(1-x)y(1-y) \\
S_w &= tx(1-x)y(1-y) + 0.5. \qquad (5.2.7)
\end{aligned}$$

Substituting the above gradients (5.2.6) into the flow equation (5.2.2) appropriately and rearranging will give us the source terms for average pressure and water phase saturation equations. We have solved the resulting two phase flow problem by iterative linearization method for (1.6e+03)-number of cells and (2e+03)-number of step size, to obtain an approximate average pressure and water phase saturation distribution as given in Figure 5.2.6 and Figure 5.2.7 respectively. The visualization in Figure 5.2.6 and Figure 5.2.7 respectively

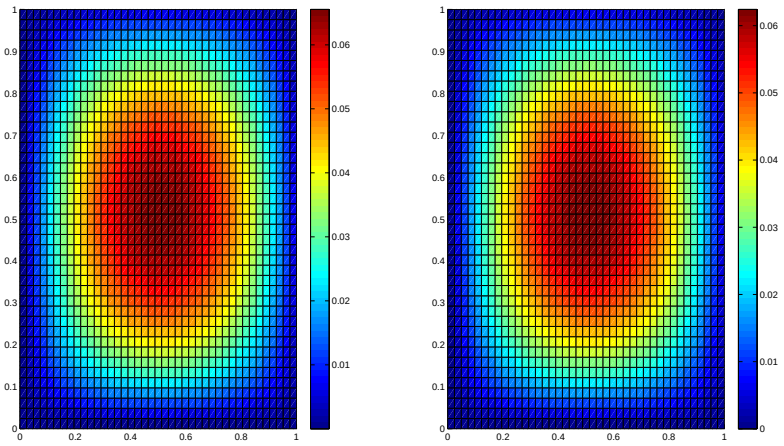

Figure 5.2.6: Approximate average pressure solution (left) and exact average pressure solution (right) for linear relative permeabilities and quadratic capillary pressure.

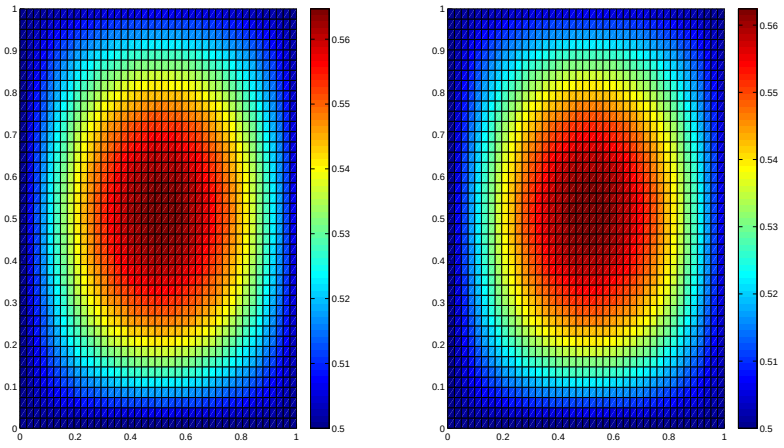

Figure 5.2.7: Approximate (left) and exact (right) saturation profile for linear relative permeabilities and quadratic capillary pressure.

reflects closely the same cell pressure and saturation profile. Even though the visualization as well as the L_2 error (L_2 norm for pressure eP = 4.2760e-05 and saturation eS = 3.2259e-05) for this particular simulation looks fine and acceptable to say that the approximated numerical solution is close to the representative exact

cell solutions, it doesn't tell us about the convergence of the numerical solution to exact solution. To validate the implementation, we have to look at the convergence rates by refining the time and space domains. The obtained results are reported in Table 5.2 for average pressure and water phase saturation numerical solutions for different space and time resolutions. As can be seen in Table 5.2 below, the errors for the implemented iterative linearization method gets smaller as the time and the control volume get smaller. From Table 5.2,

No. step	No. cells	App. Error for P_{av}	App. Error for S_w	$\frac{E_i^{P_{\text{av}}}}{E_{i+1}^{P_{\text{av}}}}$	$\frac{E_i^{S_w}}{E_{i+1}^{S_w}}$	rate for P_{av}	rate for S_w
400	25	3.5e-03	2.4-03	-	-	-	-
800	100	7.6411e-04	5.5829e-04	4.5805	4.2988	-	-
1.6e+03	400	1.7758e-04	1.3226e-04	4.3029	4.2212	-	-
3.2e+03	1.6e+04	4.2758e-05	3.2098e-05	4.1531	4.1205	-	-
7.2e+03	6.4e+03	1.0488e-05	7.9051e-06	4.0768	4.0604	-	-

Table 5.2: Error analysis for two-phase flow problem with linear mobilities and quadratic capillarity force.

we observe that the numerical solution of average pressure and water phase saturation converges to the exact solutions quadratically. Moreover, Figure 5.2.8 shows the error plot vs number of control volumes. Thus, we can conclude that the numerical solution of the designed flow problem is converging to the exact solution as the control volume and time step go to zero from the right.

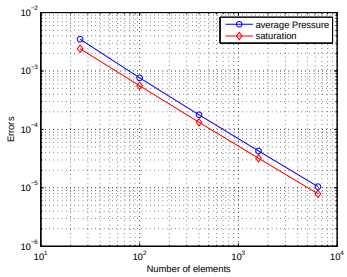

Figure 5.2.8: Error Plot of average pressure and water phase saturation for two phase flow problem with linear relative permeabilities and quadratic capillary pressure parameterizations.

5.2.5 Code Validation Test for Two-phase Flow Problem with van Genuchten Parametrization

In this case, we have considered the Van Genuchten type parametrization for capillary pressure and mobilities. From subsection 5.2.2, we can recall the van Genuchten parameterizations as,

$$\begin{aligned} P_c(S_w) &= \sqrt{S_w^{-2}-1} \\ K_{ro}(S_w) &= \sqrt{1-S_w}\left(1-S_w^{\frac{1}{\mathrm{M}}}\right)^{2\mathrm{M}} \\ K_{rw}(S_w) &= \sqrt{S_w}\left(1-\left(1-S_w^{\frac{1}{\mathrm{M}}}\right)^{\mathrm{M}}\right)^2. \end{aligned} \tag{5.2.8}$$

For this particular validation test, we have chosen N = 2 which helps us to reduce (5.2.8) to

$$\begin{aligned} P_c(S_w) &= \sqrt{S_w^{-2}-1} \\ K_{ro}(S_w) &= \sqrt{1-S_w}\left(1-S_w^2\right) \\ K_{rw}(S_w) &= \sqrt{S_w}\left(1-\sqrt{(1-S_w^2)}\right)^2. \end{aligned} \tag{5.2.9}$$

Here again we established exact solutions for the average pressure and water phase saturation equation (5.2.2) to be the same as previously used, thus

$$\begin{cases} P_{\text{av}} = tx(1-x)y(1-y)+0.2 \\ S_w = tx(1-x)y(1-y)+0.5 \end{cases} \tag{5.2.10}$$

Since the given fluid parameterizations and solutions (5.2.10) are continuously differentiable, we can obtain the first and second derivatives of each as follow,

$$\begin{aligned} \nabla P_{\text{av}} &= (t(1-2x)y(1-y), t(1-2y)x(1-x)) \\ \nabla S_w &= (t(1-2x)y(1-y), t(1-2y)x(1-x)) \\ \nabla P_c(S_w) &= \left(\frac{-t(1-2x)y(1-y)}{S_w^3\sqrt{S_w^{-2}-1}}, \frac{-t(1-2y)x(1-x)}{S_w^3\sqrt{S_w^{-2}-1}}\right) \\ \nabla K_{ro}(S_w) &= \begin{pmatrix} t(2x-1)y(1-y)(\frac{1-S^2}{2\sqrt{1-S}}+2S\sqrt{1-S}) \\ t(2y-1)x(1-x)(\frac{1-S^2}{2\sqrt{1-S}}+2S\sqrt{1-S}) \end{pmatrix} \\ \nabla K_{rw}(S_w) &= \begin{pmatrix} t(1-2x)y(1-y)(\frac{2S^{1.5}(1-\sqrt{(1-S^2)})}{\sqrt{1-S^2}}+\frac{(1-\sqrt{1-S^2})^2}{2\sqrt{S}}) \\ t(1-2y)x(1-x)(\frac{2S^{1.5}(1-\sqrt{(1-S^2)})}{\sqrt{1-S^2}}+\frac{(1-\sqrt{1-S^2})^2}{2\sqrt{S}}) \end{pmatrix}. \end{aligned} \tag{5.2.11}$$

And the second order derivatives of the capillary pressure and the average pressure can be obtained as

$$\begin{pmatrix} \frac{\partial^2 P_{\text{av}}}{\partial x^2} \\ \frac{\partial^2 P_{\text{av}}}{\partial y^2} \end{pmatrix} = \begin{pmatrix} -2y(1-y) \\ -2x(1-x) \end{pmatrix} \tag{5.2.12}$$

$$\begin{pmatrix} \frac{\partial^2 P_c(S_w)}{\partial^2 x} \\ \frac{\partial^2 P_c(S_w)}{\partial^2 y} \end{pmatrix} = \begin{pmatrix} \frac{3(t(1-2x)y(1-y))^2}{S.^4\sqrt{S.^{-2}-1}} - \frac{(t(1-2x)y(1-y))^2}{S^6(S^{-2}-1)^{1.5}} + \frac{2ty(1-y)}{S^3\sqrt{S^{-2}-1}} \\ \frac{3(t(1-2y)x(1-x))^2}{S.^4\sqrt{S.^{-2}-1}} - \frac{(t(1-2y)x(1-x))^2}{S^6(S^{-2}-1)^{1.5}} + \frac{2tx(1-x)}{S^3\sqrt{S^{-2}-1}} \end{pmatrix}.$$

Now we can collect the above gradients together and substitute into equation (5.2.2), to obtain the source terms for pressure and situation equations as follows

$$\begin{cases} -F_t = \nabla\lambda_t\nabla P_{\text{av}} + \lambda_t\nabla\cdot P_{\text{av}} + \frac{1}{2}(\nabla\lambda_d\nabla P_c + \lambda_d\nabla\cdot P_c) \\ F_s = \frac{\partial S_w}{\partial t} - \nabla K_{rw}\nabla P_{\text{av}} + K_{rw}\nabla\cdot P_{\text{av}} + \frac{1}{2}(\nabla K_{rw}\nabla P_c + K_{rw}\nabla\cdot P_c) \end{cases} \tag{5.2.13}$$

Moreover, one can obtain the boundary conditions for average pressure and saturation equation from the given exact solution.

Now we can apply our discretization scheme on the resulting two phase flow model followed by an iterative linearization solver to have a numerical solution at hand. For instance, we have solved this flow problem for $(1.6\text{e}+03)$-number of elements and $(1.6\text{e}+03)$-number of time step to obtain average pressure and water

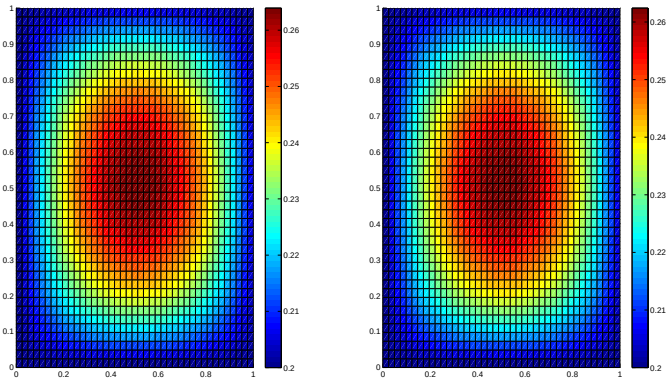

Figure 5.2.9: Approximate average pressure (left) and exact pressure (right) solutions for van Genuchten parametrization.

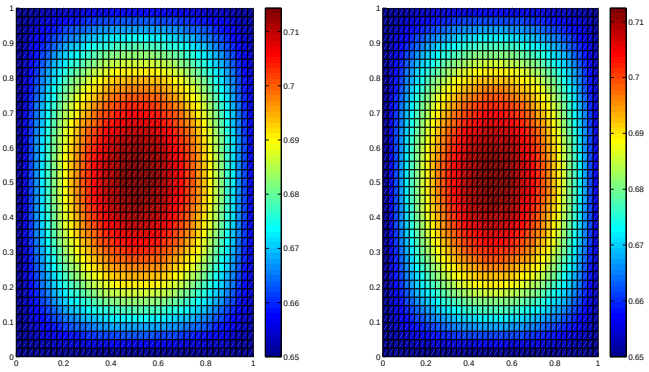

Figure 5.2.10: Approximate wetting saturation (left) and exact wetting saturation (right) solutions for van Genuchten parametrization.

phase saturation distributions as depicted in Figure 5.2.9 and Figure 5.2.10 respectively. The discrete L_2 error norm for this simulation reads, eP = 2.2266e-05 and eS = 2.7915e-05. Here again, the obtained numerical solutions are found to be promising compared to the representative exact solutions of average pressure as well as wetting phase saturation equations. But, we need to do numerical experiments on the resulting two-phase flow problem for different number of control volumes and step size in order to study the convergence of the numerical model. Table 5.3, shows the decreasing behavior of discrete L_2 average pressure and water phase saturation errors by a rate of 2 as the cell area and step size decreases by a factor of 2. In general, we can conclude that the numerical flow model converges quadratically to the constructed continuous model.

Moreover, L_2 error plot in Figure 5.2.11 for average pressure and saturation has strengthen the analysis in Table 5.3.

No. Steps	No. cells	App. Error for P_{av}	App. Error for S_w	$\frac{E_i^{P_{\text{av}}}}{E_{i+1}^{P_{\text{av}}}}$	$\frac{E_i^{S_w}}{E_{i+1}^{S_w}}$	rate for P_{av}	rate of S_w
300	25	1.7e-03	1.9e-03	-	-	-	-
600	100	3.8272e-04	4.5228e-04	4.4419	4.2009	2.1512	2.0707
1.2e+03	400	9.1426e-05	1.1050e-04	4.1861	4.0930	2.0656	2.0332
2.4e+03	1.6e+03	2.2322e-05	2.7795e-05	4.0958	3.9755	2.0341	1.9911
4.8e+03	6.4e+03	5.5359e-06	7.4612e-06	4.0322	3.7253	2.0116	1.8974

Table 5.3: Error analysis for two-phase flow with van Genuchten parametrization.

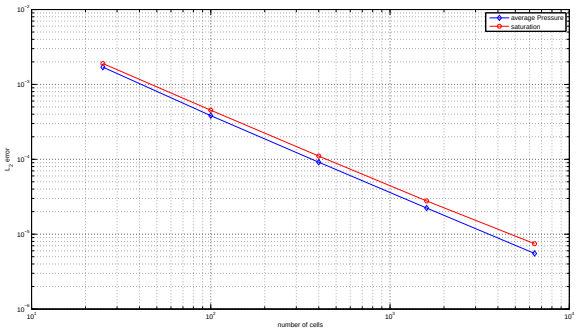

Figure 5.2.11: Error plot for two-phase flow problem with van Genuchten parameterizations.

5.2.6 Analytic Solution validation Test Case for Transport Model

In this part, we will see the convergence behaviour of convective-dispersive transport model. We define the transport model over a rectangular domain $\Omega = [0,1] \times [0,1]$ and $t \in [0,1]$. In the simple case the water flux (Darcy's velocity of water), the water saturation, porosity, and the dispersion-diffusion coefficient are set to be one. Moreover, we consider a single component transport equation. As a consequence, the general transport model (4.2.41) simplifies to give,

$$\frac{\partial C}{\partial t} + \nabla \cdot (C - \nabla C) = Q. \tag{5.2.14}$$

Here again we choose $C = tx(1-x)y(1-y)$ being the exact solution to the transport equation (5.2.14). We can construct the source term, in the same fashion as we have done for the flow equation. To find the source term Q, let us start by differentiating the given exact solution with respect to t, x and y to have

$$\nabla C = \begin{pmatrix} t(1-2x)y(1-y) \\ t(1-2y)x(1-x) \end{pmatrix} \text{ and } \begin{pmatrix} \frac{\partial^2 C}{\partial x^2} \\ \frac{\partial^2 C}{\partial y^2} \end{pmatrix} = \begin{pmatrix} -2ty(1-y) \\ -2tx(1-x) \end{pmatrix}. \tag{5.2.15}$$

Substituting these derivative results (5.2.15) into the transport model (5.2.14) will give us the source term, which results in a component transport equation with homogeneous boundary condition. This transport equation can be discretized implicitly as discussed in Section 4.2.3. Now the resulting algebraic system can be solved using linear solvers. For instance, we have solved this particular simple example for 1600-number of cells and 80-number of step size to obtain the result as shown in Figure 5.2.12 with discrete L_2 error of

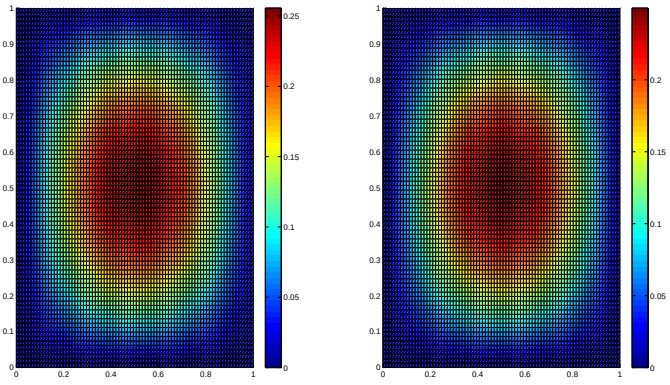

Figure 5.2.12: Comparative plot of approximate (left) and exact (right) solutions for transport model

microbial concentration, eC = 3.6642e-05. We have studied the convergence of the numerical solution to the exact solution of the transport model above (5.2.14), by refining the cells and the temporal domain and obtain the results as reported in Table 5.4.

No. step size	No. of cells	App. Error for C	$\frac{E_i^C}{E_{i+1}^C}$	rate
5	25	0.0123	-	-
10	100	0.0027	4.5556	2.1876
20	400	6.2292e-04	4.3344	2.1158
40	1600	1.4961e-04	4.1636	2.0578
80	6400	3.6642e-05	4.0830	2.0296
160	2.56e+04	9.0657e-06	4.0418	2.0150

Table 5.4: Error analysis for transport model.

As can be seen in Table 5.4, the numerical solution converges quadratically to the exact solution. Further, we plot the error against number of cells/control volumes in Figure 5.2.13.

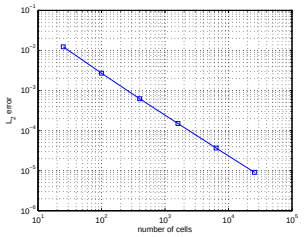

Figure 5.2.13: Error plot for component transport models.

The three test cases discussed above verify that our discretization scheme and Matlab implementation are valid and acceptable to simulate two-phase (two dimensional) flow equations. Moreover, the last test

case validates the implementation of convective-dispersive transport equation. In general, the illustrative examples considered in this thesis can be used to validate that our implementation is able to simulate two-phase flow and advection-diffusion reactive transport models. However, we observe that the iterative linearization scheme was affected by non-linearities and parameterizations.

Chapter 6

Mathematical Models for Microbial EOR Processes

In the early life of an oil reservoir, the fluid pressures are high and oil as well as water can flow to the wellbore naturally. When reservoir pressure declines, field operators often inject water into the reservoir, to maintain pressure and sweep oil to wellbores and commonly referred to as secondary oil recovery. Due to capillary forces, the reservoir rocks hold large amounts of residual oil, after secondary recovery. People from oil industry employ tertiary recovery or EOR methods to mobilize the residual oil. Most common EOR methods include surfactant flooding, polymer flooding, CO2 flooding, thermal recovery and microbial EOR, see section 2.2 for more details.

One of the microbial EOR strategy injects live microorganism and nutrient solutions into the reservoir so that microbes and their metabolic products help to mobilize the residual oil. If favorable bacteria already reside in the reservoir, it is feasible to inject nutrients only. The growth of microbes lead to production of bio-surfactant that reduce oil-water interfacial tension (IFT) and hence weaken capillary pressure (which is proportional to the oil-water IFT) that holds the residual oil in porous matrix. In the following section 6.1, we will investigate one of the most promising mechanisms of microbial EOR, i.e., reduction of IFT.

6.1 Capillary Pressure, Residual Oil and Relative Permeabilities

Reduction of oil-water IFT and selective plugging by bacterial presence are believed to have the greatest impact on oil recovery [4] and see the references there in. This section devotes to the possible reduction of IFT due to the activity of bio-surfactant on the interface between oil and water. In [4, 11], bio-surfactant concentration has been used to model oil-water IFT. However, it is also natural to correlate oil-water IFT and microbial concentration directly to avoid actual bio-surfactant production in the transport model. In [63], two separate experimental results are reported for the possible reduction of IFT. The first shows a

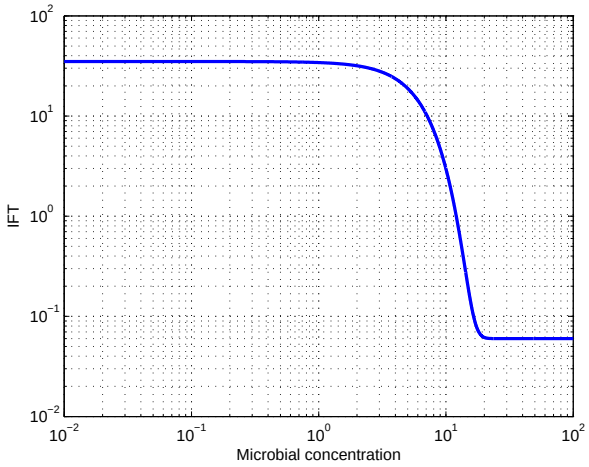

Figure 6.1.1: IFT vs microbial concentration.

drop of IFT from 35 to 0.17 mN/m, while the second shows a drop from 38 to 0.06 mN/m, due to bacterial activities. Based on these results Kai *et al.,* [5] have suggested a simple, exponential relationship between microbial concentration C and IFT, σ as

$$\sigma(C) = (\sigma_0 - \sigma_{\min})\mathrm{e}^{-\beta C} + \sigma_{\min}, \tag{6.1.1}$$

where σ_0 is the initial(maximum) IFT, $\sigma_{\min}$ is possible minimum value of IFT, β is a constant coefficient determined by the effects of microbial activity.

The relation between oil-water IFT and microbial concentration above (6.1.1) assumes an immediate effect, which is not physically true. To handle this drawback, we have considered a time aspect in the relation (6.1.1) which retards the reduction processes for a while and given as follows

$$\sigma(C) = (\sigma_0 - \sigma_{\min})\mathrm{e}^{-\frac{\beta_1 C^{\beta_2}}{C+\beta_3}} + \sigma_{\min}, \tag{6.1.2}$$

where β_1, β_2 and β_3 are microbial concentration and activity dependent positive real parameters. Specially, β_1 is very sensitive with the effect of microbial concentration on the reservoir. In other words, if the microbial concentration is too little with high effect to the reservoir system, β_1 should hold a high magnitude to cope up the model. Figure 6.1.1 depicts a curve for the proposed oil-water IFT vs microbial concentration for $\beta_1 = 0.025$, $\beta_2 = 3$ and $\beta_3 = 0.05$.

Oil reservoir environment is full of many factors that affect the growth and transport of microbes. Thus, the microbes may not get adjusted to the reservoir environment and start to produce bio-surfactant within short period of time. For instance, an experiment result in [63] shows that microbial activities take time to have an effect on the reduction of IFT. The proposed model above considers this delay of time implicitly. The growth of microbes reduce oil-water IFT. Though there is scarcity of experimental data on microbial EOR processes, the proposed IFT model (6.1.2) is similar to the report in Nielsen *et al.,* [11] of Figure 9.

In subsection 2.1.3, we have learnt the relation between capillary force and oil-water IFT for which lowering

the IFT gives a weak capillary force. Based on this relation, we will incorporate the effect of microbial concentration for the capillary pressure reduction and improvement of fluid mobilities.

6.1.1 Effect of Microbial Concentration on Capillary Pressure and Relative Permeabilities

In Section 6.1, we have proposed oil-water IFT as a function of microbial concentration. In this section, we will couple the reduction of IFT to the capillary pressure and relative permeabilities. Following Islam [17], the van Genuchten capillary pressure can be related to oil-water IFT model (6.1.2) as follows

$$P_c(S_w, C) = P_c(S_w)\frac{\sigma(C)}{\sigma_0}, \tag{6.1.3}$$

where $P_c(S_w) = (S_w^{-\frac{1}{M}} - 1)^{\frac{1}{N}}$, $M = \frac{1}{N}$ is a model dependant van Genuchten parameter.

This modified capillary pressure becomes the original van Genuchten capillary pressure when the microbial concentration is close to zero, which is possibly the maximum capillary force. On the other hand, this capillary force decreases as the microbial concentration increases.

It is reported in [4, 17, 64] that the reduction of oil-water IFT motivates phase relative permeabilities. In other words, microbial concentration affects the relative permeabilities through the reduction of oil-water IFT. Moreover, it has been suggested that relative permeability curves become affine curves as oil-water IFT considered to be negligible. Based on this information, the relative permeability curves could be related to the oil-water IFT curve in the following manner,

$$\begin{cases} K_{rw}(S_w, C) = K_{rw}(S_w) + [S_w - K_{rw}(S_w)]\frac{\sigma_0 - \sigma(C)}{\sigma_0} \\ K_{ro}(S_w, C) = K_{ro}(S_w) + [1 - S_w - K_{ro}(S_w)]\frac{\sigma_0 - \sigma(C)}{\sigma_0} \end{cases} \tag{6.1.4}$$

where σ_0 is initial IFT (maximum IFT).

From the relation (6.1.4), one notices that the designed relative permeability curves are close to affine line as oil-water IFT is close to zero and keeps the original van Genuchten parametrization of relative permeability curves, when the microbial concentration is sufficiently small.

In this thesis, the modified capillary pressure and relative permeability curves are used to couple the two-phase flow and transport equations. This coupled reservoir model can be used to simulate the effect of microbial activity on the reservoir system such as residual oil.

6.1.2 Effect of Microbial activity on Residual Oil

After a water-flooding, crude oil remains trapped in the reservoir due to fluid-fluid capillary force. Microbial EOR is one of the most promising enhanced oil recovery mechanisms used to mobilize the residual oil after a secondary recovery of water-flooding, which is achieved by lowering the capillary force. Shen *et al.,* [64]

have done a surfactant flooding experiment and data fitting on the relation between IFT and residual oil as,

$$S_{\text{or}} = \frac{\sigma(C_s)^{\frac{3}{2}}}{A\sigma(C_s)^{\frac{3}{2}} + B}, \tag{6.1.5}$$

where, A and B are constants and C_s is surfactant concentration.

We have adapted the correlation above (6.1.5), for our particular case by replacing the surfactant concentration with microbial concentration. From the correlation (6.1.5), we observe that the residual oil start to mobilize when the IFT lies between 0 and 1. In other words, the residual oil remains trapped within the skeleton of the reservoir matrix for $\sigma \geq 1$, and start to displaced for $\sigma < 1$.

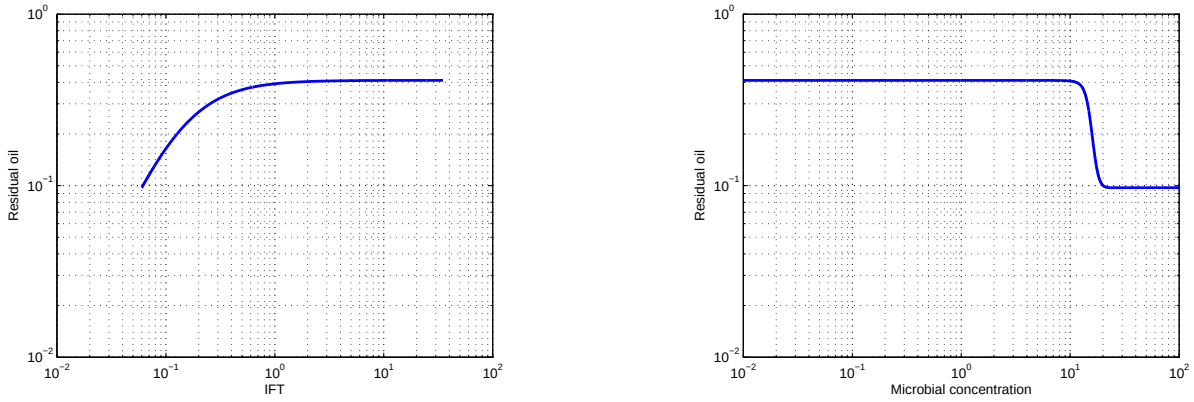

Figure 6.1.2: Residual oil vs oil-water IFT (left) and Residual oil vs microbial concentration (left).

6.2 Coupling Flow and Transport Equations

In Section 6.1, we introduced the effect of microbial concentration into the capillary pressure and phase relative permeabilities. These relations have been used to couple the two-phase flow with transport equations. The resulting coupled reservoir model can be stated as follows,

$$\begin{cases} -\nabla \cdot K(\lambda_t(S_w, C)\nabla P_{\text{av}} + \frac{1}{2}\lambda_d(S_w, C)\nabla P_c(S_w, C) = F_t & \text{in } \Omega \\ \phi\frac{\partial(S_w)}{\partial t} - \nabla \cdot (\lambda_w(S_w, C)\nabla P_{\text{av}} + \frac{1}{2}P_c(S_w, C)) = \frac{F_w}{\rho_w} & \text{in } \Omega \\ \phi\frac{\partial(SC)}{\partial t} + \nabla \cdot (q_w C - D\nabla(\phi SC)) = Q & \text{in } \Omega \\ \text{Dirichlet BC} & \text{on } \partial\Omega \\ \text{Neumann BC} & \text{on } \partial\Omega \\ \text{Initial Conditions} & \text{in } \Omega \end{cases} \tag{6.2.1}$$

System of equations in (6.2.1) have been used to simulate microbial activities on residual oil recovery in which the substrate/nutrient concentration is assumed to be sufficiently enough for microbial growth. Moreover, the mathematical model (6.2.1) is designed by considering a direct relationship between IFT and microbial concentration which removes the bio-surfactant production dynamics.

In Chapter 4, the pressure and microbial transport equations were discretized implicitly, whereas the saturation equation was discretized explicitly. The same discretization scheme is used to discretize the coupled reservoir system (6.2.1). The resulting discretized algebraic systems without boundary conditions can be rewritten as follows,

$$\begin{cases} -\nabla \cdot K(\lambda_t(S_w^{n+1}, C^{n+1})\nabla P_{\text{av}}^{n+1} + \frac{1}{2}\lambda_d(S_w^{n+1}, C^n)\nabla P_c(S_w^{n+1}, C^{n+1}) = F_t^n & \text{in } \Omega \\ \phi\frac{S_w^{n+1}-S_w^n}{\triangle t} - \nabla \cdot (\lambda_w(S_w^{n+1}, C^{n+1})\nabla P_{\text{av}}^{n+1} + \frac{1}{2}P_c(S_w^{n+1}, C^{n+1})) = \frac{F_w^n}{\rho_w} & \text{in } \Omega \\ \phi\frac{S_w^{n+1}C^{n+1}-S_w^nC^n}{\triangle t} + \nabla \cdot (q_w(S_w^{n+1}, C^{n+1})C^{n+1} - D\nabla(\phi S_w^{n+1}C^{n+1})) = Q^n \text{ in } \Omega. \end{cases} \tag{6.2.2}$$

The three equations in system (6.2.2) are coupled non-linear equations. We adopted an iterative linearization scheme to solve the system (6.2.2), for which the convergence of the method is studied for two-phase flow equations [12]. To have an iterative/semi-implicit linearization scheme, the discretization scheme (6.2.2) can be modified as

$$\begin{cases} -\nabla \cdot K(\lambda_t(S_w^{n+1,i}, C^{n+1,i})\nabla P_{\text{av}}^{n+1,i+1} + \frac{1}{2}\lambda_d(S_w^{n+1,i}, C^{n+1,i})\nabla P_c(S_w^{n+1,i}, C^{n+1,i})) = F_t^n \text{ in } \Omega \\ \phi\frac{S_w^{n+1,i+1}-S_w^n}{\triangle t} - \nabla \cdot (\lambda_w(S_w^{n+1,i}, C^{n+1,i})\nabla P_{\text{av}}^{n+1,i+1} + \frac{1}{2}P_c(S_w^{n+1,i}, C^{n+1,i})) = \frac{F_w^n}{\rho_w} \text{ in } \Omega \\ \phi\frac{S_w^{n+1,i+1}C^{n+1,i+1}-S_w^nC^n}{\triangle t} - \nabla \cdot (D\nabla(\phi S_w^{n+1,i+1}C^{n+1,i+1}) \\ \qquad - q_w(S_w^{n+1,i+1}, C^{n+1,i}, P_{\text{av}}^{n+1,i+1})C^{n+1,i+1}) = Q^n \qquad \text{in } \Omega. \end{cases} \tag{6.2.3}$$

The discretized equations (6.2.3) could be solved using iterative linearization scheme, which is summarized in Table 6.1

Step	Description
1	Given S_w^n, and C^n. Let $S_w^{n+1,0} = S_w^n$, and $C^{n+1,0} = C^n$
2	Solve the pressure equation for the new time step $\{n+1, i+1\}$, using the previous saturation, $S_w^{n+1,i}$ and concentration, $C^{n+1,i}$ profile
3	Solve the saturation equation using the pressure evaluated at the current iteration step $P_{\text{av}}^{n+1,i+1}$, but the capillary pressure and relative permeabilities are evaluated at the previous iteration, $S_w^{n+1,i}$ and $C^{n+1,i}$
4	Take the pressure and saturation profiles found at the new iteration step, $\{n+1, i+1\}$ and solve the microbial concentration equation for $\{n+1, i+1\}$
5	Iterate for i until $\|P_{\text{av}}^{n+1,i+1} - P_{\text{av}}^{n+1,i}\| \leq \varepsilon$, $\|S_w^{n+1,i+1} - S_w^{n+1,i}\| \leq \varepsilon$ and $\|C^{n+1,i+1} - C^{n+1,i}\| \leq \varepsilon$ and take $P_{\text{av}}^{n+1} = P_{\text{av}}^{n+1,i+1}$, $S_w^{n+1} = S_w^{n+1,i+1}$ and $C^{n+1} = C^{n+1,i+1}$
6	Set $n = n+1$ and go to Step 2, and repeat the above Steps up to the final time of the system

Table 6.1: Iterative linearization algorithm.

6.2.1 The Coupled Model Validation Test Case with an Analytical Solutions

In Chapter 5, we have studied numerical convergence of different two-phase flow and transport models separately. Here, we have coupled the flow problem and microbial transport models by introducing microbial concentration to the van Genuchten capillary pressure. In this Section, we will study and examine numerical convergence of the resulting coupled microbial EOR model. The dimensionless parameters used in this validation test are listed in Table 6.2. Here again, we have manufactured analytical solutions as we have done in Chapter 5, but modified van Genuchten parametrization. To construct the source terms, one can follow the same procedure as discussed in Chapter 5. Now we can differentiate the given parameters to

Parameter	value	Parameter	value
Ω	$[0,1]\times[0,1]$	t	$[0,0.5]$
K	1	ϕ	1
μ_o	1	μ_w	1
ρ_o	1	ρ_w	1
σ_0	1	$\sigma_{\min}$	0.06
β_1	1	β_2	1
β_3	1-C	D	1

Table 6.2: Parameters used to validate the coupled model.

obtain the following result,

$$\nabla P_{\text{av}} = \begin{bmatrix} t(1-2x)y(1-y) \\ t(1-2y)x(1-x) \end{bmatrix} \text{ and } \nabla S_w = \begin{bmatrix} t(1-2x)y(1-y) \\ t(1-2y)x(1-x) \end{bmatrix}$$

$$\nabla P_c(S_w, C) = \begin{bmatrix} \frac{-t(1-2x)y(1-y)}{S_w^3\sqrt{S_w^{-2}-1}}\sigma(c,t) - \alpha t^2(1-2x)y(1-y)\sigma(C,t)\sqrt{S_w^{-2}-1} \\ \frac{-t(1-2y)x(1-x)}{S_w^3\sqrt{S_w^{-2}-1}})\sigma(C,t) - \alpha t^2(1-2y)x(1-x)\sigma(C,t)\sqrt{S_w^{-2}-1} \end{bmatrix} \tag{6.2.4}$$

$$\nabla C = \begin{bmatrix} t(1-2x)y(1-y) \\ t(1-2y)x(1-x) \end{bmatrix} \text{ and } \nabla K_{ro}(S_w) = \begin{bmatrix} t(2x-1)y(1-y)(\frac{1-S^2}{2\sqrt{1-S}} + 2S\sqrt{1-S}) \\ t(2y-1)x(1-x)(\frac{1-S^2}{2\sqrt{1-S}} + 2S\sqrt{1-S}) \end{bmatrix}$$

$$\nabla K_{rw}(S_w) = \begin{bmatrix} t(1-2x)y(1-y)(\frac{2S^{1.5}(1-\sqrt{(1-S^2)})}{\sqrt{1-S^2}} + \frac{(1-\sqrt{1-S^2})^2}{2\sqrt{S}}) \\ t(1-2y)x(1-x)(\frac{2S^{1.5}(1-\sqrt{(1-S^2)})}{\sqrt{1-S^2}} + \frac{(1-\sqrt{1-S^2})^2}{2\sqrt{S}}) \end{bmatrix}.$$

Further, we need second order derivatives of capillary pressure, water phase saturation, microbial concentration and average pressure which can be obtained as

$$\begin{bmatrix} \frac{\partial^2 P_{\text{av}}}{\partial x^2} \\ \frac{\partial^2 P_{\text{av}}}{\partial y^2} \end{bmatrix} = \begin{bmatrix} -2y(1-y) \\ -2x(1-x) \end{bmatrix}, \begin{bmatrix} \frac{\partial^2 S_w}{\partial x^2} \\ \frac{\partial^2 S_w}{\partial y^2} \end{bmatrix} = \begin{bmatrix} -2y(1-y) \\ -2x(1-x) \end{bmatrix} \text{ and } \begin{bmatrix} \frac{\partial^2 C}{\partial x^2} \\ \frac{\partial^2 C}{\partial y^2} \end{bmatrix} = \begin{bmatrix} -2y(1-y) \\ -2x(1-x) \end{bmatrix}$$

$$\begin{aligned} \frac{\partial^2 P_c}{\partial x^2} &= (\frac{3(t(1-2x)y(1-y))^2}{S^4\sqrt{S^{-2}-1}} - \frac{(t(1-2x)y(1-y))^2}{S^6(S^{-2}-1)^{1.5}} + \frac{2ty(1-y)}{S^3\sqrt{S^{-2}-1}})\sigma \\ &\quad + \frac{2\alpha t^3((1-2x)y(1-y))^2}{S_w^3\sqrt{S_w^{-2}-1}}\sigma + \sigma(2\alpha t^2 y(1-y) + (\alpha t^2(1-2x)y(1-y))^2)\sqrt{S_w^{-2}-1} \\ \frac{\partial^2 P_c}{\partial y^2} &= (\frac{3(t(1-2y)x(1-x))^2}{S^4\sqrt{S^{-2}-1}} - \frac{(t(1-2y)x(1-x))^2}{S^6(S^{-2}-1)^{1.5}} + \frac{2tx(1-x)}{S^3\sqrt{S^{-2}-1}})\sigma \\ &\quad + \frac{2\alpha t^3((1-2y)x(1-x))^2}{S_w^3\sqrt{S_w^{-2}-1}}\sigma + \sigma(2\alpha t^2 y(1-y) + (\alpha t^2(1-2x)y(1-y))^2)\sqrt{S_w^{-2}-1}. \end{aligned} \tag{6.2.5}$$

Substituting the results from (6.2.4) and (6.2.5) into the coupled microbial EOR system (6.2.1) will give us source terms for average pressure, water phase saturation and microbial transport equations. The resulting mathematical model can be solved following the algorithm described in Table 6.1. For instance, we have solved this coupled mathematical model for (2.5e+3)-number of control volumes and (2.6e+3)-number of iterations in time and obtain the results for average pressure, water saturation and microbial concentration as depicted in Figure 6.2.1, 6.2.2 and 6.2.3 respectively.

We did a numerical experiment by refining the number of control volumes and number of time steps to obtain results as listed in Table 6.3 for average pressure and water phase saturation profile and Table 6.4

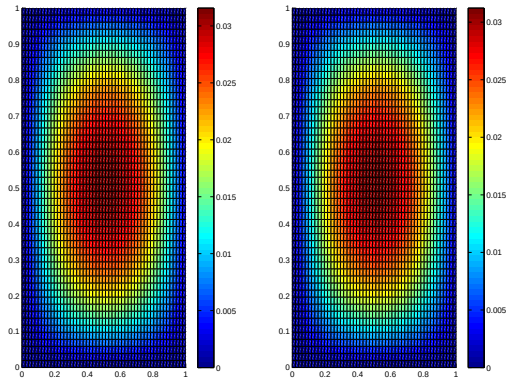

Figure 6.2.1: Approximate (left) and exact (right) average pressure solutions for the coupled system.

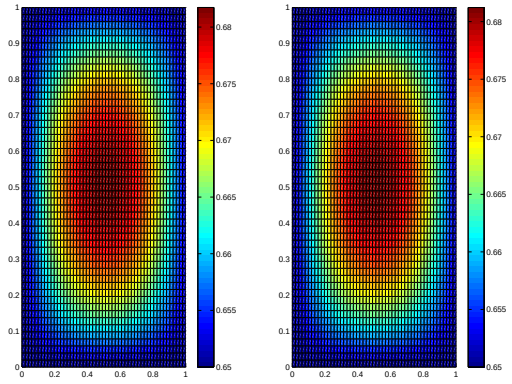

Figure 6.2.2: Approximate (left) and exact (right) water phase saturation profiles for the coupled system.

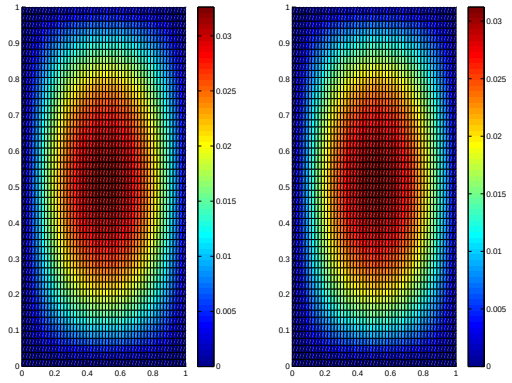

Figure 6.2.3: Approximate (left) and exact (right) microbial concentration solutions for the coupled system.

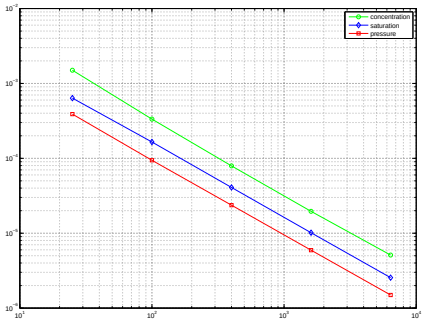

Figure 6.2.4: Error plot for the coupled system of the oil reservoir.

for microbial concentration. From Tables 6.3 and 6.4, one can learn that numerical solutions of average pressure, water phase saturation and microbial concentration converges quadratically to the respective exact solutions as the mesh size goes to zero.

No. Steps	No. elements	App. Error, P_{av}	App. Error, S_w	$\frac{E_i^{P_{\text{av}}}}{E_{i+1}^{P_{\text{av}}}}$	$\frac{E_i^{S_w}}{E_{i+1}^{S_w}}$	rate P_{av}	rate S_w
125	25	3.8945e-04	6.3651e-04	-	-	-	
250	100	9.4043e-05	1.6502e-04	4.1412	3.8572	2.0500	1.9476
500	4003	2.3688e-05	4.0792e-05	3.9701	4.0454	1.9892	2.0163
1000	1600	5.9390e-06	1.0143e-05	3.9886	4.0217	1.9959	2.0078
2000	6400	1.4948e-06	2.5478e-06	3.9731	3.9811	1.9903	1.9932

Table 6.3: Error analysis the coupled reservoir system of pressure and saturation.

No. steps	No. elements	App. Error, P_{av}	$\frac{E_i^C}{E_{i+1}^C}$	rate C
125	25	0.0015	-	-
250	100	3.3380e-04	4.4937	2.1679
500	4003	7.9218e-05	4.2137	2.0751
1000	1600	1.9594e-05	4.0430	2.0154
2000	6400	5.1069e-06	3.8368	1.9399

Table 6.4: Error analysis the coupled reservoir system of Microbial concentration.

The convergence rates reported in Tables 6.3 and 6.4 are verified in the error plot as depicted in Figure 6.2.4.

The above numerical results could be considered as a showcase to validate our discretization scheme and Matlab code implementation.

Chapter 7

Optimal Control Theory

Developments of this chapter are based on the Book [6] and studies maximum principles of constrained optimal control policies. Thus, the results will be used to have an approximate information in order to control the microbial injection strategy of microbial EOR processes. PDE constrained optimal control problem has been addressed in either optimize then discretize or discretize then optimize. Computational results for both approaches are essentially the same for sufficiently small time step $\triangle t$, and the proper finite differences of the differential equations.

Often it is preferable to follow discretize then optimization procedure for PDE constrained optimization formulations rather than optimization then discretization approach. those of enhanced oil recovery. Thus, we go further for discretize then optimization approach to develop maximum principles for PDE constrained optimization problems. As a consequence, this chapter introduces properties and preliminary concepts of discrete optimal control problems.

7.1 Extremal of Functionals and The Fundamental Theorem of Variational Calculus

First of all, let us develop the first order variation of a functional:

$$J = \int_0^{t_f} F(z(t), \dot{z}(t), t)dt. \tag{7.1.1}$$

Assume that the functional F and the function z are well behaved, i.e., $z(t) \in C^1[0, t_f]$ and F is once continuously differentiable with respect to z and $\dot{z}$.

Now let us define the increment of the functional J as follows,

$$\triangle J = \int_0^{t_f} [F(z + \delta z, \dot{z} + \delta \dot{z}, t) - F(z(t), \dot{z}(t), t)]dt. \tag{7.1.2}$$

Then, we can have the first order Tylor's expansion of $F(z+\delta z, \dot{z}+\delta\dot{z}, t)$ around the origin by truncating the higher order terms,

$$F(z+\delta z, \dot{z}+\delta\dot{z}, t) = F(z, \dot{z}, t) + \frac{\partial F}{\partial z}\delta z + \frac{\partial F}{\partial \dot{z}}\delta\dot{z}. \tag{7.1.3}$$

Rearranging (7.1.3) would give the increment of the functional as follows;

$$\delta J = \int_0^{t_f} [\frac{\partial F}{\partial z}\delta z + \frac{\partial F}{\partial \dot{z}}\delta\dot{z}]dt. \tag{7.1.4}$$

The increment functional (7.1.4) is linear with respect to δz and δz and referred to as the first variation of the functional J.

Definition 7.1.1 *i. A functional J attains a relative minimum at z^* if*

$$\triangle J = J(z) - J(z^*) \geq 0 \tag{7.1.5}$$

for all $z \in \Omega$ such that $\|z - z^*\| < \epsilon$, where, ϵ is small positive real number.

ii. Similarly, a functional J is said to have a relative maximum at z^* if,

$$\triangle J = J(z) - J(z^*) \leq 0 \tag{7.1.6}$$

for all $z \in \Omega$, provided that there exists a small positive number ϵ such that $\|z - z^*\| < \epsilon$.

The functional J is said to have an absolute or global maximizer z^*, if inequality (7.1.5) is satisfied for arbitrarily large ϵ. On the other hand, the functional J is said to have an absolute or global maximum at z^*, if z^* satisfies inequality (7.1.6) for large ϵ. The functional J is said to have global maximizer or minimizer, if the functional J is strictly convex and at least once continuously differentiable.

Theorem 7.1.2 *[6] (Fundamental Theorem of Variational Calculus): If z^* is a minimizer/maximizer of a functional J, it is necessary that the first variation of J must vanish on z, i.e.,*

$$\delta J(z^*, \delta z) = 0, \tag{7.1.7}$$

for all δz such that $z + \delta z \in \Omega$.

7.2 Optimal Control Problem Formulation

In this chapter we will see investigations to determine the control policy that extremize (maximize/minimize) a specific performance criterion, subject to the constraints imposed by physical nature of the problem. Researchers in applied science, [6, 66] have been using Pontryagin maximum principle [65], to handle these kind of optimization problems.

Optimal control policies arises in diverse field of studies like reservoir (EOR process) and control (transportation problem) engineering/mathematics to list few. The controls associated with EOR processes are physical state histories of the injected fluids. In other word, EOR process is concerned with the determination of

injection policies that lead to a maximum production of oil with minimum cost of injected fluids, subject to differential equations that describe the flow dynamics. In this particular study, the constraint set consists of conservation models needed to specify the dynamic state of the process given by microbial distributions, and fluid saturations. The conservation equation in its general form can be written as:

$$\dot{z} = f(z, \nabla z, \nabla^2 z, v), \tag{7.2.1}$$

where z is a state vector, v is a vector of controls that enter the problem over the volumetric domain, ∇ is the gradient operator that describes the convective flow effects, ∇^2 is the Laplacian operator that describes the dispersion or diffusion effects, and f defines for the set of nonlinear functions that represents the conservation relation. In our case z could be a combination of pressure, saturation and component bacteria concentrations.

Initial and boundary constraints should also be specified, and can be given by,

$$\begin{aligned} g(z, \nabla z, u) &= 0 \quad \text{on} \quad \partial\Omega \\ z &= z_0, \quad \text{at} \quad \text{t} = 0, \end{aligned} \tag{7.2.2}$$

where u is a vector of controls that enter into the system through the boundary of the system domain.

A performance functional is considered to be in the class of algebraic functionals in which its general form can be described as,

$$J = \int_0^{t_f} F_1(z(\partial\Omega), u(t))dt + \int_0^{t_f} \int_\Omega F_2(z(\Omega, t), v(\Omega, t), t)dAdt, \tag{7.2.3}$$

where F_1-represents the boundary contribution to the performance equation, whereas, F_2-represents the contribution through the volume domain.

Summing up the above equations in (7.2.1), (7.2.2) and (7.2.3) will give the following optimal control problem;

$$\begin{aligned} \max & \int_0^{t_f} F_1(z(\partial\Omega), u(t))dt + \int_0^{t_f} \int_\Omega F_2(z(\Omega, t), v(\Omega, t), t)dAdt \\ \text{S.t.} \;& \dot{z} = f(z, \nabla z, \nabla^2 z, v) \\ & g(z, \nabla z, u) = 0 \quad \text{on} \quad \partial\Omega \\ & z = z_0, \quad \text{at} \quad \text{t} = 0. \end{aligned} \tag{7.2.4}$$

The aim of this thesis is to determine, the control variables u and v that maximizes the objective function and satisfies the constraint conditions. To solve problem (7.2.4), one can apply either discretize then optimize (direct method) or optimize then discretize (indirect method). This thesis applies discretize then optimize approach. Thus, we need to study the discrete maximum principle. The discrete maximum principle would be equivalent to continuous maximum principle for small time step, see [6].

7.3 Discrete Maximum Principle

As can be seen in chapter 4, the flow and transport models can be approximated as a set of non-linear discrete algebraic equations by the help of finite volume methods. These algebraic systems could result in either explicit or implicit form depending on the temporal discretization. The explicit form can be given as,

$$z_{n+1} = f(z_n, u_n) \tag{7.3.1}$$

and the implicit form,

$$f(z_{n+1}, z_n, u_n) = 0, \tag{7.3.2}$$

where z_{n+1} are state variables evaluated at the new time level and u_n are the control variables evaluated at the old time level n.

The discrete performance function can be given as,

$$J = \sum_{n=0}^{N-1} F(z_n, u_n, v_n). \tag{7.3.3}$$

Thus, we can have either explicit optimal control problem

$$\begin{aligned} \max & \sum_{n=0}^{N-1} F(z_n, u_n, v_n) \\ & \text{S.t. } z_{n+1} = f(z_n, u_n), \end{aligned} \tag{7.3.4}$$

or implicit optimal control problem,

$$\begin{aligned} \max & \sum_{n=0}^{N-1} F(z_n, u_n, v_n) \\ & \text{S.t. } f(z_{n+1}, z_n, u_n) = 0. \end{aligned} \tag{7.3.5}$$

The necessary conditions for extremal of both (either explicit or implicit) discrete optimal control problems can be proposed using the discrete maximum principle of Pontryagin [65]. The Pontryagin maximum principle reduces the optimal control problem (7.3.4) and (7.3.5) into state, costate and optimal control models. The state models are equivalent to the discretized reservoir model whereas the costate model are used to obtain the costate functions. See the following consecutive subsections for further information and how to develop state, costate and control models. Though we considered the boundary and volumetric controls above, the interest of this thesis will end up without the contributions from the boundary controls.

7.3.1 Necessary Conditions for Explicit Discretization

This section discusses finding on admissible sequence of controls so that it maximizes/minimizes the explicit optimal control problem (7.3.4). In order to obtain the required controls, we need to have at least the

necessary conditions for the control vectors be a maximizer or minimizer of the given optimization problem. To do so, let us form the augmented performance function which includes the constraint equations and can be given as,

$$J_A = \sum_{n=0}^{N-1} \Big\{ F(z_n, u_n) - \lambda_{n+1}(z_{n+1} - f(z_n, u_n)) \Big\}, \tag{7.3.6}$$

where λ_{n+1} are the costate variables.

One can easily notice that the augmented performance function (7.3.6) is equivalent to the objective function of problem (7.3.4), when the state constraints are satisfied. In other word, the augmented performance function (7.3.6) has the same extremal (i.e., maximum or minimum) as the performance function (7.3.4), when the constraint set of problem (7.3.4) is satisfied.

The Hamiltonian of problem (7.3.4) can be defined as

$$H_n = F(z_n, u_n) - \lambda_{n+1} f(z_n, u_n). \tag{7.3.7}$$

Thus, the augmented performance function (7.3.6) can be rewritten as

$$J_A = \sum_{n=0}^{N-1} H_n - \lambda_{n+1} z_{n+1} \tag{7.3.8}$$

and the first variation of J_A is given as,

$$\delta J_A = \sum_{n=0}^{N-1} \frac{\partial H_n}{\partial z_n} \delta z_n - \sum_{n=0}^{N-1} \lambda_{n+1} \delta z_{n+1} + \sum_{n=0}^{N-1} \frac{\partial H_n}{\partial u_n} \delta u_n + \sum_{n=0}^{N-1} [\frac{\partial H_n}{\partial \lambda_{n+1}} - z_{n+1}] \delta \lambda_{n+1}. \tag{7.3.9}$$

To have the new costate variable λ_n, the variations δz_{n+1} and δz_n can be related as follows,

$$-\sum_{n=0}^{N-1} \lambda_{n+1} \delta z_{n+1} = -\sum_{n=1}^{N} \lambda_n \delta z_n. \tag{7.3.10}$$

Rearranging the right hand side of equation (7.3.10), and substituting the result into (7.3.9) will give,

$$\delta J_A = \lambda_0 \delta z_0 + \sum_{n=0}^{N-1} [\frac{\partial H_n}{\partial z_n} - \lambda_n] \delta z_n + \sum_{n=0}^{N-1} \frac{\partial H_n}{\partial u_n} \delta u_n + \sum_{n=0}^{N-1} [\frac{\partial H_n}{\partial \lambda_{n+1}} - z_{n+1}] \delta \lambda_{n+1} - \lambda_N \delta z_N \tag{7.3.11}$$

Fundamental Theorem of variational calculus states that for $z(t)$ to be the minimizer/maximizer of the functional J_A, it is necessary to have,

$$\delta J_A = 0. \tag{7.3.12}$$

If the control and state variables are unbounded, the variations δz, $\delta \lambda$ and δu are free and unconstrained. The necessary conditions for an extremal of explicit control problem (7.3.4) are therefore,

- **State Model:** since the variation $\delta \lambda_{n+1}$ is free,

$$\frac{\partial H_n}{\partial \lambda_{n+1}} - z_{n+1} = 0 \tag{7.3.13}$$

- **Costate Model:** since the state variation δz_n is free,

$$\frac{\partial H_n}{\partial z_n} - \lambda_n = 0 \tag{7.3.14}$$

- **Transversality Condition:** since the state variations δz_N and δz_0 are independent, we have

$$\text{Final transversality:} \lambda_N \cdot \delta z_N = 0 \tag{7.3.15}$$

and

$$\text{Initial transversality:} \lambda_0 \cdot \delta z_0 = 0 \tag{7.3.16}$$

- **Optimal Control:** If the control is on the constraint boundary of the admissible set U, then the necessary condition for a maximum is,

$$\sum_{n=0}^{N-1} \frac{\partial H_n}{\partial u_n}^{\mathrm{T}} \delta u_n \leq 0 \tag{7.3.17}$$

and the condition for a minimum is

$$\sum_{n=0}^{N-1} \frac{\partial H_n}{\partial u_n}^{\mathrm{T}} \delta u_n \geq 0. \tag{7.3.18}$$

When the control variable does not lie on the boundary of the admissible set U then δu_n is considered to be a free variation, and therefore,

$$\frac{\partial H_n}{\partial u_n} = 0. \tag{7.3.19}$$

7.3.2 Necessary Conditions for Implicit Discretization

An implicit discretization of the form (7.3.2) has been arising so frequently in numerical simulation of real life applications. For instance, we have developed an implicit form for average pressure, water phase saturation and component transport equations, see chapter 4. To have an optimal admissible sequence of controls $u \in U$, we need to develop the necessary conditions for extremal of the functional:

$$J = \sum_{n=0}^{N-1} F(z_n, u_n), \tag{7.3.20}$$

subject to the implicit flow constraint (7.3.2). To develop the maximum principle for such optimization problem, we form the augmented performance functional,

$$J_A = \sum_{n=0}^{N-1} \left\{ F_n(z_n, u_n) + \lambda_{n+1}^{\mathrm{T}} f_n(z_{n+1}, z_n, u_n) \right\}. \tag{7.3.21}$$

Then the first variation of J_A, i.e., $\delta J_A = 0$, gives the necessary condition for an extremal of the function J_A, if the control variable u is unconstrained, whereas if u is constrained and lies on the boundary of the constraint, the necessary condition for u to be a maximum is $\delta J_A \leq 0$.

For the sake of clarity and ease the manipulation, let us define the Hamiltonian for the augmented performance functional as

$$H_n(z_{n+1}, z_n, \lambda_{n+1}, u_n) = F_n(z_n, u_n) + \lambda_{n+1}^{\mathrm{T}} f_n(z_{n+1}, z_n, u_n). \tag{7.3.22}$$

Then, the augmented functional (7.3.21) can be rewritten as

$$J_A = \sum_{n=0}^{N-1} H_n(z_{n+1}, z_n, \lambda_{n+1}, u_n). \tag{7.3.23}$$

Thus, the first order variation of (7.3.23) is given as

$$\delta J_A = \sum_{n=0}^{N-1} (\frac{\partial H_n}{\partial z_{n+1}})^{\mathrm{T}} \delta z_{n+1} + \sum_{n=0}^{N-1} (\frac{\partial H_n}{\partial z_n})^{\mathrm{T}} \delta z_n + \sum_{n=0}^{N-1} (\frac{\partial H_n}{\partial \lambda_{n+1}})^{\mathrm{T}} \delta \lambda_{n+1} + \sum_{n=0}^{N-1} (\frac{\partial H_n}{\partial u_n})^{\mathrm{T}} \delta u_n \tag{7.3.24}$$

Now to come up with consistent state indexing in the variation above, we need to rewrite the sum

$$\sum_{n=0}^{N-1} (\frac{\partial H_n}{\partial z_{n+1}})^{\mathrm{T}} \delta z_{n+1},$$

in other but, equivalent way as

$$\sum_{n=0}^{N-1} (\frac{\partial H_n}{\partial z_{n+1}})^{\mathrm{T}} \delta z_{n+1} = (\frac{\partial H_{N-1}}{\partial z_N})^{\mathrm{T}} \delta z_N - (\frac{\partial H_{-1}}{\partial z_0})^{\mathrm{T}} \delta z_0 + \sum_{n=0}^{N-1} (\frac{\partial H_{n-1}}{\partial z_n})^{\mathrm{T}} \delta z_n. \tag{7.3.25}$$

We have substituted the expression (7.3.25) into the augmented variational form (7.3.24) to obtain

$$\begin{aligned} \delta J_A = {} & (\frac{\partial H_{N-1}}{\partial z_N})^{\mathrm{T}} \delta z_N - (\frac{\partial H_{-1}}{\partial z_0})^{\mathrm{T}} \delta z_0 + \\ & \sum_{n=0}^{N-1} (\frac{\partial H_{n-1}}{\partial z_n})^{\mathrm{T}} \delta z_n + \sum_{n=0}^{N-1} (\frac{\partial H_n}{\partial z_n})^{\mathrm{T}} \delta z_n + \sum_{n=0}^{N-1} (\frac{\partial H_n}{\partial \lambda_{n+1}})^{\mathrm{T}} \delta \lambda_{n+1} + \sum_{n=0}^{N-1} (\frac{\partial H_n}{\partial u_n})^{\mathrm{T}} \delta u_n. \end{aligned} \tag{7.3.26}$$

The sequence u_n defined inside the admissible control set U_{adm} is said to be a local maximizer, it is necessary that the first variation of the augmented performance function attains zero at each u_n, i.e., $\delta J_A = 0$, and the Pontrygian's maximum principle states that if u_n maximizes the performance function, it has to maximizes the Hamiltonian function H_n, which defines the following models,

- **State Model:** since the variation $\delta \lambda_{n+1}$ is free,

$$\frac{\partial H_n}{\partial \lambda_{n+1}} = 0 \rightleftharpoons f(z_{n+1}, z_n) = 0 \tag{7.3.27}$$

- **Costate Model:** since, the state variation δz_n is free,

$$\frac{\partial H_n}{\partial z_n} + \frac{\partial H_{n-1}}{\partial z_n} = 0 \tag{7.3.28}$$

- **Transversality Condition:** Since the state variations δz_N and δz_0 are independent, we have

$$\text{Final transversality:}(\frac{\partial H_{N-1}}{\partial z_N})^{\mathrm{T}}\delta z_N = 0 \tag{7.3.29}$$

and

$$\text{Initial transversality:}(\frac{\partial H_{-1}}{\partial z_0})^{\mathrm{T}}\delta z_0 = 0. \tag{7.3.30}$$

- **Optimal Control:** If the control is on the constraint boundary of the admissible set U, then the necessary condition for a maximum is

$$\sum_{n=0}^{N-1} \frac{\partial H_n}{\partial u_n}^{\mathrm{T}} \delta u_n \leq 0 \tag{7.3.31}$$

and the condition for a minimum is

$$\sum_{n=0}^{N-1} \frac{\partial H_n}{\partial u_n}^{\mathrm{T}} \delta u_n \geq 0. \tag{7.3.32}$$

When the control variable does not lie on the boundary of the admissible set U then δu_n is considered to be a free variation and therefore,

$$\frac{\partial H_n}{\partial u_n} = 0. \tag{7.3.33}$$

Though we have seen the maximum principles for explicit and implicit discrete optimal control problems separately, we may integrate these results in Chapter 8 to optimize a microbial EOR processes for which, we adopt an iterative linearization method and gradient accent (classical optimization method) optimization approach to address the discretized optimization problem.

Chapter 8

Economic Mathematical Modeling for 2D Microbial EOR

The main task regarding slug injection design is investigating a way to mobilize the residual oil as much as possible. Though a high injection concentration has been the basis for slug design in most microbial EOR processes, it is reported in [11] that slug size has negligible effect on oil recovery. Since oil reservoir is full of factors that affect the activity of microbes, slug injection strategy needs detail investigations in laboratory experiments and simulation models. To the best of the author's knowledge, there is no literature to suggest the best slug injection strategies for microbial EOR processes. The course of this chapter aims to investigate a mathematical model that determines the best possible way of injection policies to lower the residual oil while maximizing oil production via reduction of IFT mechanism. Though we concentrate on IFT reduction mechanism, microbial EOR processes have many mechanisms (like selective plugging by bacteria and their metabolites, viscosity reduction by gas production or degradation of long-chain saturated hydrocarbons to name a few) that contribute for residual oil recovery.

8.1 Mathematical Model for Production-Injection Wells

Since oil reservoir fields are considered to be large enough in size, we can consider wells as a source or sink models instead of boundary models. In Chapter 3, we have formulated a two-phase Darcy's flow and advection-dispersion reactive transport models. Moreover, we have coupled these flow and transport models to predict the activity of microbial concentration in oil reservoir environment. In this section, we will introduce mathematical models for production and injection wells being used as source/sink terms to the microbial EOR process model. Microbial EOR process has been performed by injecting water, microbial concentration and nutrients through injection wells and the growth of microbes produce bio-surfactant that helps to mobilize residual oil. Let us assume, we have I-number of injection wells and P-number of production

wells. Thus, the total injection and production volumetric flow rates can be described as:

$$Q_{\mathrm{w}}^{\mathrm{in,T}} = \sum_{I} Q_{\mathrm{w}}^{\mathrm{in,I}}, \text{ and } Q_{\mathrm{c}}^{\mathrm{in,T}} = \sum_{I} Q_{\mathrm{c}}^{\mathrm{in,I}},$$
$$Q_{\mathrm{w}}^{\mathrm{out,T}} = \sum_{I} Q_{\mathrm{w}}^{\mathrm{out,I}}, \text{ and } Q_{\mathrm{o}}^{\mathrm{out,T}} = \sum_{P} Q_{\mathrm{o}}^{\mathrm{out,P}}, \tag{8.1.1}$$

where $Q_{\mathrm{o}}^{\mathrm{out}}$, $Q_{\mathrm{w}}^{\mathrm{out}}$ and $Q_{\mathrm{c}}^{\mathrm{out}}$ stand for outflow volumetric rates of oil, water and microbial concentration respectively whereas Q_{w}^{in}, and Q_{c}^{in} stands for inflow volumetric rates of water and microbial concentration respectively. Furthermore, we assume that each well located at the node/grid points of control volumes. This makes the well model coincide with the discrete microbial EOR equations.

8.1.1 Performance of Production Wells

A well allows a fluid to be injected into oil reservoir and conversely, it has been used to extract fluids from subsurface. Wells have been drilled either vertically or horizontally. Without loss of generality let us consider vertically drilled wells for this particular study. For such wells, fluids flow radially in the formation [1]. To the best of the author's knowledge mathematical representation of wells determines the well as a separate structure and not part of the reservoir models. The vertical flow performance could be used to describe the relation between the bottom-hole pressure of a well and surface production rate. We can assume that a volumetric flow rate is proportional to the difference between the phase reservoir pressure, $P_{\alpha}^{\mathrm{cell}}$, in the grid cell and the bottom-hole pressure, P_{b}, in the well as follows

$$Q_{\alpha}^{\mathrm{out}} = PI(P_{\alpha}^{\mathrm{cell}} - P_{\mathrm{b}}), \tag{8.1.2}$$

where PI is production performance index.

To obtain a mathematical model for PI, we have done dimension reduction only on the control volume where the production well is located by assuming fluids flow horizontally and radially. Based on this assumption the Darcy's law for two-phase flow in differential form becomes

$$q_{\alpha} = -K\frac{K_{r\alpha}}{\mu_{\alpha}}\frac{dP_{\alpha}}{dr}. \tag{8.1.3}$$

But, the volumetric flow rate has been modeled as

$$\frac{Q_{\alpha}^{\mathrm{out}}}{2\pi rh} = q_{\alpha}, \tag{8.1.4}$$

where r is radius and h is piezometric hight.

Combining equations (8.1.3) and (8.1.4) give us the following relation

$$\frac{Q_{\alpha}^{\mathrm{out}}}{2\pi rh} = -K\frac{K_{r\alpha}}{\mu_{\alpha}}\frac{dP_{\alpha}}{dr}. \tag{8.1.5}$$

Now we can integrate equation (8.1.5) as follows

$$\int_{r_w}^{r_{\mathrm{cell}}} \frac{Q_{\alpha}^{\mathrm{out}}}{2\pi rh} dr = -\int_{P\mathrm{b}}^{P_{\alpha}^{\mathrm{cell}}} K\frac{K_{r\alpha}}{\mu_{\alpha}} dP_{\alpha}, \tag{8.1.6}$$

where r_w is wellbore radius, $r_{\text{cell}} \simeq 0.14\sqrt{\triangle x^2 + \triangle y^2}$ for isotropic medium [67], and P_α^{cell} is phase pressure at the grid cell where the associated well is installed.

After integrating equation (8.1.6), we have the following relation,

$$\frac{Q_\alpha^{\text{out}}}{2\pi h} \ln\left(\frac{r_{\text{cell}}}{r_w}\right) = -K\frac{K_{r\alpha}}{\mu_\alpha}\left(P_\alpha^{\text{cell}} - P_{\text{b}}\right). \tag{8.1.7}$$

Rearranging equation (8.1.7), will give us the following performance index, PI

$$\frac{Q_\alpha^{\text{out}}}{P_\alpha^{\text{cell}} - P_{\text{b}}} = -K\frac{K_{r\alpha}2\pi h}{\mu_\alpha \ln\left(\frac{r_{\text{cell}}}{r_w}\right)}. \tag{8.1.8}$$

Since we are developing model for production wells, we don't like dragging minus signs around all the time, the performance index is almost always defined as,

$$\frac{Q_\alpha^{\text{out}}}{P_\alpha^{\text{cell}} - P_{\text{b}}} = K\frac{K_{r\alpha}2\pi h}{\mu_\alpha \ln\left(\frac{r_{\text{cell}}}{r_w}\right)} \tag{8.1.9}$$

The performance mathematical model of production well (8.1.9) is developed using phase pressure. However, we have used average pressure formulation for reservoir models in previous chapters. To be consistent with the formulated microbial EOR process model, we should rewrite the mathematical well performance model in terms of average pressure, P_{av}, as follows

$$\begin{cases} Q_{\text{o}}^{\text{out}} = K\frac{2\pi h K_{ro}}{\mu_\alpha \ln\left(\frac{r_{\text{cell}}}{r_w}\right)}(P_{\text{av}} + \frac{1}{2}P_c(S_w, C) - P_{\text{b}}), \\ Q_{\text{w}}^{\text{out}} = K\frac{2\pi h K_{rw}}{\mu_\alpha \ln\left(\frac{r_{\text{cell}}}{r_w}\right)}(P_{\text{av}} - \frac{1}{2}P_c(S_w, C) - P_{\text{b}}), \\ Q_{\text{c}}^{\text{out}} = CQ_w^{\text{out}}. \end{cases} \tag{8.1.10}$$

Here again the average pressure, capillary pressure and relative permeabilities are evaluated at the node/grid point of a control volume for which the associated well is located. The compatibility of formulation (8.1.10) with the formulated microbial EOR mathematical model makes the well performance model more interesting for further investigation and easily inserted into the flow model as a source or sink terms.

8.2 Introducing Wells to the Coupled Microbial EOR Model

In previous sections, we were dealing with mathematical models for production wells and microbial EOR processes in separate sheet. Since the aim of this thesis is to increase sweep efficiency via controlling the injection strategy, we need to integrate the microbial EOR system with these well models.

Let us recall the coupled reservoir model as follows without boundary conditions to make the presentation clear and understandable

$$\begin{cases} -\nabla \cdot K(\lambda_t(S_w, C)\nabla P_{\text{av}} + \frac{1}{2}\lambda_d(S_w, C)\nabla P_c(S_w, C)) = F_t & \text{in } \Omega, \\ \phi\frac{\partial(S_w)}{\partial t} - \nabla \cdot (\lambda_w(S_w, C)\nabla P_{\text{av}} + \frac{1}{2}P_c(S_w, C)) = \frac{F_w}{\rho_w} & \text{in } \Omega, \\ \phi\frac{\partial(SC)}{\partial t} + \nabla \cdot (-D\nabla(\phi SC) + q_w C) = Q & \text{in } \Omega. \end{cases} \tag{8.2.1}$$

Here, $F_t = \frac{F_w}{\rho_w} + \frac{F_o}{\rho_o}$, where, F_w is a source/sink term associated with water phase saturation. Similarly, F_o is source/sink term for non-wetting phase saturation and Q represents source/sink term for microbial concentration.

Based on the developments above, we have two slug injection variables, volumetric inflow rates of water and microbial concentration, and three outgoing variables namely water, microbial concentration and oil. In this thesis, the injection variables are considered to be control/input variables in order to control the supply of microbes and water for which we hope to mobilize the residual oil efficiently. On the other hand, the volumetric production rates are determined by state/reservoir variables. As a result, the coupled microbial EOR system (8.2.1) can be modified to give

$$\begin{cases} -\nabla \cdot K(\lambda_t(S_w, C)\nabla P_{\text{av}} + \frac{1}{2}\lambda_d(S_w, C)\nabla P_c(S_w, C)) = -\sum_P (Q_o^{\text{out},P} + Q_w^{\text{out},P}) + \sum_I Q_w^{\text{in},I} & \text{in } \Omega, \\ \phi\frac{\partial(S_w)}{\partial t} - \nabla \cdot (\lambda_w(S_w, C)\nabla P_{\text{av}} + \frac{1}{2}P_c(S_w, C)) = -\sum_P Q_w^{\text{out},P} + \sum_I Q_w^{\text{in},I} & \text{in } \Omega, \\ \phi\frac{\partial(SC)}{\partial t} + \nabla \cdot (q_w C - D\nabla(\phi SC)) = \sum_I Q_w^{\text{in},I} Q_c^{\text{in},I} + \sum_P C Q_w^{\text{out},P} & \text{in } \Omega, \end{cases} \tag{8.2.2}$$

where Q's are as in Section 8.1. Here, one can consider wellbore pressure as a control variable. However, we assume that the wellbore pressure can be adjusted so that the well potential is maximum. Moreover, it is assumed that the initial and boundary conditions of the described mathematical model above (8.2.2) are known. In general, boundary conditions are determined from the reservoir geometry and the distribution of injection and production wells. We consider injection and production wells are installed inside the reservoir domain. The above developments represent constraint sets that has to be satisfied while we are in search of cost efficient injection strategies.

8.2.1 Numerical Simulation for the Integrated Models of Wells and Microbial EOR

In subsection 6.2.1, we have shown a validation test for the coupled flow and transport reservoir model by introducing a simple IFT model in the van Genutchen capillary pressure parametrization. In this section, we will see the effect of injected microbial concentration on the residual oil by IFT reduction mechanism. Without loss of generality, we consider one injection well and one production well for this particular simulation. In this thesis, we assume that the microbes are injected with water simultaneously. Moreover, we used the modified van Genutchen parameterizations given in Section 6.1.1 for which the effect of microbial growth on the reduction of IFT has been fully described.

Table 8.1 summarizes fluid and rock properties being used to simulate the integrated microbia EOR processes. Note that the parameters listed in Table 8.1 are academic and may not be physical.

8.2.1.1 The Effect of Pure Water Injection

Assume the reservoir pressure is not able to drive fluids to the wellbore and the initial reservoir comprises 40% crude oil and 60% water with no microbial concentration. Here we inject water to maintain the

Parameter	value	Parameter	value
Ω	$[0,1] \times [0,1]$	P_b	0.3
t	$[0,1]$	$\frac{r_{\text{cell}}}{r_w}$	1
K	1	h	$\frac{1}{2\pi}$
μ_o	1	μ_w	1
ρ_o	1	ρ_w	1
σ_0	0.40	P_e	1
$\sigma_{\min}$	0.06	β_3	0.05
β_1	0.5	β_2	3
D	1	ϕ	1

Table 8.1: Parameters used to simulate the coupled model reservoir.

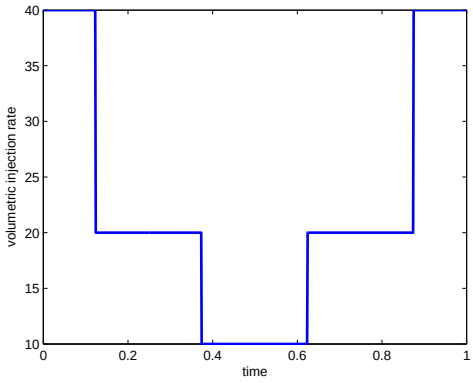

Figure 8.2.1: Initial Water injection strategy.

reservoir pressure and the injection strategy follows as shown in Figure 8.2.1. This injection strategy gives the final time reservoir profile as shown in Figure 8.2.2. Here, the injected water plays an important role to displace the trapped oil nearby the injection well. However, when we go far away from the injection well, the injected water has little contribution in displacing the the trapped oil. This suggests that design of production/injection wells installation is crucial in order to drive out the residual oils.

8.2.1.2 The Effect of Water and Microbes Injection

We used the results in Figure 8.2.2 as reservoir initial condition to see the effect of microbial activity after water flooding. In this test case, we introduce microbes into the reservoir by injecting water and microbial concentration simultaneously. Figure 8.2.3 describes the initial injection strategy of water and microbial concentration. Based on this injection policy, we have obtained a final time reservoir condition as shown in Figure 8.2.4 for average pressure, water, oil and microbial concentration distributions. As shown in Figure 8.2.4, the microbial concentration profile is very low inside the reservoir. This might be caused by either the parameters used for this simulation didn't allow the microbes growth or the water velocity is high to

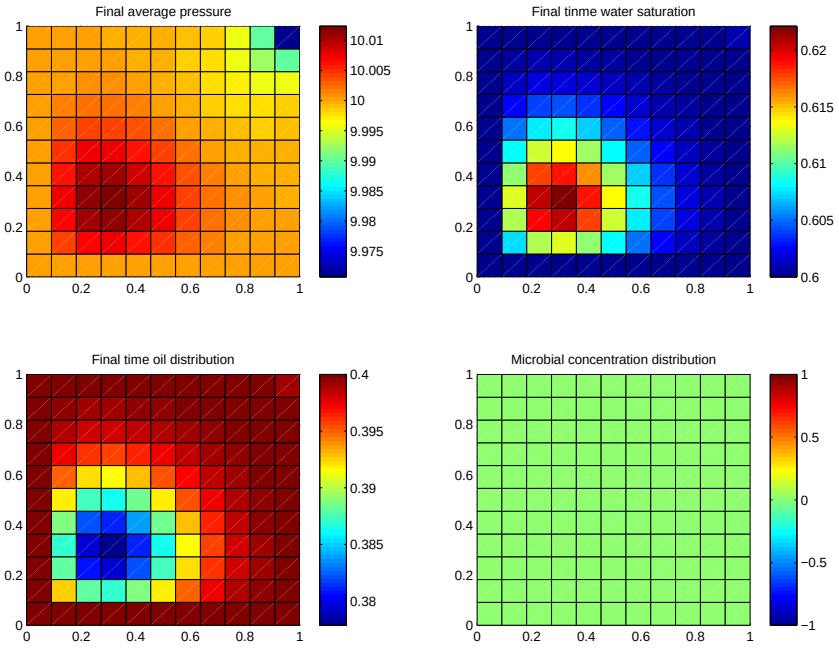

Figure 8.2.2: Final Reservoir Profile for water injection.

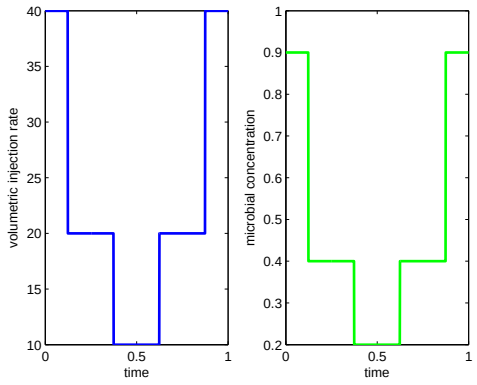

Figure 8.2.3: Injection policy for water (left) and microbial concentration (right).

transport microbes and drive out through production well without functioning. Moreover, the residual oil profile in Figure 8.2.4 is slightly reduced as compared to the residual oil distribution in Figure 8.2.2, which means the injected microbes had a little contribution to the reservoir system in this simulation. This may also affect the optimization process significantly. Because, the IFT and relative permeabilities remain unchanged with this negligible microbial concentration.

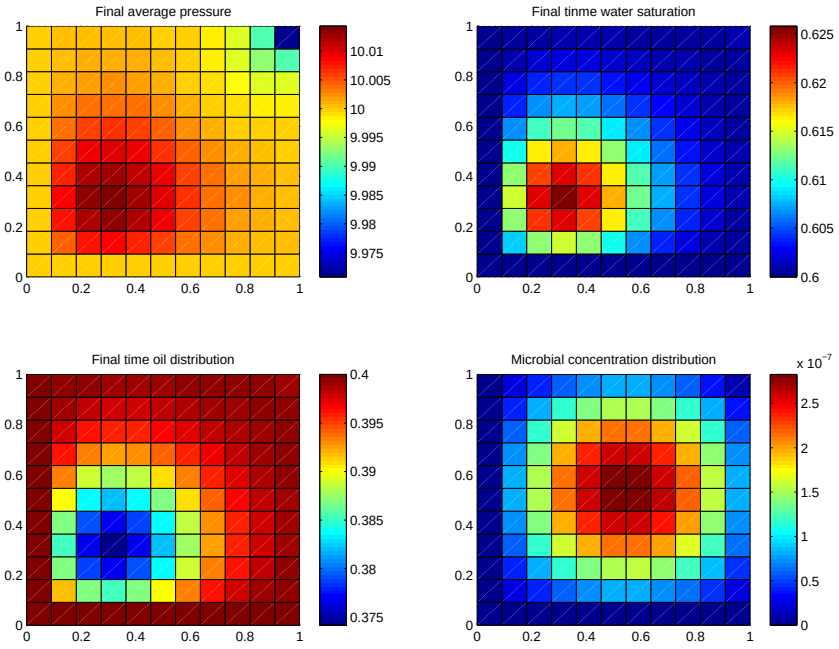

Figure 8.2.4: Final time reservoir condition for water and microbial concentration injection.

8.3 Slug Size Injection Strategy

Slug injection policies have been playing an important role to mobilize the residual oil via reduction of capillary forces. Since the injection mechanism includes different slug size, composition and component mass fraction of concentrations, it is difficult and most challenging to optimize microbial EOR processes. We aim to design injection policies that minimizes the residual oil and cost of injected fluids while maximizing production yields. Though small costs have their own effect in optimization process, cost of water is assumed to be negligible and thus, zero. Thus, the cost functional for which we need to care about can be described as follows,

$$\begin{aligned} J = \text{cost of produced oil } + \text{ cost of produced microbila concentration concentration} \\ - \text{ cost of mass fraction of injected concentration.} \end{aligned} \tag{8.3.1}$$

The cost function (8.3.1) can be rewritten in mathematical language as follows,

$$J = \sum_{P} \int_0^T (O_{\mathrm{c}} Q_o^{\mathrm{out,P}} + C_{\mathrm{c}} C Q_w^{\mathrm{out,P}}) dt - \sum_{I} \int_0^T C_{\mathrm{cin}} Q_c^{\mathrm{in,I}} Q_w^{\mathrm{in,I}}, \tag{8.3.2}$$

where O_{c}, C_{c}, and C_{cin} are costs associated with produced oil, produced microbial concentration, and injected microbes respectively in Norwegian Kroner (NOK).

Non-dimensional form of cost functional (8.3.2) can be obtained as

$$J = \sum_{P} \int_0^T (Q_o^{\text{out,P}} + R_{\text{c}} C Q_w \text{out}, \text{P}) dt - \sum_{I} \int_0^T R_{\text{cin}} Q_c^{\text{in,I}} Q_w^{\text{in,I}}, \tag{8.3.3}$$

where R_{c} and R_{cin} are cost ratios. The performance functional (8.3.3) determines the maximum potential of microbial effect to mobilize the trapped oil while maximizing the profit. We are in search of injection policies that lowers the residual oil, provided that these injection policies and reservoir variables have to satisfy the reservoir model (8.2.2). The discussion above gives us continuous economic model for efficient microbial EOR processes. In the maximization formulation (8.3.3), the cost of microbes is measured with NOK/Kg whereas the cost of oil is measured with NOK/m^3.

The resulting microbial EOR optimization model is not amenable to analytical solutions. As a consequence, it must be treated numerically. Since we are following discretization then optimization methods, the formulated optimal control strategy will be discretized in the same fashion as we discussed in Chapter 4. Then iterative linearization followed by optimization methods will be applied.

8.4 Numerical Optimization Methods and Results

Due to the inclusion of specifications, varying parameters, uncertainties, limited resources and history dependent property of real life problems, mathematical models from engineering and applied science disciplines arise with high degree of complexity. Moreover, adding economical aspects further increase the difficulty of the simulation models. Thus, they become complex and challenging to solve. For instance, the above formulated microbial EOR is highly nonlinear and impossible to give qualitative analysis. As a consequence, numerical optimization methods should be used for the formulated optimization problem to predict the optimal injection variables. There are plenty of numerical optimization methods to handle problems ranging from unconstrained linear optimization problem to chance constrained optimal control formulations. Among these deterministic methods are popular and accepted specially for smooth optimization problems. For instance, we will combine an iterative linearization method for two-phase flow problems and gradient/steepest accent method for standard non-linear optimization to solve the formulated optimization model of microbial EOR processes.

8.4.1 Maximum Principle and Solution Algorithm

We have discretized flow and transport equations in Chapter 4, but we have continuous performance function in this chapter. To be consistent with the discretized version of flow and transport equations, we can also discretize the performance functional using midpoint rule for numerical integration. Since some terms in the objective functional as well as source/sink terms assumed to be located on the grid points of the cell, we do not need to integrate them with respect to space. The objective functional (8.3.3) is discretized in time to

give the following discrete performance model

$$J_{\text{dis}} = \sum_{P}\sum_{n=0}^{\mathrm{n_f}}[Q_{o,n}^{\text{out,P}} + R_c(CQ)_{w,n}^{\text{out,P}}]\triangle t - \triangle t\sum_{I}\sum_{n=0}^{\mathrm{n_f}} R_{\text{cin}}Q_{c,n}^{\text{in,I}}Q_{w,n}^{\text{in,I}}, \tag{8.4.1}$$

where $\mathrm{n_f}$ is the number of iterations in time.

Now we have discrete optimal control formulation for microbial EOR processes which can be rewritten as follows,

$$\begin{aligned}\max &\sum_{P}\sum_{i=0}^{\mathrm{n_f}}[Q_{o,n}^{\text{out,P}} + R_c(CQ)_{w,n}^{\text{out,P}}]\triangle t - \triangle t\sum_{I}\sum_{i=0}^{\mathrm{n_f}} R_{\text{cin}}Q_{c,n}^{\text{in,I}}Q_{w,n}^{\text{in,I}}\\ &\text{s.t.,} \begin{cases} \text{equation 8.2.2} \\ \text{Boundary \& initial conditions}\end{cases}\end{aligned} \tag{8.4.2}$$

Here, we consider that the average pressure, saturation and transport equations in the constraint set of problem (8.4.2) are discretized in space as discussed in Chapter 4. To make the presentation clear and easily understandable, let us label the performance function, the pressure, saturation and transport equations with, $F^n = F(P_{\text{av}}^n, S_w^n, C^n, u_c^n, u_w^n)$, $f_p^n = f_p(P_{\text{av}}^{n+1}, P_{\text{av}}^n, S_w^{n+1}, S_w^n, C^{n+1}, C^n, u_c^n, u_w^n)$, $f_s^n = f_s^n(P_{\text{av}}^{n+1}, P_{\text{av}}^n, S_w^{n+1}, S_w^n, C^{n+1}, C^n, u_c^n, u_w^n)$ and $f_c^n = f_c(P_{\text{av}}^{n+1}, P_{\text{av}}^n, S_w^{n+1}, S_w^n, C^{n+1}, C^n, u_c^n, u_w^n)$ respectively, where u_c^n and u_w^n are control variables for microbial concentration and water volumetric inflow rate. First let us construct the Hamiltonian function of problem (8.4.2) as defined in [6, 68]

$$H^n = F^n + \mathrm{s}\lambda^{n+1}f_s^n + \mathrm{c}\lambda^{n+1}f_c^n. \tag{8.4.3}$$

Moreover, the Lagrangian of optimization problem in (8.4.2) can be defined as,

$$L^n = H^n + \mu f_p^n, \tag{8.4.4}$$

where μ is a row vector of Lagrange multiplier, whereas $\mathrm{s}\lambda^{n+1}$ and $\mathrm{c}\lambda^{n+1}$ are co-reservoir functions associated with saturation and microbial transport equations respectively. Note that the multiplication of Lagrange multipliers as well as costate variables with reservoir constraints are done componentwise.

The state/reservoir as well as costate/co-reservoir models of the resulting economic model of microbial EOR process can be formulated in the same fashion as discussed in Chapter 7. However, here we have additional mixed algebraic constraint which arises from the average pressure formulation. Now we can differentiate the Lagrangian (8.4.4) with respect to reservoir variables to develop co-reservoir model that contributes in a shadow to maximize the performance functional (8.4.1) and is stated as follows

$$\frac{\partial L^n}{\partial S_w^n} + \frac{\partial L^{n-1}}{\partial S_w^n} = 0 \text{ and } \frac{\partial L^n}{\partial C^n} + \frac{\partial L^{n-1}}{\partial C^n} = 0. \tag{8.4.5}$$

Similarly, the reservoir model should be satisfied and can be extracted by differentiating the Lagrangian (8.4.4) with respect to the co-reservoir variables

$$\frac{\partial L^n}{\partial \mathrm{s}\lambda^{n+1}} = 0 \text{ and } \frac{\partial L^n}{\partial \mathrm{c}\lambda^{n+1}} = 0. \tag{8.4.6}$$

Finally, the Lagrange multipliers should satisfy the complementarity slackness condition, which can be obtained as follows

$$\mu f_p^n = 0, \text{ for } \mu \in \mathbb{R}. \tag{8.4.7}$$

The candidate control variables is said to be a local maximizer of the performance functional, the necessary conditions (8.4.5)– (8.4.7) have to be satisfied at the candidate value.

Based on the above developments of necessary conditions, we will suggest a numerical method that searches a local maximizer for the optimization problem (8.4.2).

8.4.1.1 Description of Solution Algorithm

In this section, we will develop a new mathematical algorithm that searches a local maximum for economic problem (8.4.2) using the necessary conditions (8.4.5)–(8.4.7).

The proposed algorithm starts with solving the slack complementarity condition that is

$$\mu f_p(P_{\text{av}}^{n+1,i+1}, P_{\text{av}}^{n+1,i}, S_w^{n+1,i+1}, S_w^{n+1,i}, C^{n+1,i+1}, C^{n+1,i}, u_c^{n+1,i}, u_w^n) = 0, \text{ for } \mu \in \mathbb{R}. \tag{8.4.8}$$

Let us assume the variables with exponent $\{n+1, i\}$ are known, then equation (8.4.8) results in bilinear systems of equations. If either μ or $P_{\text{av}}^{n+1,i+1}$ is known, the bilinear system (8.4.8) becomes linear. If this linear system is solvable, the bilinear system is solvable [69]. Since the coefficient matrix of the pressure equation is linearly independent by construction, equation (8.4.8) is solvable for any fixed Lagrange multipliers. Note that, equation (8.4.8) becomes freely solvable when $\mu = 0$.

Now solve the complementarity slackness condition (8.4.8) using non-linear solver to obtain the average pressure and Lagrange multipliers at the new time step. Fix the Lagrange multiplier and combine the resulting linear system average pressure equations with reservoir models in (8.4.5) as follows,

$$\frac{\partial L^n}{\partial \text{s}\lambda^{n+1}} = 0, \ \frac{\partial L^n}{\partial \text{c}\lambda^{n+1}} = 0 \text{ and } \mu^{n+1,*} f_p^{n,i} = 0 \tag{8.4.9}$$

for $n = 1 : n_f$, where $\mu^{n+1,*}$ is known.

Solve equation (8.4.9) using iterative linearization method as we have done in previous numerical experiments. Now using the information of average pressure, water phase saturation and microbial concentration, we are able to solve the co-reservoir model for $\text{s}\lambda^n$ and $\text{p}\lambda^n$,

$$\frac{\partial L^n}{\partial S_w^n} + \frac{\partial L^{n-1}}{\partial S_w^n} = 0, \ \frac{\partial L^n}{\partial C^n} + \frac{\partial L^{n-1}}{\partial C^n} = 0 \tag{8.4.10}$$

for $n = n_f : -1 : 1$.

Once we obtained the necessary solution for a given injection variables, we can correct the injection policy such that the new control vector is able to maximize the performance functional. This is done by finding an

accent direction, that is in the direction of the gradient of L^n with respect to the injection variables. And we can correct the injection policy using the following simple gradient accent formula

$$u^n_{k+1} = u^n_k + \alpha \nabla_u L^n, \tag{8.4.11}$$

where α is a positive real number which determines how far we should go to get close to the optimal injection value, and can be obtained by either direct or backtracking method. In this study we have used backtracking method to search for possibly best α.

Take u^n_{k+1} as a new guess and repeat the above procedures until a pre-specified condition is satisfied. That is,

$$|J^n_{k+1} - J^n_k| < \epsilon, \tag{8.4.12}$$

where ϵ is tolerance error.

8.4.2 Optimization Results and Sensitivity Analysis

The proposed optimization model is non-concave in both reservoir and control variables. In this case the maximum principle conditions (8.4.5) – (8.4.7) may not be sufficient and the discussed algorithmic optimization approach may result in local optimal injection policies. In general, without concavity formulation, stationary points (points that satisfy the maximum principle conditions) may not be optimal solutions for the corresponding optimization problem and the set of all stationary points may not be connected [70, 71]. Moreover, the existence of mixed type constraints further increase the complexity of the solution processes. Thus, the proposed optimization method searches an optimal way to inject microbes and water in order to improve sweep efficiency and performance functional locally, if there is no further simplification on the proposed microbial EOR optimization model.

Let us use initial injection policy of water as described in 8.2.1.2 and reservoir parameters as listed in Table 8.1 to evaluate the performance of the optimization algorithm discussed in subsubsection 8.4.1.1. Note that the cost of microbes are not considered for these particular simulations. Thus, we can apply the algorithm proposed in subsubsection 8.4.1.1 to obtain an optimal injection profiles, final time reservoir conditions and functional performance profiles for the following three cases for numerical optimization experiments with different cost of microbes and initial slug size.

For instance, let us start with a 25NOK/Kg cost of microbes, 1000NOk/m^3 cost of produced oil and initial injection profiles as given in subsubsection 8.2.1.2. We have applied the proposed optimization algorithm on the resulting microbial EOR optimization problem to obtain an optimal water and microbial injection strategy and the finial reservoir conditions as depicted in Figure 8.4.1 and Figure 8.4.2 respectively. The final time reservoir condition in Figure 8.4.2 shows that the suggested optimal injection policy performs better to mobilize the residual oil as compared to the results in subsubsection 8.2.1.2, where they obtained from the classical injection policy. Moreover, the microbes distribution all over the reservoir is higher as compared to the distribution obtained from subsubsection 8.2.1.2. Particularly, we observe that the microbes are densely distributed around the injection well with this optimal injection of water and microbial concentration. Beside

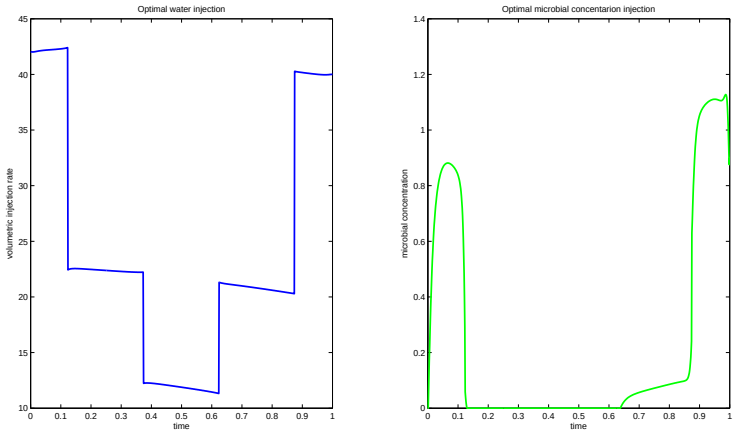

Figure 8.4.1: Optimal Injection Policy.

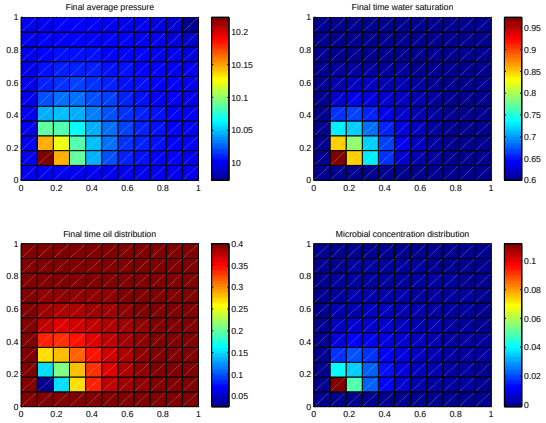

Figure 8.4.2: Final Reservoir Condition with injection strategy of Figure 8.4.1.

of the obtained optimal injection profiles and reservoir conditions, we have got a performance status at each optimization iteration as depicted in Figure 8.4.3 for which it is considered to be a major output of this optimization processes. The final value of the performance functional (where we have obtained it from the optimal injection strategy of water and microbial concentration) is improved by 10.10% as compared to the initial performance value, where it is found with initial injection profiles.

The above Figures 8.4.1 and 8.4.2 were produced by assuming the cost of microbes as 25NOK/Kg and oil costs 1000NOK/m^3. Now let us consider a zero cost with larger initial slug size of microbial concentration throughout the operating time as compared to initial injection given in Figure 8.2.3. But, we assume the cost of produced oil stays the same as before. Thus, the discrete optimization model of microbial EOR (8.4.2)

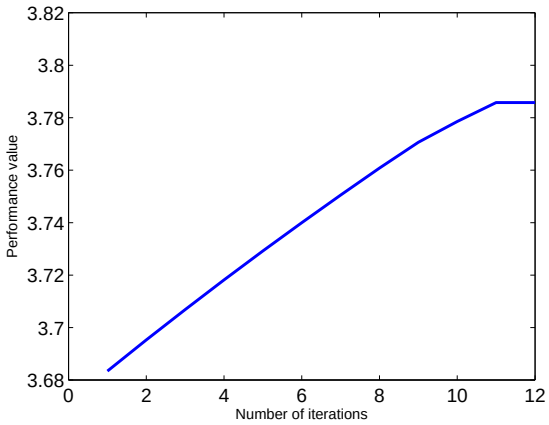

Figure 8.4.3: Performance functional.

could be reduced to

$$\max \sum_{P} \sum_{i=0}^{\mathrm{n_f}} Q_{o,i}^{\mathrm{out,P}} \triangle t$$
$$\text{S.t.,} \begin{cases} \text{equation 8.2.2} \\ \text{Boundary \& initial conditions.} \end{cases} \tag{8.4.13}$$

In problem (8.4.13), the control variables appear only in the constraint equations. Let us consider an initial constant slug size of 0.9Kg/m^3 throughout the operating time. Moreover, let us keep initial water injection and all fluid and rock parameters as before. We have solved problem (8.4.13) using the algorithm in subsubsection 8.4.1.1 and it converges to a local optimal injection policy within two optimization iterations giving a performance value of 4.021 which is a 2.57% improvement as compared to a performance value found with initial injection strategies. The corresponding optimal injection strategy is given as in Figure 8.4.4. The optimal injection trajectory of microbial concentration in Figure 8.4.4 is almost similar to the optimal injection policy for microbial concentration in Figure 8.4.1 except at the half way of operating time. Even if the model is free to choose a lager slug size of microbial concentration, the optimization gradient direction forces to have a small slug size in most of the operating time. However, the total slug size for zero cost is higher than that of the total slug size as obtained from Figure 8.4.1. Moreover, from Figure 8.4.4 we can observe that optimally controlled water injection profile is higher than the optimal injection of water in Figure 8.4.1. This shows water injection profile is also influenced by the cost of microbes. We have also obtained a reservoir profile for an injection profile of Figure 8.4.4 and the final time water, oil and microbial concentration distributions are given in Figure 8.4.5. Even though the total injection policies of a zero cost slug size is higher than slug size of a total injection policy in Figure 8.2.3, the final time reservoir condition of Figure 8.4.5 is identically similar to Figure 8.4.2.

The third test case considers a higher cost of microbes (i.e., 100 NOK/Kg) and the same initial injection strategies as the first test case has used. We have solved the resulting optimization problem for given parameters in Table 8.1 to obtain an optimal injection policy as depicted in Figure 8.4.6

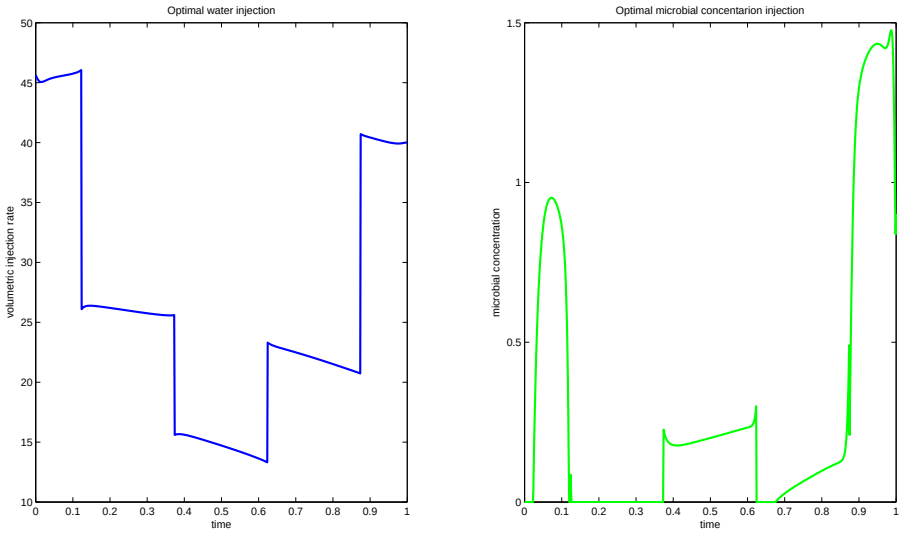

Figure 8.4.4: Optimal injection policy with zero cost of microbes

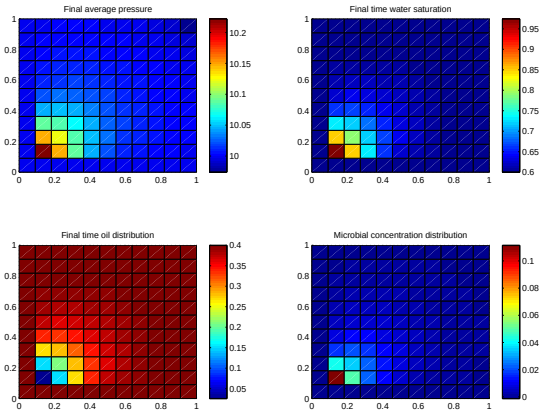

Figure 8.4.5: Final time fluids distribution for Injection 8.4.4

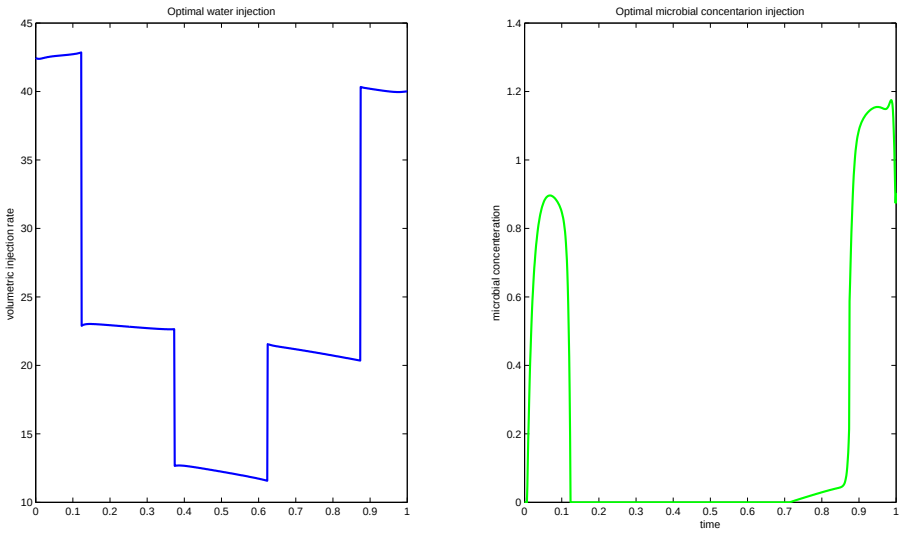

Figure 8.4.6: Optimal water (left) and microbial concentration (right) injection profiles corresponding to the highest cost of microbes

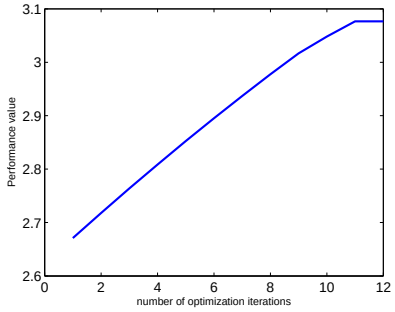

Figure 8.4.7: Performance functional for high cost of microbes

Figure 8.4.6 is identical to Figure 8.4.1 almost everywhere. But, we can observe from Figure 8.4.6 that the optimization searcher tries to lower the slug injection due to the high cost of microbes. Moreover, we have obtained a similar reservoir condition as we have obtained in previous test cases and the performance functional related to this high cost of microbes is given in Figure 8.4.7. We observe that the oil industry will get a profit improvement of 41.84% using the optimal injection policy instead of the initial injection strategy.

In the three cases above, the distribution of microbial concentration over the specified reservoir medium is higher than the distribution obtained from the initial slug injection which is given in Figure 8.2.4. However, the microbial concentration distribution is still very low implying the microbial growth is very limited. As a consequence, IFT and capillary force might be remain unchanged (i.e., the IFT might keep its maximum value specially for fluids that are not near to an injection well) for the IFT parameters given in Table

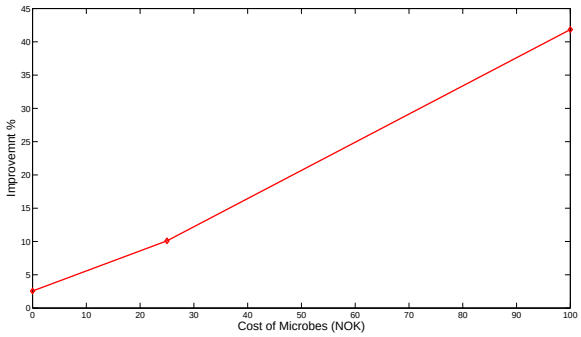

Figure 8.4.8: Effect of microbial concentration cost on performance functional.

8.1.

The cost of microbial concentration has no effect on the final time reservoir profile. However, it has a little effect on the optimal injection policy and higher effect on the performance functional as expected. We have produced a figure that describes the effect of microbial cost on the improvement of the performance functional and shown in Figure 8.4.8. As we have seen in Figure 8.4.8, the improvement is higher for higher cost slug injection and the optimizer had a small improvement for a zero cost slug injection. In general, the optimization results obtained above are performing better as compared to the performance obtained from initial injection policies. Thus, this thesis can be seen as a good start for future investigation on microbial EOR optimization design.

Chapter 9

Conclusion and Future Work

Microbial EOR technology is environment friendly residual oil recovery method as compared to other oil enhancing methods. Now a days, laboratory experiments and mathematical simulations of microbial EOR process have got an attention in academia and industry in order to understand, manege and forecast the processes takes place in oil reservoirs.

This thesis presents an average pressure formulation of two phase flow equations coupled to reactive transport model. These equations were discretized by a cell centered finite volume method in space and implicit Euler method in temporal variable. The resulting non-linear system of algebraic equations are solved using an iterative linearization method. We have done a number of numerical experiments to validate and analyse the convergence of our Matlab code implementation for 2D two-phase flow problems with different fluid parameterizations and advection-diffusion transport models. All reported numerical results in Chapter 5 agree to validate our discretization scheme and Matlab code implementation of fluid flow and transport phenomenon in porous media.

This study has investigated an IFT reduction mechanism of microbial EOR process. We have developed a new constitutive relation between IFT and microbial concentration for which it is used to couple the flow and transport models. The resulting coupled system of equations are referred to as a microbial EOR model which is used to study the fluid dynamics and the effect of microbes on the residual. The work of this thesis adopted an iterative linearization two-phase flow solver for this complex microbial EOR mathematical model. Even though the convergence of the method is not verified theoretically, a Matlab code validation test and convergence analysis of the proposed method for microbial EOR model was reported in Chapter 6. The discussed numerical result verifies the validation and the convergence of our Matlab code implementation.

Further, we have proposed a new optimization model to investigate the effect of slug size injection strategy for microbial EOR technology. The designed optimization model has bilinear formulations with respect to control variables in the objective as well as constraint set. Moreover, this optimization problem is also highly

non-linear with respect to reservoir variables. These all and the dynamic nature of the designed optimization model make the solution processes challenging. Nevertheless, we have proposed a new deterministic optimization method that combines an iterative linearization and gradient accent methods to treat it numerically. Furthermore, we have implemented the proposed method in Matlab and tested it for different fully coupled microbial EOR optimization models. The obtained optimization results perform better on the economics of microbial EOR technology as compared to the traditional slug injection policy. A performance improvement of 2.57% upto 41.84% were reported in Chapter 8. The performance functional and injection profile were sensitive for the cost of microbes, whereas the final reservoir conditions were not sensitive to microbial cost.

The numerical simulations of this thesis are performed on microbial EOR models that comprise two-phase flow and a single component (i.e., microbial concentration) advection-diffusion reactive transport models. This is seen as a first step in the direction of microbial EOR optimization simulations. The future works have to consider the dynamics of other components like nutrient and bio-surfactant distributions. The future work will further consider other microbial EOR mechanisms such as, viscosity reduction, degradation of rocks, bio-clogging and wettability alteration to name a few.

Even though we have got a significant improvement in microbial EOR based on the proposed local optimization simulation, proposing a global convergent, efficient and stable optimization method is of a great importance to see the effect of the slug injection policy for the proposed microbial EOR optimization model. Moreover, the model itself needs to be enrich in economic aspects by weaken the assumptions used in this thesis. For example, water transport and treatment costs are not considered in this thesis. It is also important if the future work integrates wells installation design to our microbial EOR optimization model.

In general, the microbial EOR technology is not well understood. Thus, it is the author's wish to study further on the simulation of microbial EOR optimization calibrated by laboratory/field experiments in order to understand and optimize microbial EOR good enough.

Appendices

Symbols

Symbols	Units	Description
ϕ	[-]	porosity
K	m^2	absolute Permeability
τ	[-]	tortuosity
M	[-]	Mobility ratio
λ_D	1/Pa.s	displacing fluid mobility
λ_d	1/Pa.s	displaced fluid mobility
$\tilde{S}$	[1/m]	ratio of surface area to volume of a rock
Θ	[-]	effective water content
w_c	[-]	water content
S_α	[-]	saturation of phase α
λ_α	1/Pa.s	phase mobilities
P_c	Pa	capillary pressure
r_c	m	curvature radius
σ	[N/m]	fluid-fluid interfacial tesnsion
$\beta_1, \beta_2, \beta_3$	[-]	interfacial tension model parameters
P_α	Pa	phase pressure
P_{av}	Pa	average pressure
q_α	m/s	Darcy's velocity of phase alpha
μ_α	Pa.s	phase viscosity
ρ_α	Kg/m^3	phase densities
C_{ij}	Kg/m^3	component i concentration in phase j
D_i	m^2/day	component i diffusion coefficient
K_s	[-]	half saturation constant
S_{or}	[-]	residual oil
Q^{in}	m^3/s	volumetric inflow rate
Q^{out}	m^3/s	volumetric outflow rate

r_w	m	well radius
r_{cell}	m	approximate cell radius
PI	m^3/Pa.s	well performance index
P_b	Pa	wellbore pressure
h	m	hydraulic head
a_b	Kg/m^2	the amount of bacteria attached to the pore walls
$G_{\max}$	[-]	maximum microbial growth rate
O_c	NOK/m^3	cost of oil per meter cube
C_{in}	NOK/Kg	cost of microbes per kilogram
ñ	[-]	unit normal vector pointing outward the boundary
x	m	Position in x direction
y	m	Position in y direction
$\triangle x$	m	cell length
$\triangle y$	m	cell width
t	[s]	operating time

Abbreviations

UoB	University of Bergen
IMPES	Implicit Pressure Explicit Saturation
EOR	Enhanced Oil Recovery
REV	Representative Elementary Volume
IFT	Interfacial Tension
PDEs	Partial Differential Equations
ODE	Ordinary Differential Equation
MPFA	Multi Point Flux Approximation
1D	one dimensional
2D	two dimensional
PI	Performance Index
Matlab	Matrix Laboratory

Bibliography

[1] J. M. Nordbotten and M. A. Celia, *Geological Storage of CO2: Modeling Approaches for Large-Scale Simulation*, A John Wiley & Sons, 2012.

[2] J. Bear, and A. Verruijt, *Modeling Groundwater flow and pollution: With Computer Programmngs for Sample Cases*, Theory and Application of Transport in Porous Medium, 1988.

[3] Corry A., *Mechanics of Immisible Fluids in Porous Media. Water resource publication*, 1994.

[4] S. M. Nielsen, A. A. Shapiro, M. L. Michelsen and E. H. Stenby. 1D Simulations for Microbial Enhanced Oil Recovery with Metabolite Partitioning. Transport in Porous Media 85:785–802, 2010.

[5] K. Skiftestad. Numerical Modelling of Microbial Enhanced Oil Recovery with Focus on Dynamic Efects: An Iterative Approach. Master's Thesis, Uiniversity of Bergen, Norway, 2015.

[6] W. F. Ramiraz, *Application of optimal control theory to enhanced oil recovery*, 1987.

[7] Y. Cao, B. Eikemo and R. Helmig, Fractional Flow formulation for Two-Phase Flow in Porous Media, University of Stutgurt, 2007.

[8] O. A. Omoniyi, and F. Abdulmalik. A review of Microbial Enhanced Oil Recovery: Currunt Development and Future Prospective. *IJSER*, 6:1378–1389, 2015.

[9] G. Dagan, U. Hornung and P. Knabner, (Editors) *Mathematical Modelling for Flow and Transport Through Porous Media*, Kluwer Academic Publishers, 1991.

[10] D.W. Peaceman, H.H. Rachford Jr. Numerical Calculation of Multidimensional Miscible Displacement. *Society of Petroleum Engineers* 4:26–36, 1964.

[11] S.M. Nielsen, and A.A. Shapiro. Microbial Enhance Oil Recovery–a modeling study of the potential of spore-forming bacteria. *Compot. Geosci.*, 20:567–580, 2015.

[12] F.A. Radu, J.M. Nordbotten, I.S. Pop, K. Kumar. A robust linearization scheme for finite volume based discretizations for simulation of two-phase flow in porous media. *J. Comput. Appl. Math.*, 289:134-141, 2015.

[13] F. List and F. A. Radu. A study on iterative methods for solving Richards equation. Computational Geosciences 20(2):341-353, 2016.

[14] F. A. Radu,K. Kumar, J. M. Nordbotten and I. S. Pop. A convergent mass conservative numerical scheme based on mixed finite elements for two-phase flow in porous media, arXiv:1512.08387, 2015.

[15] S. M. Nielsen, Shapiro, A., E. H. Stenby and M. L. Michelsen. *Microbial Enhanced Oil Recovery - Advanced Reservoir Simulation*, Kgs. Lyngby, Denmark: Technical University of Denmark (DTU), 2010.

[16] N. Tufenkji. Modeling Microbial Transport in Porous Media: Traditional Approaches and Recent Developments. *Advances in water resource,* 30:1455–1469, 2007.

[17] M. R. Islam. Mathematical modeling of Microbial Enhanced Oil Recovery. *Society of Petroleum Engineers*, 1990.

[18] A. R. Kukreti and Y. Rajapaksa. A numerical model for simulating two phase flow through porous media. *Appl. Math. Modelling,* 13:268–281, 1989.

[19] P. Bastian, *Numerical Computation of Multi-phase Flows in Porous Media*, Ph.D. thesis, Christian-Alberchts-Universitat Kiel, Submited, 1999.

[20] P. Binning and M. A. Celia. Practical Implementation of the Fractional Flow Approach to Multi-phase Flow Simulation. *Advances in Water Resource,* 2:461–478, 1999.

[21] , S. A. Bradford, Y. Wang, H. Kim, S. Torkzaban, and J. Simunek. Modeling Micro-organism Transport and Survival in the Sub-surface. *J. Environ. Qual.* 43:421–440, 2014.

[22] J. F. Schijven and S. M. Hassanizadeh. Removal of Viruses by Soil Passage: Overview of Modeling, Processes, and Parameters. *Critical Reviews in Environmental Science and Technology,* 30:49–127, 2000.

[23] M. Behesht, R. Roostaazad, F. Farhadpour and M. R. Pishvaei. Model Development for MEOR Process in Conventional Non-Fractured Reservoirs and Investigation of Physico-Chemical Parameter Effects. *Chem. Eng. Technol.* 31:953–963, 2008.

[24] Zhang, R.M. Knapp and M.J. Mclnerney, U. of Oklahoma, A Mathematical Model for Microbially Enhanced Oil Recovery Process. *Society of Petroleum Engineers Inc*, 1992.

[25] S. O. Babatunde. Modeling of oil reservoirs with focus on microbial induced effects. Master's Thesis, University of Bergen, Norway, 2015.

[26] A. Costa. Permeability-porosity relationship: A reexamination of the Kozeny-Carman equation based on a fractal pore-space geometry assumption. *Geophysical Research Letters*, 33:1–5, 2006.

[27] Y. Mualem. A new model for predicting the hydraulic conductivity of unsaturated porous media. *Water Resources Research*, 12:513–522, 1976.

[28] M.Th.van Genuchten. A closed-form equation for predicting the hydraulic conductivity of unsaturated soils. *Soil Sc. Soc. of America*, 44(5):892–898, 1980.

[29] S. Kokal, and A. Al-Kaabi, *Enhanced oil recovery:challenges & opportunities*, EXPEC Advanced Research Centre, Saudi Aramco, 2010.

[30] V. Alvarado and E. Manrique, Enhanced Oil Recovery: An Update Review. *Energies*, 3:1529–1575, 2010,

[31] E.J. Manrique, M. Gurfinkel, V. Muci. EOR Field Experiences in Carbonate Reservoirs in the United States. *SPE Reserv. Eval. Eng.* 10:667–686, 2007.

[32] Kowalewski, E. Ruesltten, I., Boassen , T., Sunde E., Stensen, J.., Lilleb. Analyzing Microbial Improved Oil Recovery Processes from Core Floods. *IPTC*, 2005.

[33] L. W. Lake, *Emhenced Oil Recovery*, Eglewood Cliffs, 1989.

[34] S. M. Skjveland, J. Kleppe, *Recent Advances in Improved Oil Recovery Methods for North Sea Sandstone Reservoirs*, Norwegian Petroleum Directorate, 1992.

[35] S. Thomas. Enhanced Oil Recovery An Overview. *Oil & Gas Science and Technology Rev. IFP*, 63(1): 9–19, 2008.

[36] G. Cheraghian, S. S. K. Nezhad, Mosayyeb Kamari, Mahmood Hemmati, Mohsen Masihi and Saeed Bazgir. Adsorption polymer on reservoir rock and role of the nanoparticles, clay and SiO2. *Int Nano Lett.,* 2014.

[37] I. Lazar, I. G. Petrisor and T. F. Yen. Microbial Enhanced Oil Recovery. *Petroleum Science and Technology,* 25:353–1366, 2007.

[38] J. I. Adetunji,*Microbial Enhanced Oil Recovery*, PhD thesis, 2012

[39] A. I. Laskin, S. Sariaslani and G. M. Gadd (Editors) *Advances in Applied Microbiology*, Accadamic London 94, 2009.

[40] I.M. Banat, and S.S. Cameotra, Potential Commecial Applications of Microbial Surfactant. *App. Microbial Biotech,* 56(5):493–508, 2000.

[41] R. T. Armstrong, D. Wildenschild. Microbial Enhanced Oil Recovery in Fractional-Wet Systems: A Pore-Scale Investigation. *Transport in Porous Media,* 92:819–835, 2012.

[42] S. L. Marshall, Fundamental Aspects of Microbial Enhanced Oil Recovery: A Literature Survey, 2008.

[43] O. Polivka and J. Mikyska. Compositional Modelling of Two-Phase Flow in Porous Media Using Semi-Implicit Scheme. *Int. J. of Appl. Math.,* 45:55–63, 2015.

[44] G. Chavent, A Fully Equivalent Global Pressure Formulation for Three-Phase Compressible Flow, arXiv:0901.1462, 2008.

[45] H. K. Dahle, M.A. Celia, S. M. Hassanizadeh and K. H. Karlsen, A total pressure-saturation Formulation of Two-phase flow incorporating Dynamic effects in the Capillary Pressure Saturation Relationship. *Computational Methods in Water Resource XIV*, 2:1067–1074, 2002.

[46] B. Amaziane, M. Jurak, A. Zgalji c. Keko, Modeling and Numerical Simulations of Immiscible Compressible Two-Phase Flow in Porous Media by the Concept of Global Pressure. *Transp. Porous. Med.,* 84:133–152, 2010.

[47] A. Kvashchuk. A robust implicit scheme for two-phase flow in porous media. Master's Thesis, University of Bergen, Norway, 2015.

[48] D. A. Lopez-Falcon, M. A. Diaz-Viera, and A. Ortiz-Tapia. Transport, Growth, Decay and Sorption of Micro-organisms and Nutrients through Porous Media: A Simulation with COMSOL. *COMSOL Conference, Boston MS, USA*, 2008.

[49] O. Langsrud. Simulation of two phase flow by finite element methods. *Society of Petroleum Engineers*, 1996.

[50] K. Kumar, I.S. Pop and F.A. Radu, Convergence analysis of mixed numerical schemes for reactive flow in a porous medium. *SIAM J. Num. Anal*, 51:2283-2308, 2013.

[51] K. Kumar, I.S. Pop and F.A. Radu, Convergence analysis for a conformal discretization of a model for precipitation and dissolution in porous media. *Numerische Mathematik* 127:715–749, 2014.

[52] Z. Chen. *Finite Element Methods and Their Applications*, Springer Berlin Heidelberg, 2005.

[53] J. Fish, T. Belytschko, *A First Course in Finite Elements*, John Wiley & Sons, Ltd, 2007.

[54] S. C. Brenner, L. R. Scott. *The Mathematical Theory of Finite Element Methods*, Springer Science+Business Media, LLC, 2008.

[55] J. W. Thomas, *Numerical Partial Differential Equations: Finite Difference Methods*, Springer-Verlag, City of New York, State of New York, 1995.

[56] R. Eymard, T. Gallouet and R. Herbin, *Finite Volume Methods Schemes and Analysis*, Lecture Note, 2008.

[57] Z. Chen, G. Huan and Y. Ma, *Computational Methods for Multiphase Flows in Porous Media*, Society for Industrial and Applied Mathematics, 2006.

[58] Francisco Marcondes, Clovis R. Maliska, Mário C. Zambaldi, A Comparative Study of Implicit and Explicit Methods Using Unstructured Voronoi Meshes in Petroleum Reservoir Simulation. *J. Braz. Soc. Mech. Sci. & Eng.,* XXXI(4):353–361 2009.

[59] C.J. van Duijn, S.M. Hassanizadeh, I.S. Pop, and P.A. Zegeling. Non-equilibrium Models for Two Phase Flow in Porous Media: the Occurrence of Saturation Overshoots. *ICAPM*, 59–70,2013.

[60] , S. W. Tylor, P. R. Jaffe. Substrate and bio-mass Transport in Porous Medium. *Water Resource Research*, 26:2181–2194, 1990.

[61] K. Abidoye and D. B. Das. Scale dependent dynamic capillary pressure effect for two-phase flow in porous media. *Advances in Water Resources,* 74:212–230, 2014.

[62] I. Langmuir. Adsorption of Gases on Glass, MICA and Platinum. *Journal of the American Chemical Society*, 9:1361–1403, 1918.

[63] E. Kowalewsk, I.Rueslatten, T. Boassen, E.Sunde, J. A.Stensen, B. L. P. Lillebo, G.Bodtker, and T.Torsvik. Analyzing microbial improved oil recovery processes from core floods. *IPTC*, 2005.

[64] P. Shen, B. Zhu, X. B. Li, and Y. S. Wu. The influence of interfacial tension on water/oil two-phase relative permeability. *Society of Petroleum Engineers*, 2006.

[65] F. Clarke, The Pontryagin Maximum Principle and a Unified Theory of Dynamic Optimization. *Proceedings of the Steklove Institute*, 268:58–69, 2009.

[66] E. N. Bodine, L. J. Gross, S. Lenhart. Optimal Control Applied to a Model for Species Augmentation. *mathematical biosciences and engineering*, 5:669-680, 2000.

[67] Lie, K.-A., Krogstad, S., Ligaarden, I. S., Natvig, J. R., Nilsen, H. M., and Skaflestad, B. (2012). Open-source matlab implementation of consistent discretisations on complex grids. *Computational Geosciences*, 16(2):297–322, 2012.

[68] Richard F. Hartl, Suresh P. Sethi, Raymond G. Vickson. A Survey of the Maximum Principles for Optimal Control Problems with State Constraints. *SIAM*, 37:181–218, 1995.

[69] Charles R. Johnson, Helena Šmigoc, Dian Yang, Solution Theory for Systems of Bilinear Equations, arXiv:1303.4988 [math.RA], 2013.

[70] A. M. Kassa and S. M. Kassa. A branch-and-bound multi-parametric programming approach for non-convex multilevel optimization with polyhedral constraints. *J Glob Optim,* 64:745–764, 2015.

[71] A. M. Kassa and S. M. Kassa. A multi-parametric programming algorithm for special classes of non-convex multilevel optimization problems. *IJOCTA*, 3(2):89–98, 2013.